Integration of Nanoparticle Cell Lysis and Microchip PCR as a Portable Solution for One-Step Rapid Detection of Bacteria

by

Weijie Wan

A thesis
presented to the University of Waterloo
in fulfillment of the
thesis requirement for the degree of
Doctor of Philosophy
in
Systems Design Engineering

Waterloo, Ontario, Canada, 2011

AUTHOR'S DECLARATION

I hereby declare that I am the sole author of this thesis. This is a true copy of the thesis, including any required final revisions, as accepted by my examiners.

I understand that my thesis may be made electronically available to the public.

Abstract

Bacteria are the oldest, structurally simplest, and most abundant forms of life on earth. Its detection has always been a serious question since the emerging of modern science and technology. There has been a phenomenal growth in the field of real-time bacteria detection in recent years with emerging applications in a wide range of disciplines, including medical analysis, food, environment and many more. Two important analytical functions involved in bacteria detection are cell lysis and polymerase chain reaction (PCR). Cell lysis is required to break cells open to release DNA for use in PCR. PCR is required to reproduce millions of copies of the target genes to reach detection limit from a low DNA concentration. Conventionally, cell lysis and PCR are performed separately using specialized equipments. Those bulky machines consume much more than needed chemical reagents and are very time consuming. An efficient, cost-effective and portable solution involving Nanotechnology and Lab-on-a-Chip (LOC) technology was proposed. The idea was to utilize the excellent antibacterial property of surface-functionalized nanoparticles to perform cell lysis and then to perform PCR on the same LOC system without having to remove them from the solution for rapid detection of bacteria.

Nanoparticles possess outstanding properties that are not seen in their bulk form due to their extremely small size. They were introduced to provide two novel methods for LOC cell lysis to overcome problems of current LOC cell lysis methods such as low efficiency, high cost and complicated fabrication process. The first method involved using poly(quaternary ammonium) functionalized gold and titanium dioxide nanoparticles which were demonstrated to be able to lyse *E. coli* completely in 10 minutes. The idea originated from the excellent antibacterial property of quaternary ammonium salts that people have been using for a long time. The second method involved using titanium dioxide nanoparticles and a miniaturized UV LED array. Titanium dioxide bears photocatalytic effect which generates highly reactive radicals to compromise cell membranes upon absorbing UV light in an aqueous environment. A considerable reduction of live *E. coli* was observed in 60 minutes. The thesis then evaluates the effect of nanoparticles on PCR to understand the roles nanoparticles play in PCR. It was found that gold and titanium dioxide nanoparticles induce PCR inhibition. How size of gold nanoparticles affected PCR was studied as well. Effective methods were discovered to suppress PCR inhibition caused by gold and titanium dioxide nanoparticles. The pioneering work paves a way for the integration of nanoparticle cell lysis and LOC PCR for rapid detection of bacteria. In the end, an integrated system involving nanoparticle cell lysis and microchip PCR was demonstrated. The prototyped system consisted of a physical microchip for both cell lysis

and PCR, a temperature control system and necessary interface connections between the physical device and the temperature control system. The research explored solutions to improve PCR specificity in a microchip environment with gold nanoparticles in PCR. The system was capable of providing the same performance while reducing PCR cycling time by up to 50%. It was inexpensive and easy to be constructed without any complicated clean room fabrication processes. It can find enormous applications in water, food, environment and many more.

Acknowledgements

First of all, I would like to express my sincerest and deepest gratitude to my supervisor Professor John T.W. Yeow. This work would have been impossible without his invaluable guidance, generous support and constant encouragement throughout my PhD life.

My gratitude is extended to the members of my PhD Advisory Committee, Professor Maud Gorbet in Department of Systems Design Engineering for her invaluable suggestions on my experiments, Professor Jonathan Kofman in Department of Systems Design Engineering for his insightful recommendations and Professor C. Perry Chou in Department of Chemical Engineering for his generous support and invaluable suggestions. I am honored to have Professor Jun Yang in Department of Mechanical and Materials Engineering at the University of Western Ontario as the external examiner.

I am thankful to Mr. Dale Weber in Department of Biology for teaching and helping me in using the TEM machine and in preparing bacteria samples for TEM imaging. I am thankful to Dr. Michele M. Van Dyke in Department of Civil Engineering for her help in performing real-time PCR experiments.

I am indebted to Ms. Vicky Lawrence for her assistance for the past four years.

I am especially thankful to Ms. Yun Wang, Mr. Yanhui Bai, Mr. Sangtak Park and Ms. So-Ra Chung for their long-term help through out my PhD study.

Special thanks to Miss Xiaodan Xu for her every support during the most difficult time of my life.

This research was made possible by the financial support from the Natural Sciences and Engineering Research Council (NSERC) of Canada, the Ontario Graduate Scholarship in Science and Technology (OGSST), the University of Waterloo President's Graduate Scholarship and the University of Waterloo Graduate Scholarship.

Dedication

This work is dedicated to my parents Mr. Guohua Wan and Ms. Liying Xu.

Table of Contents

List of Figures

List of Tables

.

Chapter 1

Introduction

Lab-on-a-Chip (LOC) device refers to device that provides one or several biochemical analytical functions on a single microchip of small size ranging from a few square millimeters to a few square centimeters. The history of LOC devices can be traced back to 1975, when the first LOC device, a gas chromatograph used to separate a mixture of various gases, was invented [1]. However, the real boost and serious growth in LOC devices were not seen until 1990 when the term "μ-TAS" was first proposed by Andreas Manz [2] who demonstrated a microchip incorporating sample separation and detection. Miniaturizing a conventional biochemistry laboratory down to the size of a silicon microchip is the driving concept behind LOC technology. Although a reduction in size to the microscale usually does not involve changing the nature of chemical reactions at the molecular level, laws of scale for surface per volume, molecular diffusion and heat transport enable dramatic increases in throughput. Moreover, being able to perform multifunctional operations is also highly desirable. Ideally, each LOC device may have one or more sample injection reservoirs, sample mixing chambers, sample separation channels, chemical reaction chambers and a monitor and measuring system. There are many benefits of using LOC devices. Due to their small sizes, they consume tiny amounts of biochemical reagents. This is desirable since many reagents are expensive. Moreover, using small amounts of chemicals result in a reduction of analysis time and a faster response as chemicals can mix and react more quickly. Furthermore, since some reagents and reaction products can be very harmful to humans, LOC devices minimize human interaction with chemicals and reaction products. High throughput analysis is enabled by massive parallelization due to compactness of the system. Small size also enables portability of LOC devices, which enables many new applications such as point-of-care diagnosis and detection that cannot be achieved before. Because fabrication of LOC devices is based on highly developed semiconductor processing techniques, it is fairly easy to manufacture LOC devices in large quantities, therefore reducing costs. For the past few years, research activities and investment from both government and industry have been growing amazingly in this rapid emerging field. And thanks to the microfabrication technology and the polymer fabrication technology, realization of LOC devices becomes possible. Many university

laboratories working on LOC or LOC related research have been emerging with more and more publications. Companies also invest generously in this promising field with a global market of approximately 817.6 million US dollars in 2009. Custom-made LOC devices and entire measuring systems are now commercially sold by companies such as Agilent Technologies, Evotec Technologies, Caliper Life Sciences, Hitachi and Fluidigm Technology [3]. LOC devices are currently undergoing an important transition from primarily research-and-development tools to applied applications in chemical analysis, drug discovery and development, clinical diagnostics and many more.

For the past few years, a little word with big potential has been brought into the focus of not only scientists and engineers but also the general public from all over the world. The word is “Nanotechnology”. For scientists and engineers, it is considered “the next industrial revolution” and for the general public, it is known as “the next big idea”. In the media, "Nanotechnology" has captured headlines at almost every online technical, scientific and medical journal. The Nobel Prize has been awarded several times for Nanotechnology research [4] and the Feynman Prize, a prestigious award in the field of Nanoscience and Nanotechnology, was created to recognize the accomplishments of nanoscientists [5]. Science magazine named a development as Breakthrough of the Year in 2001 [6]. Nanotechnology is big business. According to the National Research Council Canada, the economic and social impact of nanotechnology is huge: discoveries and applications of nanotechnology could lead to a new industrial revolution and to commercial markets as large as $1.5 trillion per year within ten years. The figure, if true, makes Nanotechnology one of the fastest-growing industries in history, even larger than the combined telecommunications and information technology industries at the beginning of the technology boom in 1998. One widely-cited market report noted that in 2005, Nanotechnology was incorporated into more than 30 billion US dollars worth of manufactured goods [7, 8]. It is not surprising that Nanotechnology is already a priority for well-known companies like IBM, HP, Xerox and GE, all of whom have developed massive research capabilities for studying and developing devices and products using Nanotechnology. The market is not only for the well-recognized companies but also for a host of start-ups and smaller concerns that are jumping into the game as well. In the academy, major universities across the world - from MIT in

the United States to Delft University of Technology in the Netherlands and the National Nanoscience Center in China - are building new faculties, facilities and research groups for Nanotechnology. Nanotechnology research also crosses scientific disciplines. Chemists, biologists, doctors, physicists and engineers are all involved in the development of Nanotechnology. Innovations in this rapidly emerging field have already boosted many commercial inventions from faster-burning rocket fuel additives to new cancer treatments and simple-to-use detectors for biotoxins such as anthrax. Generally speaking, when the size of a material reaches the nanoscale, new properties unlike those possessed by its bulk counterparts may present. Moreover, small size means larger surface-area-to-volume ratio which greatly enhances properties that depend on surface interactions. During the past few decades, focus has been put on trying to understand the basic mechanisms that dominate at the nanoscale and properties of nanomaterials. As an engineer, it is not only necessary to explore basic understandings towards mechanisms and phenomenon but also equally important to be able to utilize the knowledge to build and create better solutions to solve problems with specific requirements. Nanotechnology provides a new tool that enables many new applications that were not possible to achieve before.

1.1 Motivation

Bacteria are the oldest, structurally simplest, and most abundant forms of life on earth [9, 10]. They were discovered to exist 3.0 to 3.5 billion years ago. There are about 4,800 different kinds of bacteria to date [9, 10]. Bacteria detection has always been a serious question since the emerging of modern science and technology. There are a number of reasons to be able to detect bacteria. From a medical standpoint, it is important to know which bacteria are causing diseases, so that the appropriate treatment can be suggested, and it is also critical to be able to identify bacterial contamination in medical facilities. Law enforcement agencies use bacteria detection to look for signs of bioterrorism and to determine whether or not an area is safe to enter. Agricultural and food inspectors need to know if pathogenic species are in a food supply to ensure food safety. Scientists are also interested in bacterial identification, since it is a large part of their work to explore the world. Researchers need to know which bacteria they are working with, and they must be able to confirm that their samples are

not contaminated by other species. There are different methods to detect bacteria. The most widely and probably easiest way to detect bacteria is culture collection where bacteria is cultured on appropriate nutrient substrate from a small sample collected from the origin. The method is effective but it can take hours or days to show usable results and may miss most types of bacteria. There has been phenomenal growth in the field of real-time bacteria detection in recent years with emerging applications in a wide range of disciplines, including medical analysis, food, environment and many more [11-13]. LOC technology seems to be an excellent fit for solving the problem as mentioned in the previous section.

As is known, different life species differ in DNA coding region no matter how similar they look alike. Therefore, an accurate and direct way to identify a specific kind of microorganism species is to detect a specific sequence of its DNA coding region that is unique to the species. In many cases, the concentration of the target bacteria is low leading to a low concentration of DNAs which is either not possible to detect or possible to detect with unacceptable accuracy. Therefore, a commonly used technique named *polymerase chain reaction* (PCR) is used to amplify a specific region of DNA or RNA from a very small number of templates to millions of copies of target segments to facilitate detection. Besides PCR, a process named cell lysis is needed to break cells open to release intracellular materials such as DNAs prior to PCR. Both functions are indispensable in many LOC applications such as water quality monitoring and blood test. They have attracted much attention for the past two decades. Miniaturizing cell lysis and PCR at microchip level has been a hot research area for a long time. There are many publications about miniaturizing cell lysis [14-17] and PCR [18-21] on a microchip individually. However, miniaturizing each function on a microchip is not the ultimate goal of LOC devices. Integrating several functions on a single microchip is the current trend of LOC research.

As mentioned in the previous paragraphs, cell lysis and PCR are common routines in many Biomedical and LOC applications including bacteria detection while nanomaterials, especially nanoparticles, show very interesting properties with a great potential to benefit bio-related applications. The major motivation of my research work is to promote Nanotechnology in Biomedical and LOC applications, more specifically, to study the properties of nanoparticles and to design,

fabricate, test and optimize an integrated system utilizing nanoparticles to perform cell lysis followed by LOC PCR on a single microchip without having to remove nanoparticles from the solution after cell lysis for rapid detection of bacteria. The motivation of my research can further be divided into several projects with clear objectives.

Objective 1: Discover novel cell lysis methods for LOC applications using Nanotechnology

There are two means to fulfil the objective. One is inspired by the excellent antibacterial property of quaternary ammonium salts that people have been using to fight against pathogenic bacteria for a long time. Nanoparticles have large surface-area-to-volume ratio which enhances properties that depend on surface area. By engineering nanoparticles with poly(quaternary ammonium) functional groups on the surface, an easy and convenient way of performing cell lysis on the microchip level is expected. The other one to fulfil the objective is to utilize the photocatalytic effect induced by titanium dioxide nanoparticles and a miniaturized UV light source to generate highly oxidative radicals to attack cell membranes to break cells open on the microchip level.

Objective 2: Understand the roles gold and titanium dioxide nanoparticles play in PCR

This is a pre-requisite to integrate nanoparticle cell lysis and PCR together. As proposed in the research motivation, nanoparticles used in cell lysis step are not to be removed. They become part of PCR solution. In order for the integrated system to work, both cell lysis and PCR with nanoparticles have to work properly. Therefore, how nanoparticles affect PCR when they are part of the reaction solution has to be studied. If PCR inhibition were observed, methods have to be discovered to minimize the inhibition effect caused by nanoparticles. In fact, there are very few references in the literature about the effect of gold nanoparticles on PCR while there are no references existed about the effect of titanium dioxide nanoparticles on PCR at all. Therefore, the research serves as a pioneering work in exploring the effect of nanoparticles on PCR.

Objective 3: Develop an integrated system with nanoparticle cell lysis and LOC PCR for rapid detection of bacteria.

After achieving Objective 1 and 2, an integrated system with nanoparticle cell lysis and LOC PCR on a same microchip is to be developed for rapid detection of bacteria.

1.2 Thesis Organization

The thesis is organized in a way described as follows. Chapter 1 gives a brief introduction to LOC devices and Nanotechnology, describes the research motivation and sets research objectives. Chapter 2 introduces background information which is necessary to understand the context and experiments appearing in later chapters. Chapter 3 describes research activities towards novel cell lysis methods for LOC applications using poly(quaternary ammonium) modified nanoparticles, and using photocatalytic effect induced by titanium dioxide nanoparticles and a miniaturized UV array. Chapter 4 is devoted to the effort in understanding roles nanoparticles play in PCR and in answering the question that if PCR inhibition is induced by nanoparticles, what means can be taken to suppress the effect. Chapter 5 is all about the integration of nanoparticle cell lysis and PCR together in the same reaction chamber without removing nanoparticles from the solution for rapid detection of *E. coli*. Chapter 6 draws all conclusions about the work that I have carried out and pinpoints research opportunities for the future.

Chapter 2

Background

This chapter is devoted to introducing background knowledge that is useful to readers in the next few chapters. Section 2.1 introduces cell lysis methods for general purposes as well as for Lab-on-a-Chip (LOC) applications. Section 2.2 introduces *polymerase chain reaction* (PCR) as well as microchip PCR. Section 2.3 introduces Nanotechnology with a focus on how people explore the nano world as well as nanomaterials. Section 2.4 introduces background knowledge of *Escherichia coli* (*E. coli*), the bacteria sample used in my experiments. Section 2.5 gives background knowledge of the state-of-the-art fabrication techniques for LOC devices.

2.1 Cell Lysis

Cell lysis is the process of breaking cells open to release intracellular materials such as DNA, RNA, proteins and many more for further analysis. It is an indispensable part of many bio-related applications. There are different methods of performing cell lysis in general and for LOC applications. These include mechanical, chemical, electrical and thermal approaches described in the following sections in details.

2.1.1 Mechanical Approaches

In mechanical cell disruption, cell envelope is physically broken through mechanical forces, releasing all intracellular components into the surrounding medium. Several types of equipments for mechanical cell disruption are commercially available in large scale cell lysis. In a high-pressure homogenizer, a pump forces the sample through a restricted-orifice valve. High pressure of up to 150 Mpa is followed by instant expansion through a special exiting nozzle. Cell disruption was accomplished by three different mechanisms in this system: impingement on the valve, high liquid shear in the orifice, and sudden pressure drop upon discharge which causes explosion of the cell [22]. *Escherichia coli* was proven to be successfully lysed using the method [23]. In a bead-beating equipment, cells were agitated in suspension with small abrasive particles. Cells broke because of

shear forces, grinding between beads, and collisions with beads [24, 25]. Both methods mentioned above are not suitable for miniaturization due to the difficulty of getting agitation in a microchip. High-frequency ultrasound is another method used for mechanical cell lysis. Ultrasonication devices generate intense sonic pressure waves in liquid media. Under appropriate conditions, the pressure waves cause formation of micro bubbles which grow and collapse violently. The implosion generates a shock wave with enough energy to break cell membranes [26, 27]. In modern ultrasonic processors, lead zirconate titanate crystals are used to make piezoelectric generators. The vibrations are then propagated down a titanium metal horn or probe tuned to make the processor unit resonate at 15–25 kHz. Mechanical cell lysis methods are also introduced to LOC devices. Kim *et al.* reported a mechanical cell lysis device on a microfluidics CD [28]. In the pure mechanical cell lysis device as shown in Figure 2-1, beads caused disruption of cells by colliding with them. Interactions between beads and cells were generated in the rimming flow established inside a partially filled annular chamber in the CD rotating around a horizontal axis. The CD was spun forward and backward to maximize bead-cell interaction using a high acceleration for 5 to 7 minutes. The device was capable of lysing cells such as mammalian cells (*CHO-K1*), bacteria (*Escherichia coli*), and yeast (*Saccharomyces cerevisiae*). A lysis efficiency of approximately 65% relative to a conventional cell lysis protocol was demonstrated. Ultrasonic cell lysis has been implemented on LOC devices thanks to MEMS fabrication technique [29-31]. It generates acoustic energy which confines in a small reaction chamber to produce high energy density for fast and efficient cell lysis. The generation of ultrasound is achieved either by an external transducer or by a piezoelectric membrane. Khanna *et al.* reported nanocrystalline diamond microspikes enhanced ultrasonic cell lysis in a LOC device [32]. Despite of its high cell lysis efficiency in disrupting almost all cell species including spores which are extremely hard to lyse using other methods [33], ultrasonic cell lysis has some disadvantages including the generation of considerable heat during processing, complicated clean room fabrication steps and high cost for fabrication [34].

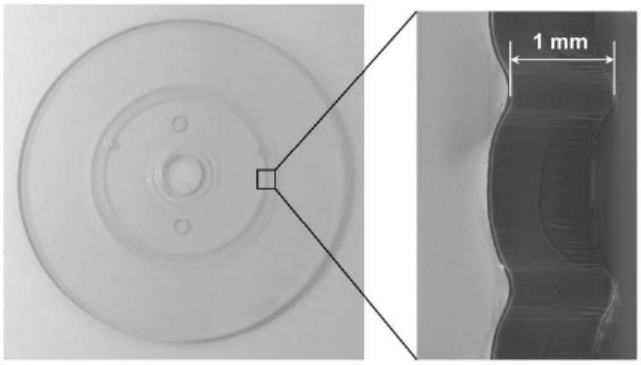

(a) (b)

Figure 2-1. A CD designed for mechanical cell lysis. (a) CD with an annular chamber (total volume of 1 mL) (b) SEM photo of a wavy inner wall of the chamber [28].

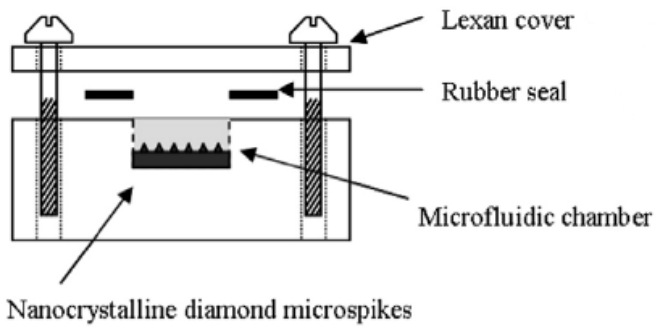

Figure 2-2. Sketch of an ultrasonic cell lysis unit [32].

2.1.2 Chemical Approaches

Chemical methods extract intracellular components from cells by either directly dissolving cell membranes or by making cell membranes permeable with solvents that create channels through the cell membrane. Conventionally, acid and alkali are used as lysing reagents. In acid hydrolysis, acids such as HCl and H_2SO_4 at a high concentration are mixed with cells at 55~100℃, intracellular materials are slowly released within 6~12 hours [35]. Cells treated with NaOH undergo a conformational change which results from dissolving of cell membranes [36]. Chemicals such as sodium dodecyl sulfate (SDS), toluene, ether, phenylethyl alcohol, dimethyl sulfoxide (DMSO), benzene, methanol, chloroform and triton have also been used for chemical cell lysis [37-39]. Schilling *et al.* reported a chemical cell lysis system for LOC applications as shown in Figure 2-3 [40]. They used a bacteria protein extraction reagent in microfluidics channels for chemical cell lysis. They

were able to lyse *Escherichia coli* and extract proteins from the matrix. An obvious advantage of chemical cell lysis method for LOC applications is that it does not involve any complicated fabrication processes. Moreover, unlike mechanical cell lysis, chemical cell lysis generally does not generate small cell membrane fragments. However, it is at the sacrifice of cell lysis efficiency as a relatively long time is required either for cell membranes to dissolve or for intracellular materials to diffuse out. One other disadvantage of chemical cell lysis is that chemical reagents must be removed from the sample before subsequent operations such as enzyme-mediated amplification or PCR can take place. This greatly complicates the design and fabrication of microchips.

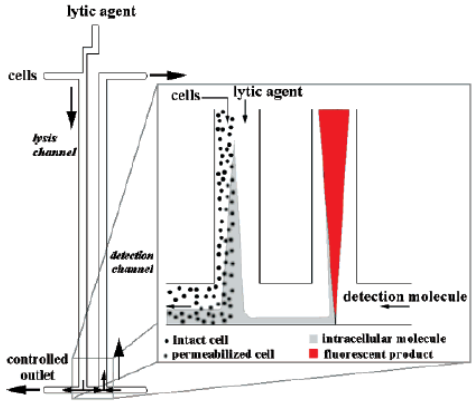

Figure 2-3. Schematic of a microfluidic device for chemical cell lysis and fractionation/detection of intracellular components [40].

2.1.3 Electrical Approaches

Cells can also be lysed when subject to exposure of a high electric field given enough amount of time. A cell exposed to an electric field gradient experiences a build-up of opposing charges across its membrane. Once the electric field intensity reaches a critical level, pores form across the membrane allowing an open path between the intracellular matrix and the external suspending medium. By applying voltage with right magnitude, duration and frequency, the pores could either reseal (reversible electroporation), or remain open (irreversible electroporation or cell lysis). The critical electric field strength required for irreversible electroporation can be calculated by

$$E_c = \frac{V_c}{f \cdot r}$$

where V_c is the applied voltage, r is the radius of the cell and f is a geometric form factor which is dependent on cell types [41]. The pulse duration required to reach the critical voltage across the membrane of a spherical cell is expressed by

$$\tau = (\frac{\rho_1}{2+\rho_2}) \cdot C \cdot r$$

where ρ_1 and ρ_2 are resistivities of the suspending medium and cytoplasm respectively, C is the capacitance of the membrane per unit area [41]. Reversible electroporation is usually used in molecular biology as a way of introducing new substance into a cell while irreversible electroporation is extensively studied for LOC cell lysis. Lee *et al.* reported a miniaturized cell lysis device using electrical cell lysis as shown in Figure 2-4 [42]. They fabricated a narrow orifice which results in an electric field strength as high as 1.2 kV/cm at an operational voltage of 50 V. 100% cell lysis was claimed to be done although time required to achieve the result was not given. Park *et al.* reported a 3D electrical cell lysis device as shown in Figure 2-5 [43]. Pairs of 3D probes were patterned on a silicon-on-insulator wafer at a separation distance of 100 nm to 1.5 µm. Dielectrophoresis was used to capture vaccinia virus particles first and then to lyse them at a high electric field strength of 10^7 V/m. The key to electrical cell lysis is to create high electric field strength. This can be done in two means. One is to increase power, which is not desirable for LOC applications. The other way is to fabricate electrode pairs with very small gaps. However, it poses a challenge for the fabrication process, which is expensive and can be very time-consuming.

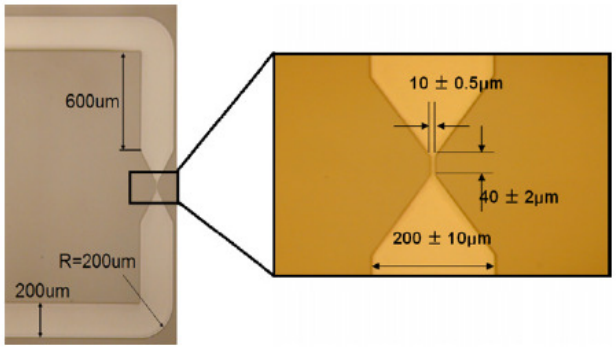

Figure 2-4. A narrow orifice for electrical cell lysis [42].

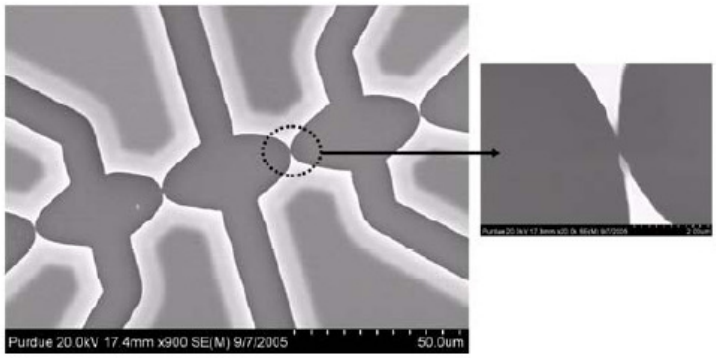

Figure 2-5. SEM images of a 3D electrical cell lysis device [43].

2.1.4 Thermal Approaches

Repeated freezing and thawing of cells disrupt them because of the repeated formation of sharp ice crystals, many of which grow inside cells, like burst in balloon using needles from the inside. It is not difficult to perform at a large scale but is not realistic for LOC applications. Elevated temperature, also named boiling method, can also lyse cells by altering cell membrane conformation. It is probably the easiest cell lysis method in terms of technical difficulties. It is easy to be integrated in LOC devices. However, it is very low in efficiency.

2.1.5 Summary of Cell Lysis Methods for LOC Applications

Table 2-1 summarizes the cell lysis methods that are available to be considered in LOC applications. An ideal cell lysis method should be low in technical difficulty, low in cost and high in efficiency. Unfortunately, none of the current cell lysis methods available to LOC applications is considered ideal. It is an opportunity as well as a challenge to find novel cell lysis methods for LOC applications that suit the need.

Table 2-1. Comparison of cell lysis methods for LOC applications [39]

Cell lysis method	Technical difficulty	Cost	Efficiency
Mechanical	High	High	High
Chemical	Medium	Medium	Low
Electrical	Medium	Medium	Low
Thermal	Low	Low	Low

2.2 Polymerase Chain Reaction (PCR)

Polymerase chain reaction (PCR) is a commonly used technology that enables researchers to produce millions of copies of a specific region of DNA in vitro. The initial idea of PCR came out in 1984 by Dr. Kary Mullis, a Nobel Chemistry Award winner in 1993 [44]. It has been widely used in many applications including gene amplification, DNA cloning, functional analysis of DNA, diagnosis of diseases and so on [45-47]. PCR is a complicated chemical process that includes a number of essential components and repeated cycles of three steps, namely denaturing, annealing and extension.

2.2.1 PCR Components and Reagents

A basic PCR setup requires several essential components and reagents. These components include DNA templates, forward and reverse primers, DNA polymerase, deoxynucleoside triphosphates (dNTPs) and buffer solution.

2.2.1.1 DNA templates

DNA templates serve as a starting point of the chemical reaction. The target gene sequence is from a specific region of the DNA templates. In fact, not only DNA can be used in PCR but also RNA. Almost all forms of DNA and RNA are suitable for PCR. These include genomic, plasmid and phage DNA, previously amplified DNA also named amplicons, complimentary DNA and messenger RNA. Typically, 0.1~1 µg of mammalian genomic DNA is used in each PCR reaction [48-51]. 0.1~1 µg of mammalian genomic DNA corresponds to 3×10^4 - 3×10^5 copies of genes. For bacterial genomic DNA or a plasmid DNA, picogram to nanogram quantities are used per reaction [48, 49]. Previously amplified DNA fragments can also be used as PCR templates. However, the amplified fragments are usually purified by gel purification if the initial PCR generated a number of non-specific bands or if a different set of primers is to be used for the subsequent PCR. On the other hand, if the amplification reaction contains only the intended target product, and the purpose of the subsequent PCR is simply to increase the overall yield using the same set of primers, no further purification is required.

2.2.1.2 Primers

A primer is a short strand of nucleic acid that serves as the starting point of DNA replication. Primers are of great importance to a successful PCR. They are required because the enzyme (DNA polymerase) that catalyzes DNA replication can only add new nucleotides to an existing strand of DNA. Primers always come in as a pair since DNA has two strands and each primer (one named forward primer and the other named reverse primer) is responsible for each strand. During annealing step, primers attach to two ends of the DNA template. In many cases, primers are designed to be exactly complementary to the two ends of the target DNA fragment to be amplified. The lengths of the primers are typically 15~30 base pairs (bps) depending on specific requirements. They are designed to avoid the possibility of mishybridization to a similar sequence nearby. In the past, primer synthesis was carried out manually using miniature glass columns similar in their shape to low-pressure chromatography columns or syringes equipped with porous filters [52]. Nowadays, they are automatically synthesized in 3' to 5' direction as opposed to that in DNA replication using computer-controlled instruments named oligonucleotide synthesizers. Basically, the synthesis is carried out by a stepwise addition of nucleotide residues to the 5'-terminus of the growing chain until the desired sequence is assembled.

2.2.1.3 DNA polymerase

DNA polymerase is essentially a type of protein that attaches to the ends of both forward and reverse primers to start synthesizing new strands of DNA from 5' to 3' direction during the extension step of PCR. No DNA polymerase is known to be able to begin a new chain (*de novo*). Therefore, they start working from the ends of the primers. Some but not all DNA polymerases have the capability of correcting mistakes during synthesis. When an incorrect base pair is recognized, DNA polymerase reverses its direction by one base pair. The incorrect base pair is excised by 3' to 5' exonuclease activity of the polymerase. The property is also referred to as "proofreading". There are several types of DNA polymerase been used throughout the evolution of PCR. Before Taq polymerase was introduced, people had to add polymerase into PCR solution at the end of each PCR cycle to supply active polymerase since the polymerase used in early days was not stable and became inactive at high

temperature above 90℃. Taq polymerase is a thermostable DNA polymerase named after the thermophilic bacterium *Thermus aquaticus*. It was originally isolated by Thomas D. Brock in 1965 [53]. Taq polymerase has the capability of withstanding the protein-denaturing high temperature during PCR. The attracting property makes it one of the most widely used polymerases in PCR nowadays. The optimum temperature to achieve a high enzyme activity for Taq is 75~80℃. It is able to replicate 1000 base pairs of DNA in less than 10 seconds at 72℃ [54]. Taq polymerase also has the capability of "proofreading".

2.2.1.4 Deoxynucleoside triphosphates (dNTPs)

A deoxynucleoside triphosphate is composed of a nucleobase, a deoxyribose and a triphosphate group. Deoxynucleoside triphosphates (dNTPs) are a mixture of deoxyadenosine triphosphates (dATPs), deoxycytidine triphosphates (dCTPs), deoxyguanosine triphosphates (dGTPs), and deoxythymidine triphosphates (dTTPs). They are the four basic building blocks from which a DNA polymerase synthesizes a new DNA strand. Their chemical structures are shown in Figure 2-6. During the extension step of PCR, dNTPs are added to DNA strand in the exercise of DNA polymerase from the 5' to 3' direction.

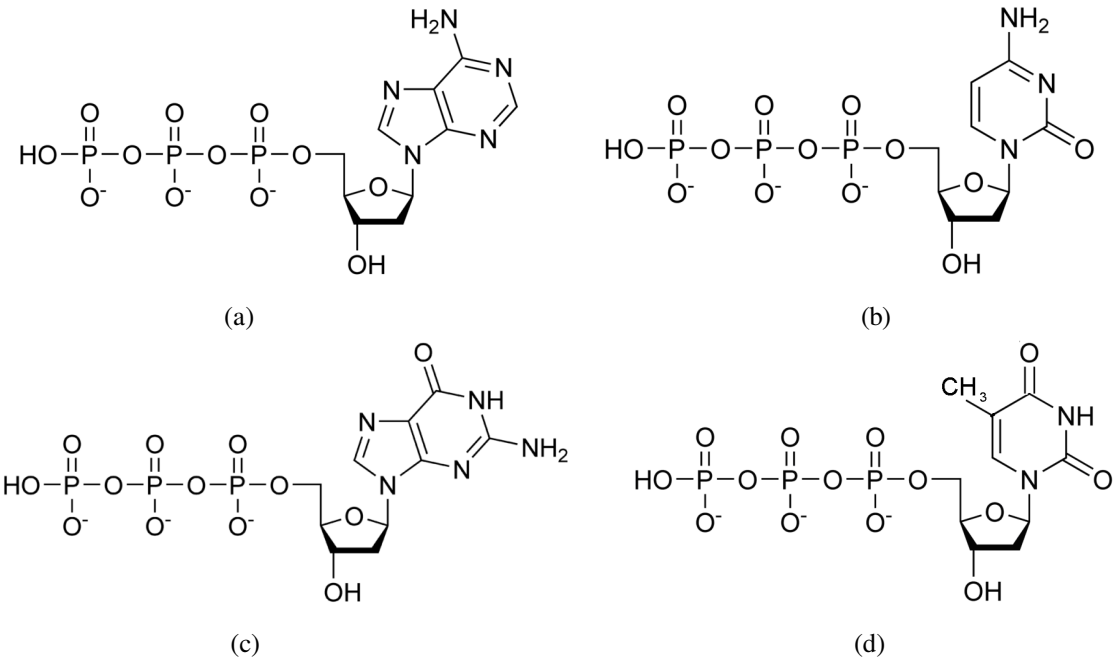

Figure 2-6. Chemical structures of dNTPs. (a) dATP; (b) dCTP; (c) dGTP; (d)dTTP.

2.2.1.5 Buffer solution

PCR buffer is necessary to create an optimal environment for PCR, especially for the optimal activity and stability of DNA polymerase. Buffers often contain Tris hydrochloride (Tris-Hcl) and magnesium chloride ($MgCl_2$). Tris-Hcl is used to adjust the pH of the solution. Magnesium ions are used as cofactors for DNA polymerase to maintain its biological activity. The concentration of each component in the buffer is specific to polymerases.

2.2.2 Principle of PCR

A standard PCR cycle involves three steps. Step 1: Denaturing. In this step, temperature is raised to 94~98℃ for 15-30 seconds. At this temperature, hydrogen bonds which hold two single-stranded DNAs together are broken and a double helix DNA becomes two single-stranded DNAs. Step 2: Annealing. In this step, temperature is lowered to 50~65℃ for 20~40 seconds. At this temperature, forward and reverse primers are annealed to the 5' ends of the target DNA fragments. 3. Extension. In this step, temperature is dependent on the DNA polymerase used. A commonly used temperature for Taq polymerase is 72℃. At this temperature, DNA polymerase starts to synthesize new DNA strands starting from the places where forward and reverse primers are left over in the 5' to 3' direction. At the end of each cycle, there is two times the amount of double-stranded DNAs compared to the amount at the beginning of the cycle. Usually, 30 to 50 repeated cycles mentioned above are required to generate enough DNA fragments for analysis depending on different applications. Figure 2-7 shows the first three cycles of a typical PCR process. As shown in the figure, the number of target fragments roughly increases exponentially with the number of cycles.

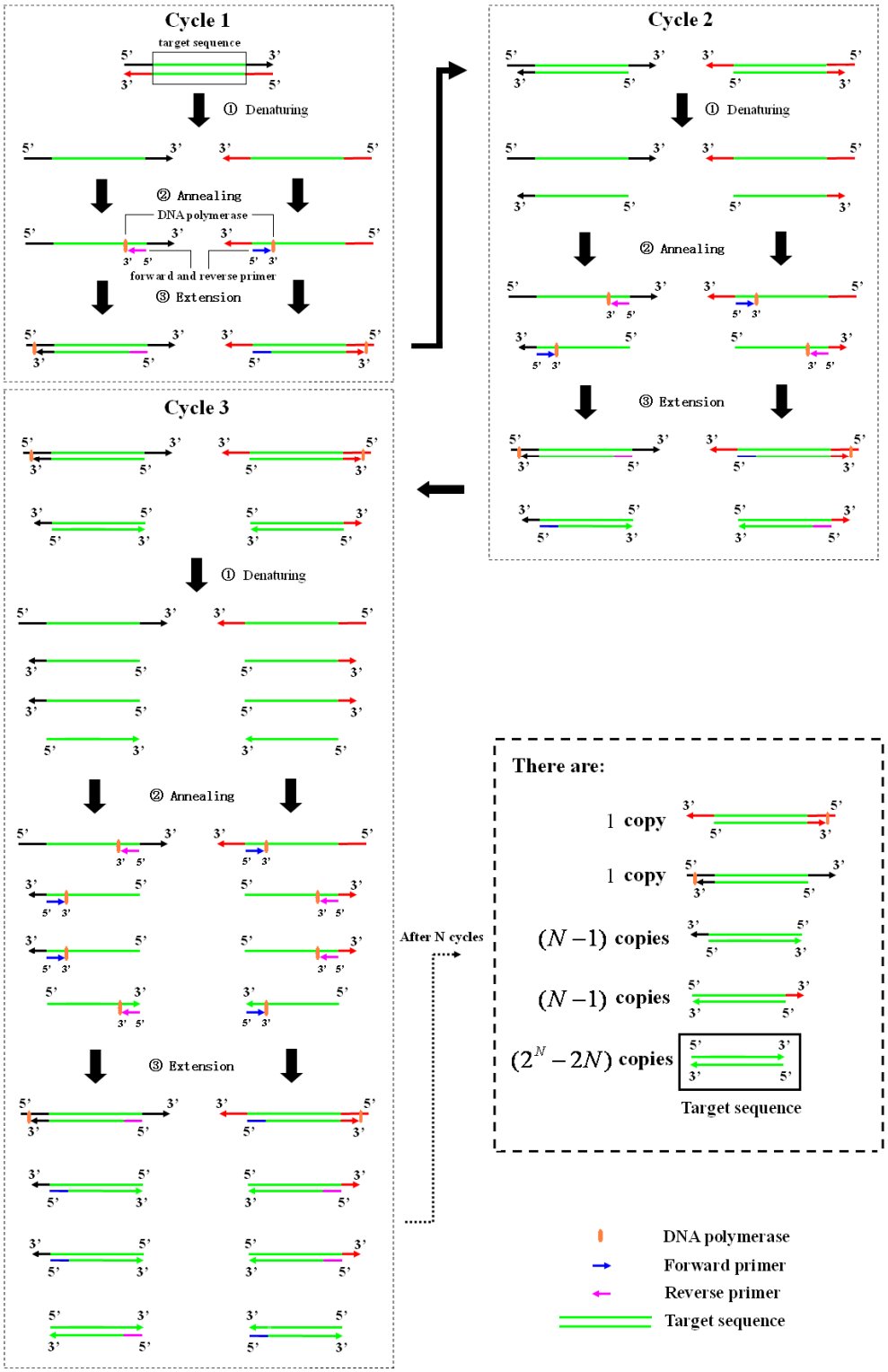

Figure 2-7. Illustration of the PCR process.

2.2.3 Real-time PCR

Real-time PCR, also named quantitative real-time PCR or kinetic PCR, is a variation from the standard PCR method to amplify and quantify a target DNA fragment simultaneously. The procedure follows the general principle of PCR with the key feature of detecting amplified DNA fragments as the reaction goes in real time. Basically, a detection step, usually through detecting fluorescent signals, is added at the end of each cycle in real-time PCR. There are two common methods for detection of PCR products. One uses non-specific fluorescent dyes, such as SYBR Green. The dye binds to any double-stranded DNAs, causing fluorescence of the dye. An increase in PCR products results in an increase of fluorescence intensity which is measured at the end of each cycle, allowing the amount of DNAs to be quantified. A major drawback of the method is that non-specific PCR products are quantified as part of the specific PCR products due to the fact that the dyes bind to all double-stranded PCR products. Therefore, the method is not suitable for accurate quantification of PCR products. The other uses sequence-specific DNA probes made up of customized oligonucleotides that release fluorescent reporters only after hybridization of the probe with its complementary DNA target. The method detects only desired PCR products. Therefore it has a very high specificity compared to the one using non-specific fluorescent dyes. Probe-based real time PCR is used in some of my experiments to provide an easy, reliable and convenient way to facilitate the analysis of results.

2.2.4 Microchip PCR

Miniaturizing and integrating analytical functions on a microchip is the driving concept behind LOC devices. As a very important function in molecular biology, PCR has been the focus of LOC research. Development of microchip PCR devices for LOC applications has been an active research area these years. Unlike conventional bulky and expensive PCR machines that cost thousands of dollars, microchip PCR devices are portable, disposable and inexpensive.

2.2.4.1 Architecture

Microchip PCR devices can be characterized into two categories, time domain and space domain. In time domain PCR, reaction solution is kept still within PCR reaction chamber while temperature

within the reaction chamber changes according to the desired temperatures for denaturing, annealing and extension steps within each PCR cycle. The advantage of the approach is that it requires less space. Moreover, the design and operation is relatively simple. A schematic of time domain PCR is shown in Figure 2-8(a). In space domain PCR, there are three fixed temperature zones corresponding to the desired temperatures for denaturing, annealing and extension steps within PCR reaction chamber. Reaction solution moves at a controlled speed passing through different temperature zones. How long the reaction solution stays at each temperature zone is determined by the length of fluidic channel as well as the flow rate. The advantage of the approach is that it does not involve temperature transition between PCR stages, therefore resulting in faster cycling. However, it requires more space and a more complicated fabrication process. A schematic of time domain PCR is shown in Figure 2-8(b).

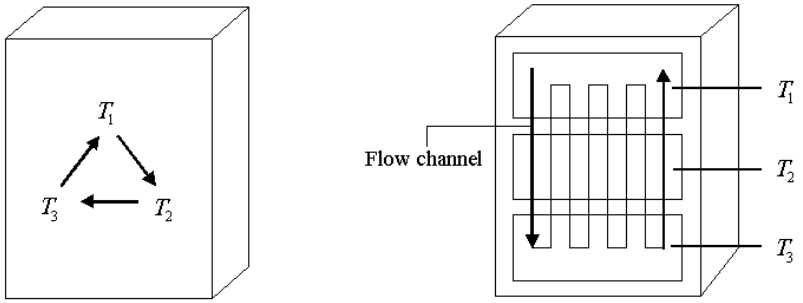

(a) (b)

Figure 2-8. Schematics of time domain and space domain PCR. (a) Time domain PCR; (b) Space domain PCR.

2.2.4.2 Fabrication

The design of microchip PCR device has many limitations when the size is reduced to the microscale. Reaction chambers, heaters and sensors are the three major considerations of a microchip PCR device. Reaction chamber is required for PCR to take place. In microchip PCR devices, the volume of reaction chamber ranges from picoliters to microliters. There are also different shapes such as capillary, serpentine, square and many more. PCR reaction chamber can be formed by using either lithography technique or soft lithography technique. Wet etching is a commonly used lithography process in microfabrication. It involves utilizing liquid chemicals or etchants to remove materials

from the wafer, usually in specific patterns defined by photoresist masks on the wafer. Reaction chambers can be fabricated by wet etching directly on substrates. The fabrication process is described in Figure 2-9.

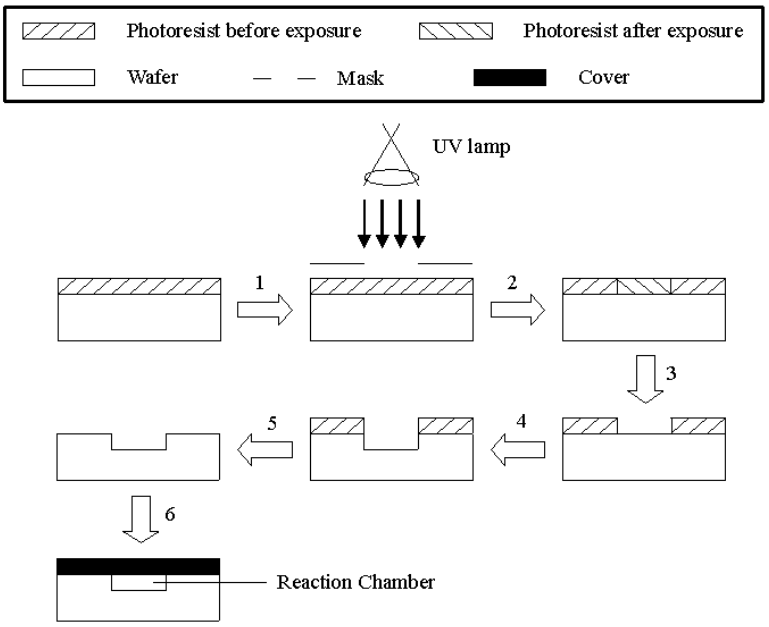

Figure 2-9. Fabrication process to form a PCR reaction chamber directly in a substrate.

Soft lithography technique is a family of techniques for fabricating or replicating structures using elastomeric stamps, molds, and conformable photomasks [55]. The development of the technology has expanded rapidly since 1995. It is a very useful tool in device design prototyping due to the fact that it has a lower cost and requires less turn-around time than traditional photolithography technology. Soft lithography molding technique involves casting prepolymers against masters or molds patterned by conventional lithographic techniques and then peeling off hardened or cured prepolymers from the molds. Commonly used prepolymers include Polydimethylsiloxane (PDMS) and Polymethylmethacrylate (PMMA). Fabrication of PCR reaction chambers using soft lithography molding technique with PDMS is shown in Figure 2-10. The process starts with spin-coating a layer of negative photoresist on top of a substrate, usually a silicone wafer followed by exposing the substrate under UV light. Photoresist developer is used to dissolve unexposed portion of the photoresist. After mixing PDMS base and the curing agent well at an appropriate ratio and degassing,

the mixture is poured on top of the master. PDMS mixture is given enough time to polymerize followed by peeling them off from the master. After flow inlet and outlet are formed on the PDMS sheet, a cover is bonded to the PDMS sheet.

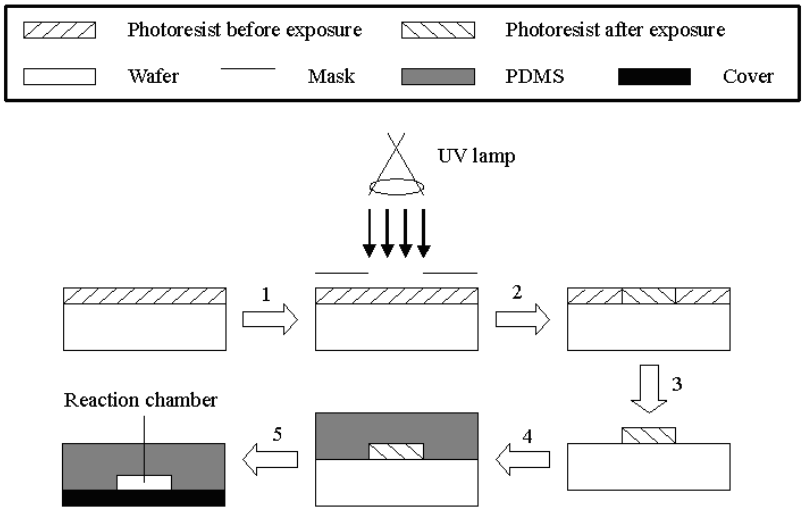

Figure 2-10. Fabrication process to form PCR reaction chambers using soft lithography technique with PDMS.

An important component of a microchip PCR device is heaters which are needed to generate desired temperatures for denaturing, annealing and extension steps in PCR. In microchip PCR devices, heaters can be embedded on-chip or be placed off-chip. Off-chip heaters are easy to obtain but assembling is required to attach them to reaction chambers. On-chip heaters need to be fabricated along with the reaction chamber using lithography but they do not require assembly and have better integrity and stability. Because PCR is sensitive to temperature and a slight change in temperature during different steps can lead to very different results, a temperature sensor is needed for accurate temperature feedback control. As the same as heaters, temperature sensors can be placed off-chip or be fabricated on-chip. They can be fabricated within reaction chambers along with heaters or can be attached to the substrate to monitor temperature. Off-chip temperature sensors can be as simple as thermocouples. Infrared cameras can also be used as off-chip temperature sensors. One way to make on-chip temperature sensors is to pattern metals whose resistance changes with temperature such as platinum. These are named *resistance temperature detectors* (RTDs). Another way to make on-chip

temperature sensors is to fabricate on-chip thermocouples, which in principal requires dissimilar metals. The fabrication is much more complicated than making on-chip RTDs.

Commonly used materials for microchip PCR reaction chambers include silicon, glass, PDMS, PMMA and so on. It has to be noted that some materials, such as silicon and glass, are not fully compatible with the PCR process. They can interact with PCR components to inhibit the reaction. Therefore, surface modification of reaction chambers and channels needs to be done to improve the performance. There are two types of surface modification, static and dynamic to be specific. Static modification is to treat the surface of reaction chambers and channels with a substance which is fully compatible with PCR, usually during microchip fabrication or prior to perform PCR. Dynamic modification involves pre-mixing PCR reagents with substances which are compatible with PCR and treating the surface of reaction chambers and channels during PCR. A full list of agents and procedures used to improve PCR compatibility is provided in [56].

2.2.5 PCR Product Analysis

Gel electrophoresis is a very useful tool in molecular biology. It is often used to separate DNA molecules using an electric field applied to a gel matrix [57]. It is known that DNA molecules are negatively charged due to a large number of phosphate groups in their backbones. Under an electric field, DNA molecules are attracted to the anode side because of electric forces. When DNA molecules are placed in wells in the gel and an electric field is applied, they move through the gel matrix at different speeds, mainly determined by their sizes or mass. This way, DNA molecules of different sizes can be separated. The gel is usually a cross-linked polymer with pores to allow DNA molecules to go through. A commonly used polymer is agarose which is composed of long unbranched chains of uncharged carbohydrate without cross links in a gel with large pores allowing for the separation of macromolecules. A gel electrophoresis apparatus consists of a power supply and a buffer-filled reaction chamber with a piece of gel immersed in it as shown in Figure 2-11.

After running through gel electrophoresis, DNA molecules are stained to be visible in ultraviolet (UV) light. Ethidium bromide and GelRed are commonly used stains for the purpose. When DNA molecules are fluorescent under UV, an image can be taken of the gel. If several samples are loaded

into wells in the gel, they run in parallel in individual lanes. They form distinct “bands” during electrophoresis. Bands in different lanes that end up at the same distance from wells contain molecules that move at the same speed. In most cases, this means that they are of the same size roughly. A DNA marker is often used along with the samples to be analyzed. It contains a mixture of molecules of known sizes. When the marker is run on one lane in the gel parallel to the unknown samples, the bands observed can be compared to those of the unknowns in order to determine their sizes. The distance a band travels is approximately inversely proportional to the logarithm of the size of the molecule [58].

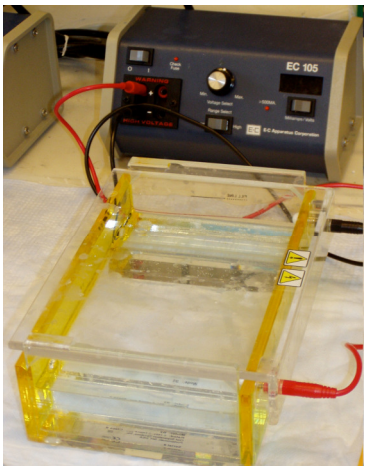

Figure 2-11. Gel electrophoresis apparatus. Courtesy of Jeffrey M. Vinocur. An agarose gel is placed in the buffer-filled box and an electrical field is applied via the power supply to the rear. DNA molecules move towards the anode.

2.3 Nanotechnology

2.3.1 A Brief History of Nanotechnology

The history of Nanotechnology can be traced back to 1959 when Dr. Richard Feynman, the 1965 Nobel Prize in Physics winner, gave a talk named “There's Plenty of Room at the Bottom” that introduced the idea of Nanotechnology for the first time. Though he never explicitly mentioned “nano-technology”, Feynman suggested that it will eventually be possible to precisely manipulate atoms and molecules [59]. In 1974, the term “Nanotechnology” was coined for the first time [60]. In 1981, Dr. Eric Drexler published a paper describing molecular nanotechnology, which established

fundamental principles of molecular design, protein engineering, and productive nanosystems and essentially expanded the idea of molecular manufacturing by integrating modern scientific ideas with Feynman's concepts [61]. Also in 1981, the first scanning tunneling microscope was invented by Binning and Rohrer. With this technology, individual atoms could be clearly identified for the first time. Although the machine is limited to examining only conducting materials, the breakthrough was essential for the development of the field of nanotechnology because theories and ideas were able to be tested experimentally. In 1985, Harold Kroto, James R. Heath, Sean O'Brien, Robert Curl and Richard Smalley discovered C_{60}, and shortly thereafter came to discover the fullerenes [62]. In 1986, atomic force microscope was invented. The instrument being able to examine non-conducting materials, overcomes some of these limitations in the scanning tunneling microscope. Year 1986 also marked the first book in Nanotechnology [63]. In 1989, manipulation of atoms was demonstrated by Don Eigler, who patterned IBM logo using 35 individual xenon atoms [64]. Since then, research and development in Nanotechnology have been carried out extensively in both industrial and academic levels. Table 2-2 lists major events and milestones in the history of Nanotechnology.

Table 2-2. A short history of Nanotechnology

Year	Events and Milestones
1959	Dr. Feynman gave a talk describing molecular machines building with atomic precision
1974	Taniguchi used term "nano-technology" in paper for the first time
1981	STM invented
1985	C_{60} discovered
1986	AFM invented
1989	IBM logo spelled in individual atoms
1991	Extensive research started on carbon nanotubes
1993	First Feynman Prize in Nanotechnology awarded
1996	$250,000 Feynman Grand Prize announced
1998	First DNA-based nanomechanical device
2001	Logic gates made entirely from nanotubes

2.3.2 Tools for Measuring Nanostructures

The history of Nanotechnology is a combination of the history of being able to see and to measure at the nanoscale and the history of being able to control features down at the nanoscale. There are several tools for measuring nanostructures that play important and indispensible roles in the development of Nanotechnology.

2.3.2.1 Scanning probe instruments

Some of the first tools to help launch the Nanotechnology revolution were the so-called scanning probe instruments. All types of scanning probe instruments are based on an idea first developed at the IBM Laboratory in Zurich in the 1980s. In scanning probe measurements, the probe, essentially a tip, slides along a surface in either one or two directions. The probe itself is at the nanoscale. As the probe slides, it can measure several different properties, depending on the specific type of the instrument. For example, in *atomic force microscopy* (AFM), electronics are used to measure the force exerted on the probe as it moves along the surface [4]. In *scanning tunneling microscopy* (STM), the amount of electrical current flowing between a scanning probe and a surface is measured. Depending on the way the measurement is done, STM can be used either to test the local geometry such as surface roughness or to measure the local electrical conducting properties. STM was actually the first of the scanning probe methods to be developed and Gerd Binnig and Heinrich Rohrer shared the 1986 Nobel Prize in Physics for its development. In *magnetic force microscopy* (MEM), the tip that scans across the surface is magnetic. It is used to sense the local magnetic structure on the surface [4]. The MFM tip works in a similar way to the reading head on a hard disk drive or audio cassette player. Figure 2-12 shows an example of one of these tips [65]. In order to get a 2-D image of the surface of interest, the probe has to scan the whole surface. Computer enhancement is often needed to make the raw results look more usable. Scanning probe microscopy is a critical tool for measuring and understanding nanostructures in Nanotechnology history as it provides a method to see objects of atomic dimensions.

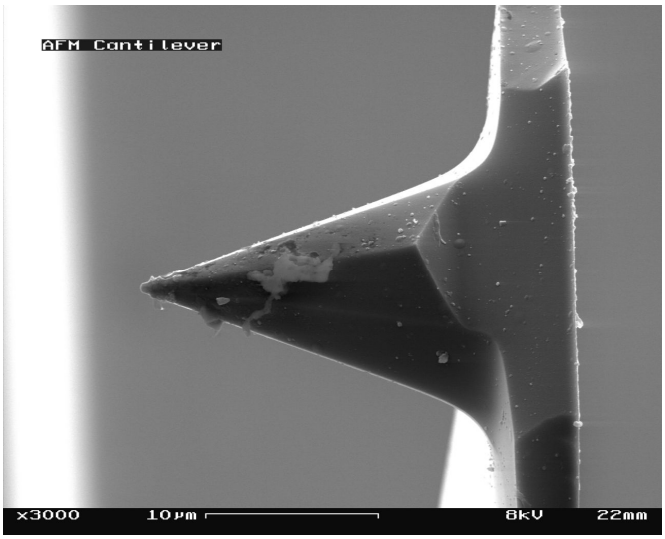

Figure 2-12. An AFM tip [65].

2.3.2.2 Spectroscopy

Spectroscopy is another tool to explore the Nano world. It refers to measuring the absorption, scattering, or other properties of the material under the condition of excitation lights with a specific wavelength. Spectroscopy is much older than scanning probe microscopy and it provides complementary insights [4]. It is widely used in the analysis of nanostructures with different energies of excitation lights. However, it suffers from a fact that all light has a characteristic wavelength and is not very helpful in studying structures smaller than its wavelength. As we know, visible light has a wavelength between 390 and 750 nanometers [66]. It is clear that it is not too much help in looking at an object only a few nanometers in size. Spectroscopy is of great importance for characterizing nanostructures as a group, but most types of spectroscopy do not tell us about structures at the nanoscale.

2.3.2.3 Electrochemistry

Electrochemistry deals with how chemical processes can be changed by the application of electric currents, and how electric currents can be generated from chemical reactions [4]. At the macroscale, the most commonly used electrochemical devices are batteries that produce electricity from chemical reactions. A typical example of the opposite process is electroplating, where metal ions in a solution

are moved by an electric field to coat an electrode surface. Electrochemistry is broadly used in the manufacturing of nanostructures, but it can also be used in their analysis. The nature of the surface atoms in an array can be measured directly using electrochemistry, and advanced electrochemical techniques including some scanning probe electrochemical techniques are often used both to construct and to investigate nanostructures [4].

2.3.2.4 Electron microscopy

Electron microscopy is based on the use of electrons rather than light to examine the structure and behavior of the material. There are different types of electron microscopy, but they are all based on the same general idea. The electron microscope uses electrostatic and electromagnetic devices to control the electron beam and focus it to form an image. These devices are similar to the role played by the glass lenses of an optical microscope which form a magnified image by focusing light on or through the specimen. In transmission, the electron beam is first diffracted by the specimen, and then, the electron microscope re-focuses the beam into a Fourier-transformed image of the diffraction pattern for the selected area of investigation. The real image thus formed is a highly magnified image with the highest resolution at the nanoscale, and can be then recorded on a special photographic plate, or viewed on a detecting screen. Under favorable conditions, electron microscopic images can have a resolution sufficient to see individual atoms, but samples must often be stained before they can be imaged. Additionally, electron microscopy can only measure physical structure, not forces like those from magnetic or electric fields. Still, electron microscopy has many uses and is broadly used in nanostructure analysis and interpretation [4].

2.3.3 Tools for Making Nanostructures

The ability of controlling and making structures at the nanoscale is as important as being able to see and measure at the nanoscale. There are several tools for making nanostructures that play important and indispensible roles in the development of Nanotechnology.

2.3.3.1 Scanning probe instruments

Besides being used to measure nanostructures, scanning probe instruments can also be used to manipulate them. A surface can be modified with the tip of a scanning probe in the same way as people can scratch, dimple, or score a soft surface as they drag their finger along it. Generally, small objects at the nanoscale which are either individual atoms or individual molecules can be moved on a surface either by pushing on them or by picking them up off the surface onto a scanning tip that moves around and puts them back down [4]. For both cases, the scanning tip acts as a sort of earthmover at the nanoscale. In the pushing application, that earthmover is simply a bulldozer. In the pick-up mode, it acts more like a construction crane or backhoe. The way to assemble materials on an atom-by-atom or molecule-by-molecule basis realizes a dream that people have had for many years. Scanning probe instruments are elegant in surface assembly or making structures at the nanoscale. They are great for research. However, they are relatively expensive and slow, which are two limitations in large-scale production if Nanotechnology is to become a real force. Although it is possible to make an array of hundreds or even thousands of probe tips that can be used at the same time, making nanostructures using scanning probe instruments is still very much like making products by hands, wonderful yet inefficient to satisfy mass demand.

2.3.3.2 Nanoscale lithography

Invented in 1796, lithography is a method for printing. Lithography originally used an image drawn in wax or other oily substance applied to a lithographic stone as the medium to transfer ink to the printed sheet. It was first introduced to microfabrication process and proved to be a very successful method to make objects at the microscale. Patterns can be created on a photosensitive substrate by selective exposure to a radiation source such as light. A mask is usually involved in the process to define the desired patterns. When it comes to the nanoscale, things become more complicated. Nanoscale lithography simply cannot use visible light as radiation light source because the wavelength of visible light is at least 400 nm, so structures smaller than that are difficult to make directly. Therefore, people are using light source with very short wavelength to create objects at the nanoscale. For example, wavelength of 193 nm is used to create patterns that are smaller than 100 nm.

2.3.3.3 Dip pen nanolithography

Another way to create patterns at the nanoscale on a surface is to write them in the same way as people write using a pen. The method is named *dip pen nanolighography* (DPN). However, such a pen at the nanoscale is needed. Fortunately, it is not too hard to find. AFM tips are ideal for the purpose. The "ink" in DPN is molecules or atoms. By manipulating AFM tips with a reservoir of "ink" on top across the surface, lines and desired patterns can be easily obtained. A good example of dip pen assembled structures is the excerpt from Dr. Feynman's speech "There's Plenty of Room at the Bottom" as shown in Figure 2-13. DPN, developed by Chad Mirkin and his collaborators at Northwestern University, has several advantages including the fact that almost anything can be used as "ink" at the nanoscale and the fact that almost any surface can be written on. Moreover, it is easy to create complex patterns in details as AFM tips are easy to manipulate. Therefore, DPN is considered a favorable choice to create complex patterns in small volumes. However, it also bears some disadvantages including the fact that it is slow therefore is not suitable for large scale nanostructure fabrication.

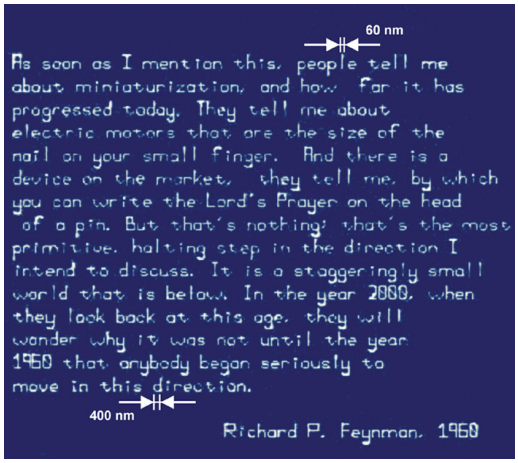

Figure 2-13. Dr. Feynman's famous speech being written at the nanoscale using dip pen nanolithography. Courtesy of the Mirkin Group, Northwestern University.

2.3.3.4 Electron beam lithography

As described in section 2.3.3.2, light-based lithography is limited to creating features no smaller than the wavelength used. Even though in principle it is possible to get around the restriction by using light

of short wavelengths, the solution can generate other problems such as blowing off desired patterns due to the high energy of light with shorter wavelengths. People come up with an idea to solve the problem by using electrons instead of light. This is the foundation of *electron beam lithography* (EBL). EBL are proven to be able to create structures at the nanoscale as shown in Figure 2-14. It also has applications in current microelectronics manufacturing and is one approach to be used to keep Moor's law on track.

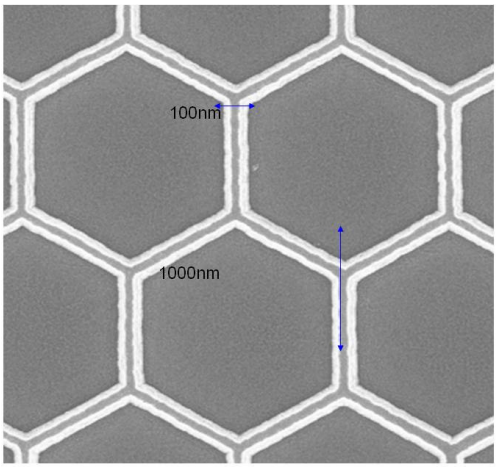

Figure 2-14. Scanning Electron Micrograph of an artificial spin ice nanostructure, fabricated by e-beam lithography from a 20 nm thick cobalt film on silicon. Courtesy of Branford Group, Imperial College.

2.3.3.5 Nanosphere lithography

Nanosphere lithography (NSL) is a powerful fabrication technique to inexpensively produce nanoparticle arrays with controlled shape, size, and interparticle spacing [67]. The method starts with depositing drops of nanosphere colloids on a substrate. Commonly used methods of deposition include spin coating and drop coating. After drying out, it leaves a layer of well distributed nanospheres on top of the substrate. The surface of the substrate is usually modified to allow nanospheres to be able to freely diffuse across the substrate. As the solvent, like water, evaporates, capillary forces draw the nanospheres together, and the nanospheres crystallize in a hexagonally close-packed pattern on the substrate [68]. After having the mask, desired materials can be deposited from a source to the substrate through the nanosphere mask with a controlled thickness. Deposition

can be done using thermal evaporation, chemical vapor deposition, electron beam deposition, or pulsed laser deposition. The substrate with nanospheres and nanostructures of desired materials is placed in a sonicating equipment to remove nanospheres, leaving nanostructures on the substrate. Figure 2-15 shows an AFM image of silver nanostructures patterned using NSL [68].

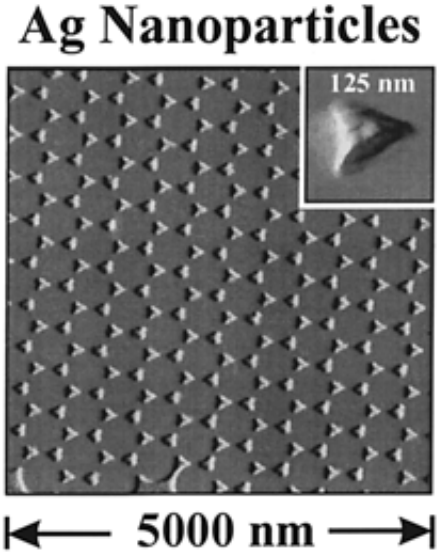

Figure 2-15. Silver nanostructures patterned using NSL [68].

2.3.3.6 Self-assembly

Self-assembly is another way to create nanostructures by mixing chemicals together and get nanostructures by letting the molecules sort themselves out. The idea behind self-assembly is that molecules will always seek the lowest energy level available to them. In other words, if bonding to another molecule accomplishes this, they will bond; if turning into another direction accomplishes this, they will turn. The most amazing property of the method is that nanostructures are formed naturally just like a compass needle points from south to north to minimize its energy with respect to earth's magnetic field. There are different forces involved in self-assembly. In general, these forces are weaker than the ones that hold molecules together such as a covalent bond. Typical forces in self-assembly include hydrogen bond which is the interaction between hydrogen atoms and oxygen atoms in water molecules, hydrophilic or hydrophobic effects which are the tendency of water to exclude or include non-polar molecules, and multipolar interactions which occur between molecules with no

total charges but uneven charge distributions. In self-assembly, particular atoms or molecules are introduced onto a surface or onto a pre-constructed nanostructure. The molecules then self-align themselves into particular positions in order to minimize the total energy. Figure 2-16 shows a TEM image of a film made by the triblock molecules in a self-assembly fashion [69]. Self-assembly is almost certainly going to be the preferred method for making large nanostructure arrays [4].

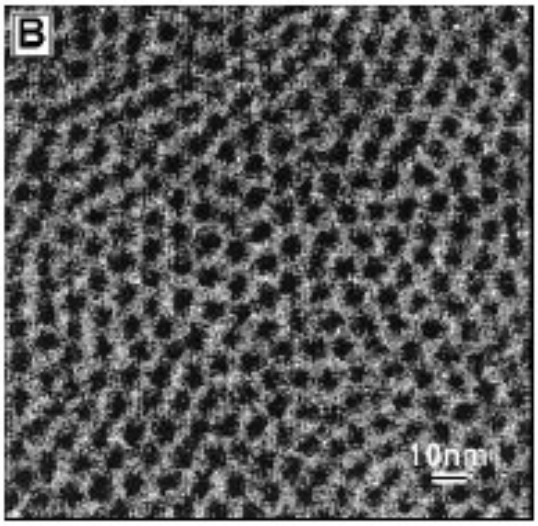

Figure 2-16. A TEM image of a film formed by the triblock molecules, revealing regularly sized and shaped aggregates that self-organize into superlattice domains [69].

2.3.4 Nanomaterials

Nanomaterials are basic building blocks of Nanotechnology. They have morphological features with at least one dimension on the nanoscale, which is defined as one tenth of a micrometer. At such scale, materials behave quite different from their bulk counterparts mainly due to increased surface-area-to-volume ratio. This leads to new phenomenon and superior properties that cannot achieved before. One good example is *carbon nanotubes* (CNTs) which are extensively studied since 1990's due to its superb electrical, mechanical and thermal properties, although the discovery of CNTs dates back to 1950's [70]. CNTs are the strongest and stiffest materials discovered so far in terms of young's modulus and tensile strength. A multi-walled CNT was experimentally demonstrated to have a tensile strength of 63 gigapascals (GPa), around 50 times higher than steel [71]. The electronic properties of CNTs are also extraordinary. Metallic CNTs can carry an electric current density of 4×10^9 A/cm^2

which is more than 1,000 times greater than metals such as copper [72]. There is great interest in the possibility of constructing nanoscale electronic devices from them. All CNTs are expected to be very good thermal conductors along the longitudinal axis and good insulators laterally to the tube axis. Measurements show that a single-walled CNT has a room-temperature thermal conductivity along its axis of about 3500 $W \cdot m^{-1} \cdot K^{-1}$ [73], almost 10 times better than copper, the most thermally conductive metal. Aside from carbon nanotubes, other materials also show very interesting properties when going from macro scale to nanoscale. Copper, which is opaque at the macro scale, becomes transparent at the nanoscale [74]. Platinum and gold, chemically inert materials at the macro scale, presents active catalytic properties at the nanoscale [75-78]. Aluminum, a stable material at the macro scale, turns into combustible substances at the nanoscale [79, 80]. Silicon, an insulator at macro scale, becomes conductors at nanoscale [81, 82]. Much of the fascination with nanotechnology stems from these unique quantum and surface phenomena that matter exhibits at the nanoscale.

Nanoparticles are nanomaterials with all three dimensions at the nanoscale. They have large surface-area-to-volume ratios which result in unique properties. Nanoparticles can be synthesized in two ways generally. One is dry synthesis and the other is wet synthesis. Dry synthesis involves both attrition and pyrolysis. In attrition, mechanical forces are applied to macro or micro scale particles by grinding them in a ball mill, a planetary ball mill, or other size reducing mechanisms. The result is smaller particles which are then air classified to recover nanoparticles. In pyrolysis, essentially a gas phase synthesis method, a vaporous precursor, either liquid or gas, is forced through an orifice at high pressure and burned. The resulting solid is air classified to recover oxide particles from by-product gases. Thermal plasma can also deliver the energy necessary to cause evaporation of small particles at the microscale. Nanoparticles are formed upon cooling while leaving the plasma region.

Wet synthesis of nanoparticles is also named sol-gel process. Such method is used primarily for the synthesis of materials starting from a chemical solution (sol, short for solution) which acts as the precursor for an integrated network (or gel) of either discrete particles or network polymers [83]. In sol-gel process, precursors undergo hydrolysis reactions to form either a network of gel or a nanoparticle colloidal suspension. A nanoparticle colloidal suspension is essentially a solid-liquid mixture which contains distinct nanoparticles dispersed to various degrees in a host liquid medium.

Nanoparticles form by sedimentation during reactions. The sol-gel approach is a cheap and low-temperature technique that allows for the fine control of the product's chemical composition. Even small quantities of dopants, such as organic dyes, can be introduced in the sol and end up uniformly dispersed in the final product. Sol-gel derived materials have many applications including electronics, optics, energy, biosensors, drug delivery, and separation technology [84].

Gold and titanium dioxide nanoparticles are commonly seen nanomaterials and have been extensively studied for the past few decades. They are used throughout my experiments described in the next few chapters. Both of them are typically synthesized using the sol-gel process and are in the form of nanoparticle colloid. Colloidal gold has a color of deep red to dirty yellowish depending on the size. Due to the unique optical, electronic, and molecular-recognition properties of gold nanoparticles, they find wide applications in a wide variety of areas, including electron microscopy, electronics and materials science [85]. A typical way of synthesizing colloidal gold is by reduction of chloroauric acid ($HAuCl_4$), although more advanced and precise methods do exist. After dissolving chloroauric acid, the solution is rapidly stirred while a reducing agent is added. A commonly used reducing agent is sodium citrate. This results in Au^{3+} ions being reduced to neutral gold atoms. As more and more of these gold atoms form, the solution becomes supersaturated, and gold gradually starts to precipitate in the form of nanoparticles. The rest of the gold atoms formed during the process stick to the existing particles. From a statistical point of view, if the solution is stirred vigorously enough, the nanoparticles will be fairly uniform in size. To prevent nanoparticles from aggregating, some sort of stabilizing agent that sticks to the nanoparticle surface is usually added. Gold nanoparticles can also be functionalized by surface modification through surface chemical reactions to produce desired properties for different applications [86]. Titanium dioxide nanoparticles are widely used in a variety of applications such as water and air purification, photocatalytic destruction of organic matters and many more. Titanium dioxide nanoparticles are synthesized by hydrolysis of precursors such as titanium (IV) isopropoxide and titanium (IV) sulfate. The nature of titanium dioxide nanoparticles such as phase and size is determined by the presence of additives such as alcohol and acid, the amount of water, and the rate of mixing.

2.4 *Escherichia coli* (*E. coli*)

Escherichia coli, abbreviated *E. coli* and named after Theodor Escherich who first described *E. coli* in 1885 as *Bacterium coli commune*, is a Gram-negative rod-shaped bacterium that is commonly found in the lower intestine of warm-blooded organisms. Gram-negative bacteria are bacteria that do not retain crystal violet dye in the Gram staining protocol [87]. *E. coli* is facultative anaerobic and lacks the ability to produce spores. *E. coli* cells are typically rod-shaped and are about 2 μm long and 0.5 μm in diameter, with a cell volume of 0.6~0.7 μm^3 [88]. As a Gram-negative bacterium, *E. coli* share many characteristics as other gram-negative bacterium such as that it has cytoplasmic membrane, it has thin peptidoglycan layer which is much thinner than in Gram-positive bacteria, proteins exist in the outer membrane which act like pores for particular molecules and many more. The most distinction between Gram-positive and Gram-negative bacterium is cell membrane. Figure 2-17 shows the cell membrane comparison between Gram-positive and Gram-negative bacterium [89].

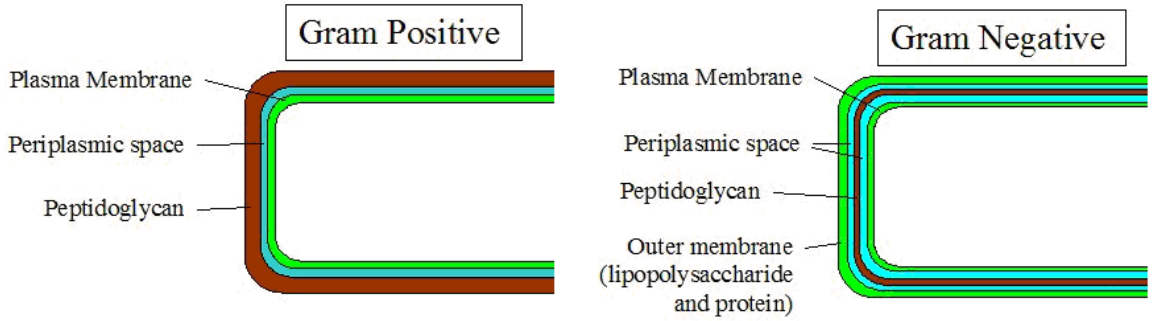

Figure 2-17. Gram-positive and Gram-negative bacteria are mainly differentiated by their cell walls [89].

E. coli is able to survive and reproduce on a wide variety of substrates such as in lysogeny broth (LB) medium. The optimal growth of *E. coli* occurs at 37℃ but some strains can reproduce at temperatures of up to 50℃ [90, 91] There are hundreds of *E. coli* strains discovered so far. A strain of *E. coli* is a sub-group within the *E. coli* species that has unique characteristics which distinguish it from other *E. coli* strains. Although the differences among *E. coli* strains can only be detected at the molecular level, they may result in differences in the physiology or lifecycle of the bacterium. For example, a strain may gain pathogenic capacity, the ability to use a unique carbon source, the ability to take upon a particular ecological niche or the ability to resist antimicrobial agents. Different strains

of *E. coli* are often host-specific, making it possible to determine the source of faecal contamination in environmental samples [92]. For example, knowing which *E. coli* strains are present in a water sample allows to make assumptions about where the contamination originates. Most *E. coli* strains are harmless, but some, such as strain O157:H7, O121, and O104:H21, can cause serious food poisoning in human beings and animals [93]. The harmless strains are part of the normal gut flora, and can benefit their hosts by producing vitamin K2 [94] and by preventing the establishment of pathogenic bacteria within the intestine [95, 96]. O157:H7 is also notorious for causing serious and even life-threatening complications such as haemolytic-uremic syndrome. Therefore, it is quite important to be able to detect *E. coli* strains fast and reliably in our everyday life.

2.5 Fabrication Tools for LOC Devices

Simply speaking, LOC is a technology which shrinks and minimizes biomedical and biochemical laboratory routines that usually require running through complicated and cumbersome laboratory equipments to a miniaturized microchip format which occupies only several square centimeters. The technology started in the early 1960s. It has undergone tremendous development since 1990s. LOC devices have several inherent advantages compared to other analytical methods, especially the ability to perform complex analytical chemistry operations without a laboratory. This has the potential to allow samples to be analyzed at the point of need rather than to take hours or maybe days at a centralized laboratory. Flow conditions and chemical reactions can be better controlled in LOC devices. Also, they require small reagent amounts which can reduce costs and reduce the amount of chemical wastes. This section focuses on aspects of the state-of-the-art technological tools available for manufacturing LOC devices.

2.5.1 Silicon-based Micromachining Technique

At the early stage of the development of LOC devices, silicon-based micromachining tools played an important role. Bulk micromachining and surface micromachining are two categories in the micromachining family.

2.5.1.1 Bulk micromachining technique

Bulk micromachining refers to the technique used to define patterns directly in the substrate itself. A generic approach to bulk micromachining is illustrated in Figure 2-18 [97]. After the substrate is cleaned, a sacrificial layer used for protection of the substrate during the etching step is deposited. A photoresist is coated on top of the sacrificial layer using a spin coater and is exposed to UV radiation through a mask with transparent and opaque areas which define the desired pattern. Photoresist is then developed using photoresist developer. Exposed areas are either eliminated or kept, depending on whether it is positive or negative photoresist. The sacrificial layer under developed photoresist is removed followed by removing the rest of the photoresist from the substrate. Next, the substrate is etched under the protection of the sacrificial layer. The last step is to remove the rest of the sacrificial layer from the substrate. The fundamental step in bulk micromachining is etching. There are different ways to achieve it. Wet etching uses chemicals to etch away unwanted parts. Commonly used etchants for silicon include potassium hydroxide (KOH) or tetramethyl ammonium hydroxide (TMAH). The thickness of the pattern is controlled by the time spent in the etchant and is highly empirical. Different materials have different behavior in terms of etching directions. Silicon is an anisotropic material, meaning etching rate is different for all directions and etching is preferred to undergo along a specific angle. This results in patterns with clear-cut sharp walls. Glass is an isotropic material, meaning etching rate is all the same for all directions. This results in patterns with walls of irregular shapes. Unlike wet etching, dry etching uses reactive gas such as fluorocarbons, oxygen, chlorine, and boron trichloride instead of liquid chemicals to bombard target areas to etch materials, just like sandblasting at the atomic level. It typically results in anisotropic etching. A standard dry etching process cannot produce large thickness as the sacrificial mask layer is removed by bombardment of the reactive gas molecules while the substrate is being etched. To overcome the problem, *deep reactive ion etching* (DRIE) is introduced, which deposits a passivation layer before the previous one is etched away completely. The process can produce structures with very high aspect ratios. *Single crystal reactive ion etching and metallization* (SCRAM) is another etching technique. It sequentially mixes anisotropic and isotropic dry etching and is used to create suspended structures with high aspect ratios. There are many LOC devices created by bulk micromachining. Figure 2-19(a)

shows a fluidic vortex diode machined by DRIE [98] and Figure 2-19(b) shows a probe fabricated by the SCREAM process used to measure deformation of cells under mechanical stress [99].

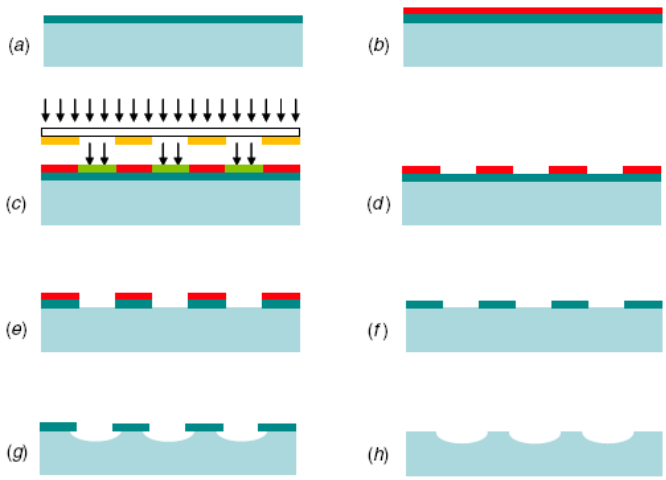

Figure 2-18. Illustration of a generic approach to bulk micromachining [97]. (a) Deposition of sacrificial layer; (b) Deposition of photoresist; (c) Patterning under UV exposure using mask; (d) Removal of patterned photoresist; (e) Removal of patterned sacrificial layer; (f) Removal of remaining photoresist; (g) Etching of substrate; (h) Removal of remaining sacrificial layer.

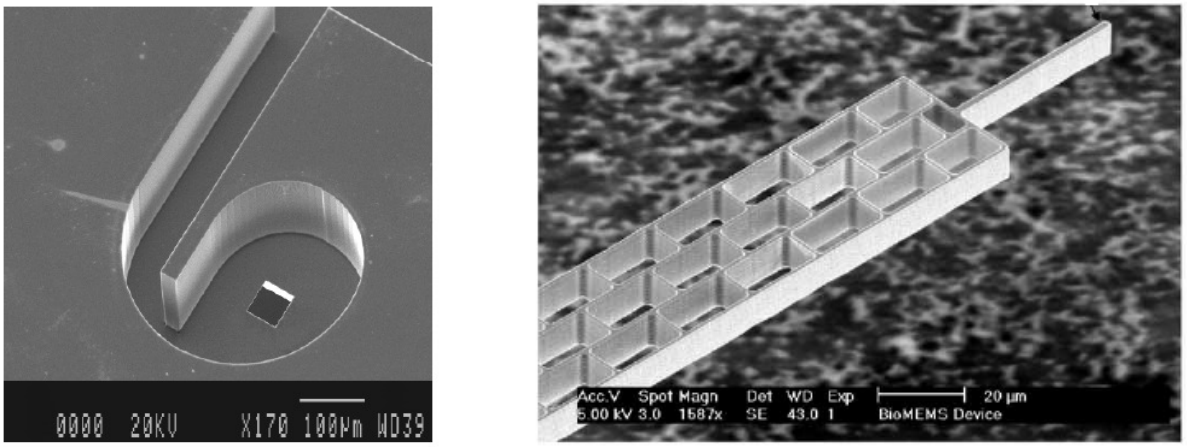

(a) (b)

Figure 2-19. LOC devices created by bulk micromachining technique. (a) a fluidic vortex diode machined by DRIE [98]; (b) a probe fabricated by the SCREAM process used to measure deformation of cells under mechanical stress [99].

2.5.1.2 Surface micromachining technique

Surface machining uses deposition or growth of thin layers on a substrate and selective etching of them. Unlike bulk micromachining, the structural material is the added thin layer instead of the substrate. The use of a sacrificial layer illustrated in Figure 2-20 is a fundamental concept in surface machining [97]. The technique is capable of creating thin suspended structures. Figure 2-21 shows a microchannel made using surface micromachining [100].

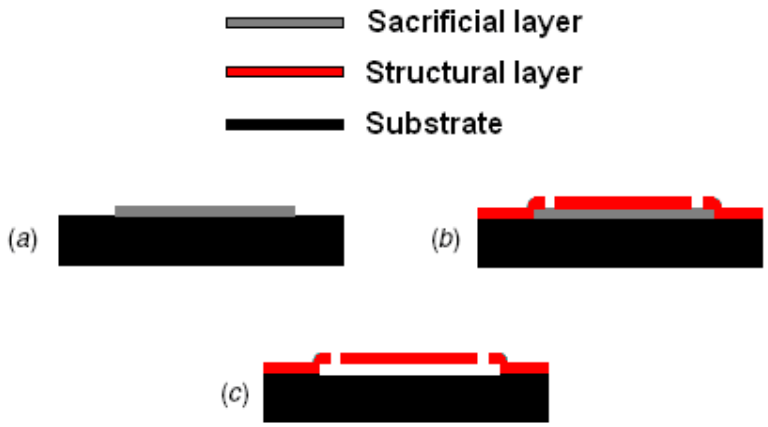

Figure 2-20. Concept of sacrificial layer in surface micromachining [97]. (a) Deposition of a sacrificial layer, conventionally a silicon oxide deposited by low-pressure chemical vapour deposition (LPCVD); (b) The structural layer is deposited, typically consisting of LPCVD polycrystalline silicon, and the accesses are defined; (c) The sacrificial layer is etched and the structure is released.

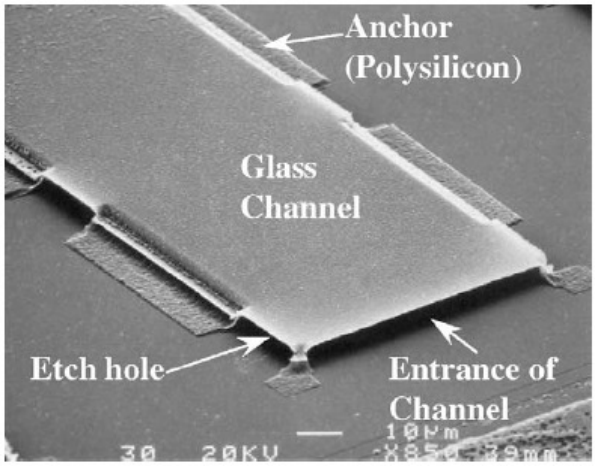

Figure 2-21. A microchannel made by surface micromachining [100].

2.5.2 Polymer Technique

Aside from silicon-based micromachining technique, polymer technologies have emerged as a unique and popular way to fabricate LOC devices. Polymers are large molecules composed of repeated units. They form long chains during polymerization process. Polymers commonly used for LOC devices include Polydimethylsiloxane (PDMS), Polymethylmethacrylate (PMMA), Polyvinylchloride (PVC), Polystyrene (PS) and many more. Polymer technologies include replication technique and direct structuring technique.

2.5.2.1 Replication technique

Figure 2-22 illustrates steps involved in the manufacturing of LOC devices by replication technique [97]. It starts with making a master which serves as a negative mould for replication. There are several ways to make a master. LIGA, a German acronym for Lithographie, Galvanoformung, Abformung meaning Lithography, Electroplating, and Molding, is a well known fabrication technique for master fabrication as described in Figure 2-23 [97]. It starts with depositing a thin metal layer as an electrode during the electrolytic deposition step followed by depositing a layer of PMMA. X-ray lithography is performed on the PMMA followed by electrolytic growth of metal. The master is released by first removing the substrate layer and the electrode metal layer by polishing and then removing PMMA by an etchant. LIGA usually results in masters made of Nickel or nickel-based alloys such as NiCO and NiFe. Silicon is also a popular material for manufacturing masters. Bulk micromachining is widely used to create masters made of silicon for microchannels. Masters with high aspect ratios can be achieved using DRIE. Conventional milling techniques can also be used to fabricate masters with a resolution on the order of 50-100 μm for users of a limited budget.

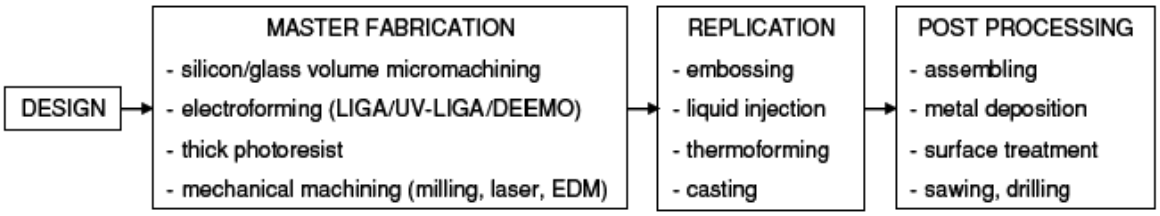

Figure 2-22. Steps involved in replication technique [97].

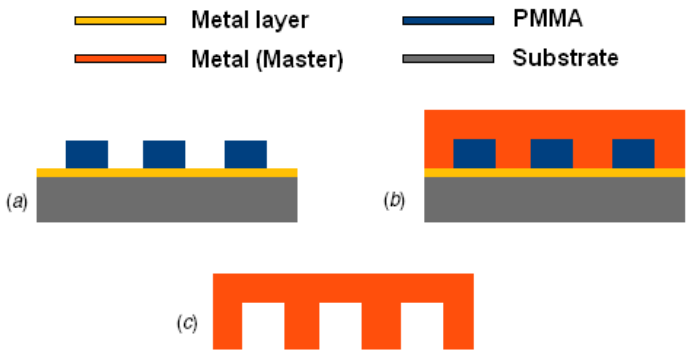

Figure 2-23. LIGA process [97]. (a) Deposition of a thin metal layer used as an electrode during the electrolytic deposition step followed by x-ray lithography of a thick layer of PMMA; (b) Electrolytic growth of metal; (c) PMMA is dissolved after removal of the substrate and the electrode metal layer by polishing to release the master.

The second step in replication technique is to get a reverse replication of a master. Embossing, liquid injection, thermoforming and casting are commonly used for the purpose. Details about embossing, liquid injection and thermoforming are shown in Figure 2-24 [101]. In embossing, a piece of thermoplastic is heated above its transition temperature and is pressed under a vacuum. It is then cooled down and the product is released from the mould. In liquid injection, an entrance for liquid plastic is created on one side of a master. The master is then heated above the transient temperature of the polymer and put under vacuum. The thermoplastic is heated and injected to the mould. The whole piece is cooled and plastic is stripped from the mould. In thermoforming, a piece of thermoplastic is inserted into a master and put under vacuum. The temperature is gradually increased to a point high enough for the plastic to deform but not to melt. A pressurized gas then brings the film into contact with the patterns. Finally, the product is removed from the mould after cooling down. However, the most frequently used replication technique in LOC devices at the moment is undoubtedly casting of PDMS as shown in Figure 2-25 [102]. The process begins by manufacturing a master using bulk machining of silicon or thick SU-8 photolithography. A mixture of silicone rubber and cross linking agent is cast on the master. After cross linking, the elastomer is carefully peeled off the substrate. Accesses such as fluid inlets and outlets are created using tools like a hole punch. The part is bonded on another substrate such as silicon or PDMS to form a complete device. There are many LOC devices created using replication technique including optical coupling elements made by LIGA [103],

a capillary electrophoresis system obtained by thermoforming [104], a microfluidic circuit made by embossing of PMMA [105] as shown in Figure 2-26 and many more.

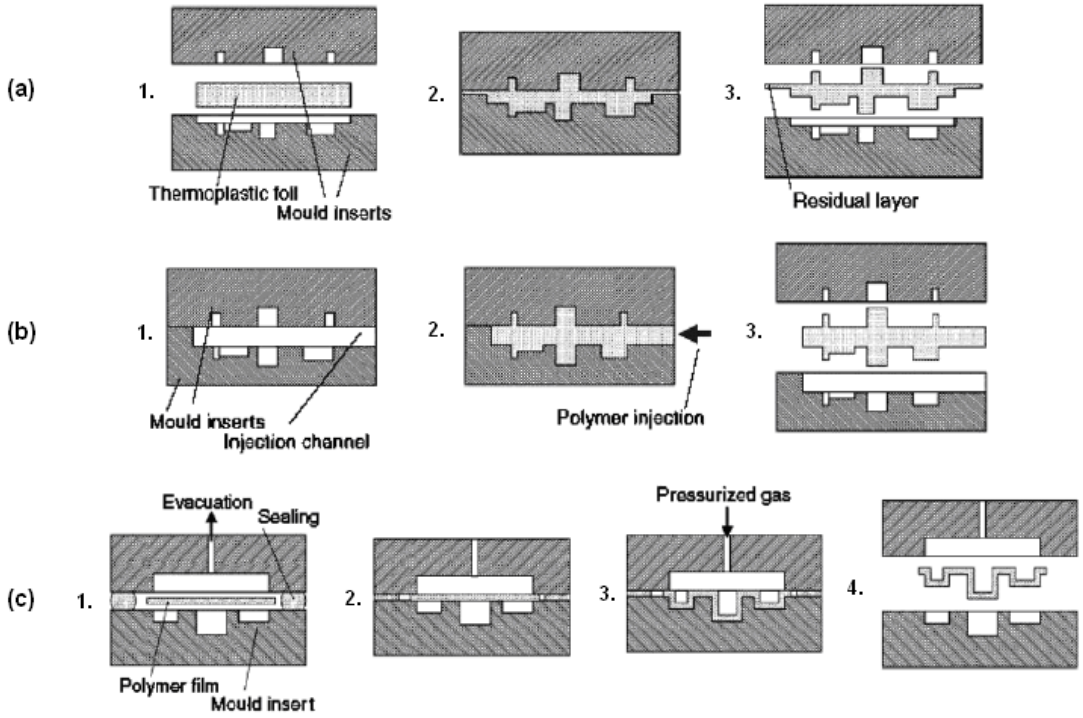

Figure 2-24. Process details of replication technique. (a) embossing; (b) liquid injection; (c) thermoforming [101].

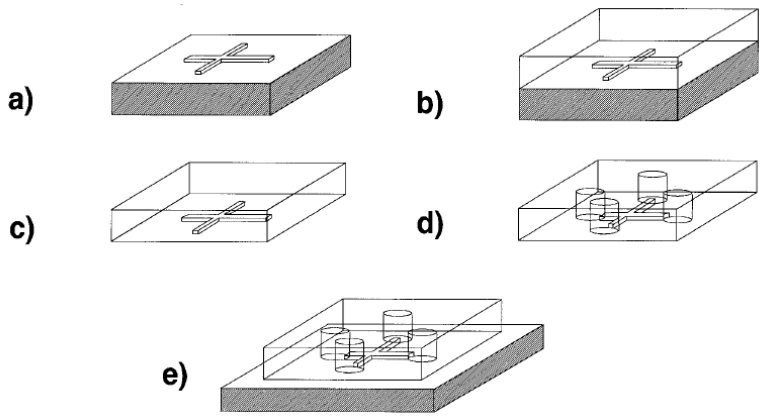

Figure 2-25. The PDMS casting process [102]. (a) Fabrication of a master; (b) A mixture of silicone rubber and cross linking agent is poured on the master; (c) After cross linking, the elastomer is carefully peeled off the substrate; (d) Accesses such as fluid inlets and outlets are created; (e) The part is bonded on another substrate form a complete device.

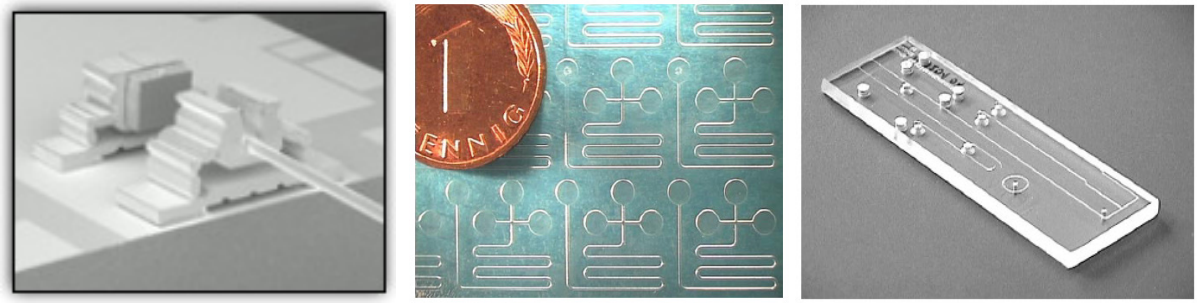

(a) (b) (c)

Figure 2-26. LOC devices created using replication technique. (a) Optical coupling elements made by LIGA [103]; (b) A capillary electrophoresis system made by thermoforming [104]; (c) A PMMA microfluidic circuit [105].

2.5.2.2 Direct structuring technique

Silicon bulk micromachining technique is used in replication technique to produce masters as described in the previous section. Silicon surface micromachining technique has also been adapted for use by polymer technologies with the purpose of avoiding the expensive assembly step and to facilitate integration. The technique, known as direct structuring, makes use of sacrificial layers and defines features directly in the polymer layer. One amazing example describing the concept is the use of frozen water as the sacrificial layer demonstrated in Figure 2-27 [106]. The process starts with plasma treatment of a pre-patterned substrate to create a hydrophobic surface. An appropriate amount of water is dropped on the surface and remains in the "valley" due to hydrophobic property of the surface. Temperature is then brought down to allow water to freeze followed by coating a layer of UV curable polymer on top. The device is ready after polymer cross-linking and melting of ice. SU-8, originally used as a negative photoresist, has many advantages as a structural material in direct structuring technique. It is transparent, has a high chemical resistance and is biocompatible [107]. The thickness of a SU-8 layer can range from 1 μm to 1 mm using a spin coater. Structures with high aspect ratios can easily be created. There are many LOC devices fabricated using direct structuring technique. Figure 2-28(a) shows a filter made of SU-8 [108] and Figure 2-28(b) shows a micromirror made of SU-8 with a SU-8 sacrificial layer [109].

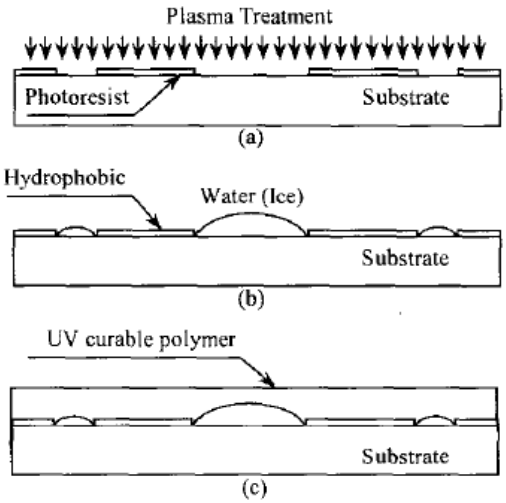

Figure 2-27. Concept of direct structuring technique using frozen water as the sacrificial layer [106]. (a) plasma treatment of a pre-patterned substrate to create a hydrophobic surface; (b) Water is frozen to create a sacrificial layer; (c) microchannels are created by coating a UV curable polymer on top.

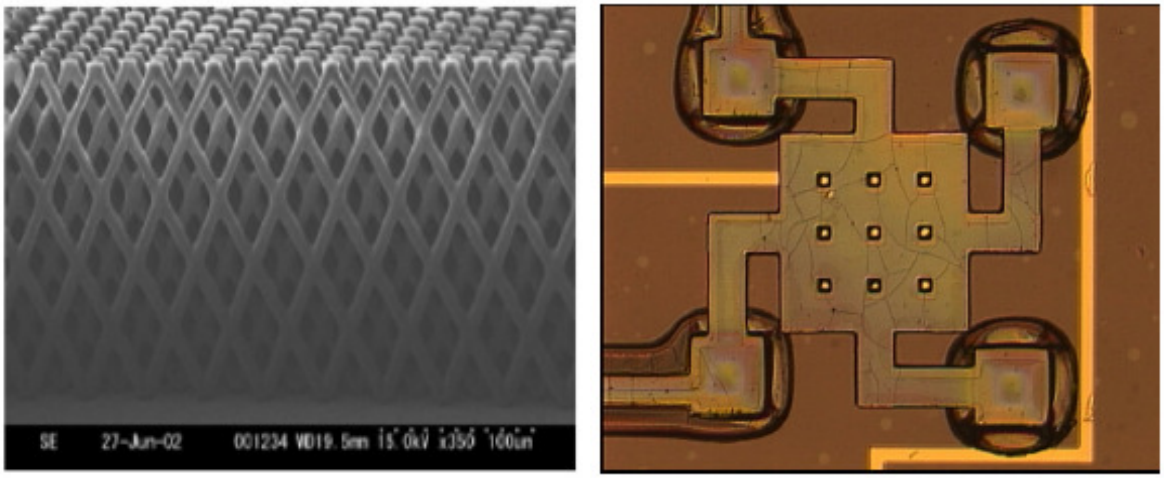

(a) (b)

Figure 2-28. LOC devices made from direct structuring technique. (a) A filter made of SU-8 [108]; (b) A micromirror made of SU-8 [109].

Chapter 3

Novel Cell Lysis Methods for Lab-on-a-Chip Applications

This chapter describes research activities towards two novel cell lysis methods for Lab-on-a-Chip (LOC) applications. Section 3.1 focuses on making use of poly(quaternary ammonium) functionalized nanoparticles which present excellent antibacterial property by disrupting cell membranes for cell lysis. Section 3.2 focuses on making use of the photocatalytic effect of titanium dioxide nanoparticles under UV irradiation for cell lysis.

3.1 Cell Lysis using Surface Modified Nanoparticles

Pathogenic bacteria cause serious illnesses to human beings as well as animals. They pose a great threat to our health. People have always been using all sorts of antibacterial reagents to fight against pathogenic bacteria. As building blocks for Nanotechnology applications, nanomaterials, especially nanoparticles, present unique properties that cannot be achieved by their bulk counterparts mainly due to their small size and the resulting large surface-area-to-volume ratio. Extensive research has been conducted on introducing and enhancing the antibacterial property using nanoparticles such as metal, metal oxide and composite [110-119]. A major problem with current research on introducing antibacterial property using nanoparticles is that it usually takes a relatively long time to get satisfying results [115, 120]. Besides, some require external excitations to induce the property [121-124]. This complicates design and system miniaturization for many applications such as LOC devices.

Quaternary ammonium cations, also known as quats, are derivatives of ammonium compounds, in which all four of the hydrogen atoms bonded to nitrogen are replaced by hydrocarbyl groups as shown in Figure 3-1 [125]. Quaternary ammonium compounds such as benzalkonium chloride, benzethonium chloride, and methylbenzethonium chloride with long side chains, have widely been used as disinfectants for a long time [126-131]. They are effective against both Gram-positive and Gram-negative bacteria [132, 133]. It is believed that the antibacterial action of quaternary ammonium compounds involves disruption of cytoplasmic and outer membrane lipid bilayers through interaction between long quaternary nitrogen functional groups and the polar head groups of acidic

phospholipids [134-138]. The result is the generalized and progressive leakage of cytoplasmic materials [139].

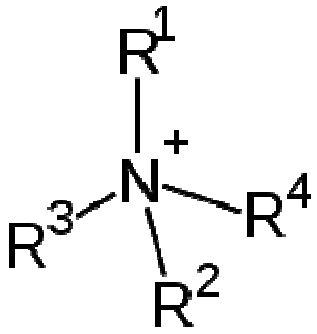

Figure 3-1. Quaternary ammonium cations. $R^1 - R^4$ are hydrocarbyl groups.

Can we engineer poly(quaternary ammonium) modified nanoparticles to take advantage of the antibacterial property induced by poly(quaternary ammonium) functional groups as well as the large surface-area-to-volume ratio of nanoparticles to achieve more efficient antibacterial effect? To answer the question, a series of experiments were conducted to demonstrate the excellent antibacterial property of surface modified gold and titanium dioxide nanoparticles without external excitations. Nanoparticle concentration and reaction time were evaluated as two important factors affecting antibacterial performance.

3.1.1 Materials

3.1.1.1 Nanoparticles

Gold and titanium dioxide were chosen as they are very common carrier nanomaterials and are readily available as commercial products [86, 140]. Nanoparticles functionalized with poly(quaternary ammonium) were obtained from Vive Nano as research prototypes. In order to compare the effect of surface modifications, polyacrylate sodium functionalized gold and titanium dioxide nanoparticles were obtained from Vive Nano as well. For convenience, poly(quaternary ammonium) modified gold and titanium dioxide nanoparticles are denoted as AuNP+ and TiO2NP+ respectively while polyacrylate sodium modified gold and titanium dioxide nanoparticles are denoted

as AuNP- and TiO2NP- respectively. Gold nanoparticles were in the range of 1~10 nm while titanium dioxide nanoparticles were in the range of 1~20 nm. TEM images of the nanoparticles used in the experiments were acquired using a TEM machine (Philips CM10) and are shown in Figure 3-2. The stock concentration of each of the nanoparticle colloidal dispersions was 1.5 mg/mL.

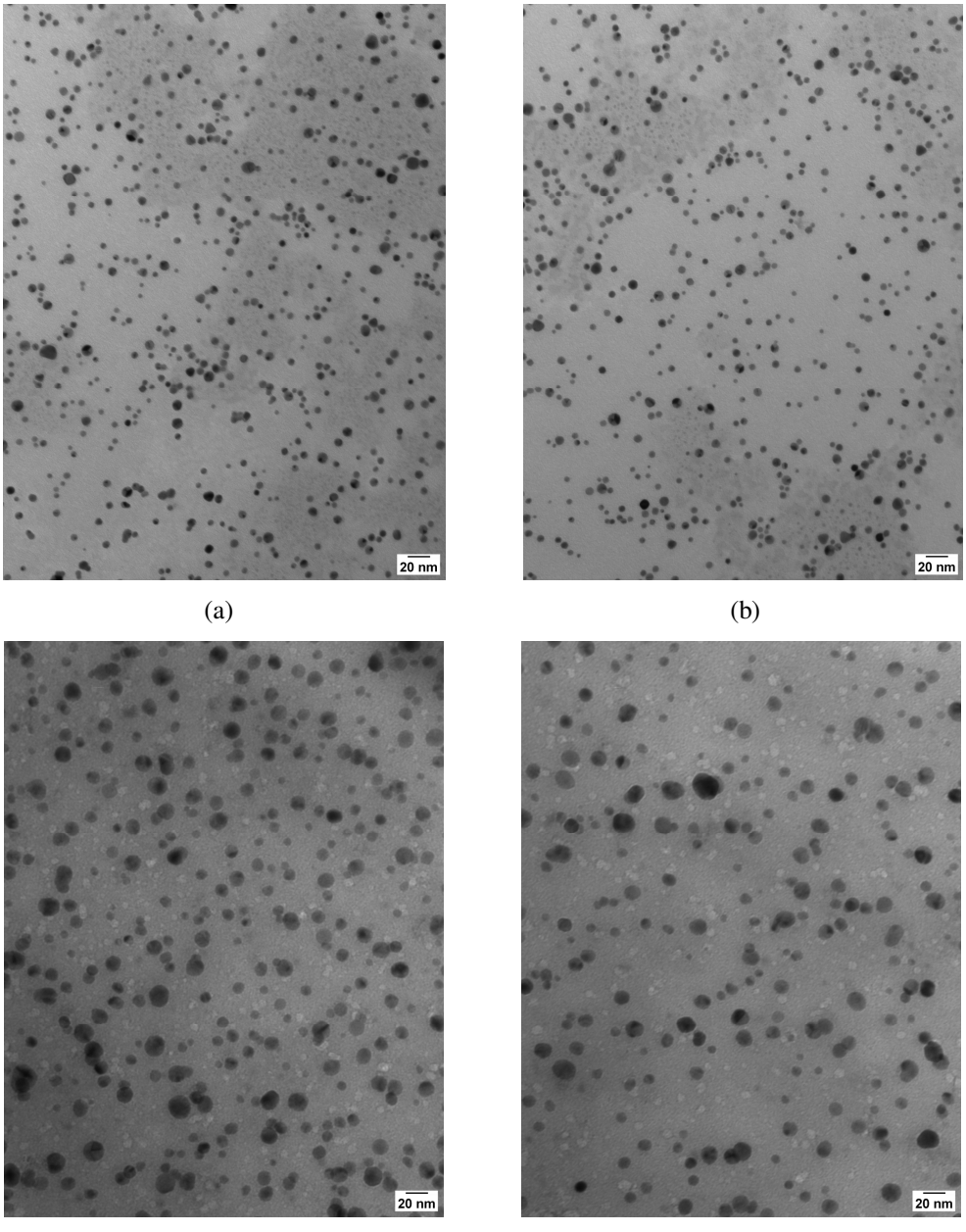

(a) (b)

(c) (d)

Figure 3-2. TEM images of the gold and titanium dioxide nanoparticles used in the experiments. (a) AuNP+; (b) AuNP-; (c) TiO2NP+; (d) TiO2NP-.

3.1.1.2 Cell samples

Escherichia coli (*E. coli*) was used to test cell lysis efficiency. Cells were grown in lysogeny broth (LB) at 37℃ over night and were washed twice using deionized water before experiments. To prepare LB, 10 g of tryptone, 5 g of yeast extract, and 10 g of NaCl were dissolved in 1 L of distilled water followed by autoclaving at 121℃. Stock cell concentration was adjusted and was measured using a spectrometer (Beckman Coulter DU520) to be at $OD_{600} = 0.60$. Cell solution was diluted as needed in different experiments.

3.1.2 Methods

3.1.2.1 Cell viability kit

In some of the experiments, cells were stained using the Live/Dead BacLight bacterial viability kit (L7012, Molecular Probe, USA) to directly view cell viability as well as to determine cell survival rates. The kit contains two fluorescent stains, SYTO 9 green-fluorescent nucleic acid stain and the red–fluorescent nucleic acid stain, propidium iodide. These stains differ both in their spectral characteristics and in their capability to penetrate healthy bacteria. When used alone, SYTO 9 stain labels both live and dead bacteria in a population. In contrast, propidium iodide penetrates only bacteria with damaged membranes, reducing the SYTO 9 fluorescence when both dyes are present. Therefore, live bacteria with intact membranes fluoresce green, while dead bacteria with damaged membranes fluoresce red. The excitation/emission maxima is around 480/500 nm for the SYTO 9 stain while 490/635 nm for the propidium iodide stain. The background remains virtually nonfluorescent. Images were captured using a fluorescence microscope (Nikon Eclipse E600FN) and a digital camera (Nikon Digital Sight DS-U1) through a dual-band filter so that both cells with and without intact cell membranes can be seen at the same time. The kit can also be utilized to create fluorescence spectroscopy protocols to quantitatively analyze cell viability rates by using a spectrofluorometer (Jasco FP-6500). The recommended steps provided by Invitrogen Inc. are as follows,

i. Measure the fluorescence emission spectrum with an excitation wavelength of 470 nm and an emission wavelength ranging from 490 to 700 nm.

ii. Calculate the ratio of the integrated intensity of the portion of each spectrum between 510 to 540 nm to that between 620 to 650 nm, that is

$$Ratio_{G/R} = \frac{F_{cells,green}}{F_{cells,red}}$$

iii. Calculate the ratio at different reaction time spots, for example 5, 10, 15, 30, 45 and 60 minutes. Correlate the ratio with the cell viability rate.

To correlate the green/red fluorescence ratios with cell viability rates, characterization is needed for pre-defined cell viability rates. The procedure is as follows,

i. Mix five different proportions of the bacterial suspensions in 1 cm quartz fluorescence cuvettes as shown in Table 3-1. The total volume of each of the five samples is 1 mL.

Table 3-1. Recipe of various proportions of live:dead cells for fluorescence spectroscopy

Ratio of live:dead cells	Live cell suspension (mL)	Dead cell suspension (mL)
0:100	0	1
10:90	0.1	0.9
50:50	0.5	0.5
90:10	0.9	0.1
100:0	1	0

ii. Prepare a combined reagent mixture in a microfuge tube by adding 10 µL of SYTO 9 and 10 µL of propidium iodide. Add 3 µL of the mixture to each of the five samples and mix thoroughly by pipetting up and down several times. Incubate at room temperature in the dark for 15 minutes.

iii. Measure the fluorescence emission spectrum (excitation wavelength of 470 nm, emission wavelength of 490-700 nm) of each cell suspension in the spectrofluorometer as shown in Figure 3-3(a). Calculate the ratio of the integrated intensity of the portion of each spectrum between 510-540

nm to that between 620-650 nm for each bacterial suspension. Plot the ratio of integrated green fluorescence to integrated red fluorescence versus cell viability rate as shown in Figure 3-3(b).

iv. Since green/red fluorescence ratio versus cell viability rate is considered linear, cell viability for a specific green/red fluorescence ratio is determined using Figure 3-3(b).

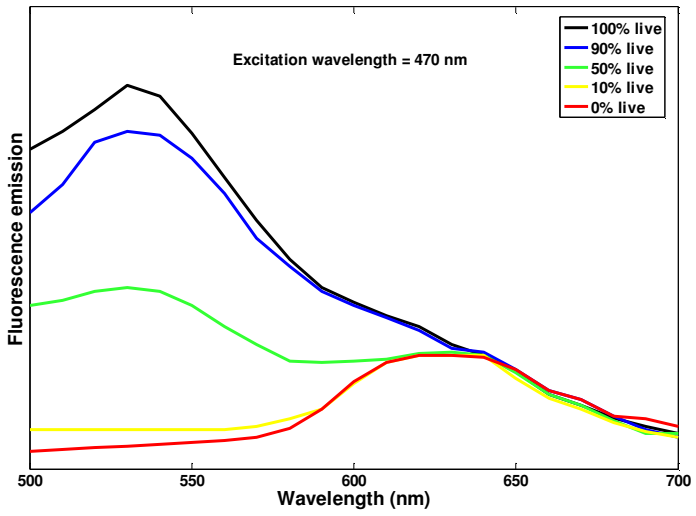

(a)

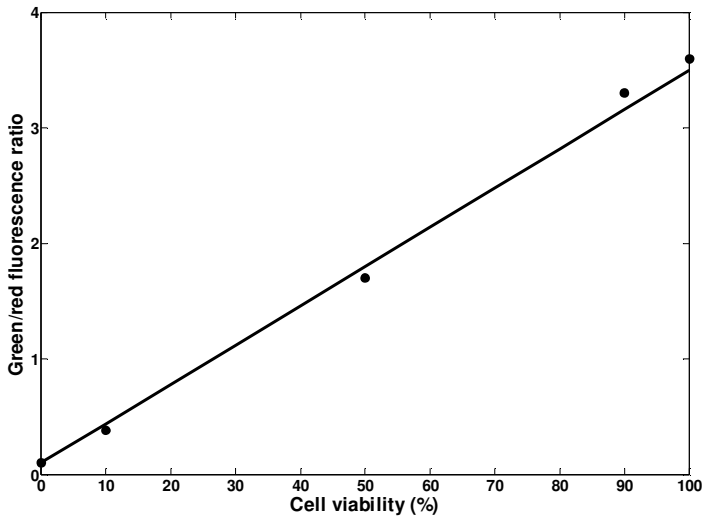

(b)

Figure 3-3. Analysis of relative viability of *E. coli* suspensions by fluorescence spectroscopy. (a) Fluorescence emission spectra of various proportions of live and dead *E. coli*; (b) Green/red fluorescence ratio versus cell viability with curve fitting.

3.1.2.2 Bacteria colonies

To qualitatively visualize bacteria growth, bacteria was cultured using the spread plate method on LB agar plates. A freshly made agar plate was taken followed by pipetting 0.1 mL of the solution of interest onto surface of the agar plate. Then, the sample was spread evenly over the surface using a sterile glass spreader. Finally, the plate was placed in the oven at 37℃ over night. Images were taken right after removing the plates from the oven. LB and agar mixture was prepared by dissolving 15 g of agar to 1 L of LB followed by autoclaving at 121℃. When LB and agar mixture was still hot, 10 mL of the mixture was taken and poured in a sterilized petri dish followed by spreading the solution evenly. The prepared LB agar plates were stored at 4℃.

3.1.2.3 Transmission electron microscopy (TEM)

TEM was used to examine nanoparticles as well as cell morphology after experiments. For examining nanoparticles, 3 µL of each of nanoparticle dispersions was dropped on Formvar coated copper TEM grids. The grids were dried in a vacuum oven at room temperature and examined using a TEM machine (Philips CM10) at 60 kV. For examining bacteria, 5 batches of freshly cultured *E. coli* were washed twice using deionized water and were transferred to 1.5 mL microcentrifuge tubes respectively. 1 mL of each of deionized water, poly(quaternary ammonium) functionalized gold nanoparticle colloidal dispersion, poly(quaternary ammonium) functionalized titanium dioxide nanoparticle colloidal dispersion, polyacrylate sodium functionalized gold nanoparticle colloidal dispersion, and polyacrylate sodium functionalized titanium dioxide nanoparticle colloidal dispersion was added to the microcentrifuge tubes respectively. The suspensions were mixed and shaken well, and left undisturbed for 5 minutes. Each suspension was centrifuged down to a pellet and washed once with the phosphate buffer (P.B.) composed of 0.2 M monobasic sodium phosphate and 0.2 M dibasic sodium phosphate, followed by suspending in 2.5% glutaraldehyde in P.B. for 1 hour at 4℃. Each suspension was then washed with P.B. 3 times and was suspended in 0.5% osmium tetroxide in P.B. for 16 hours at room temperature. Each suspension was then diluted to 8 mL with deionized water and was suspended in approximately 1 mL of 2% warm agar followed by pouring suspensions carefully on fresh microscope glass slides in a thin layer and cutting them into small 2×2 mm blocks.

The cells were dehydrated by passing them through a graded acetone series and embedded in plastic. Samples were first trimmed using razor blades and then cut with a glass knife on a Leica ultramicrotome followed by staining with lead citrate and 4% uranyl acetate. After rinsing with distilled water, samples were dried and examined in a TEM machine (Philips CM10) operated at 60 kV.

3.1.3 Results and Discussion

Experiments were conducted to compare the effect of surfactants on the antibacterial activity by mixing *E. coli* solution with each of the nanoparticle colloidal dispersions in sterilized test vials followed by adding fluorescent staining components. Figure 3-4 shows fluorescent images recorded right after mixing 10 µL of the *E. coli* stock solution with 100 µL of each of the nanoparticle colloidal dispersions for 10 minutes. As shown in Figure 3-4(b) and (d), most cells stained red as opposed to green in the control sample in Figure 3-4(a), which indicates that most cells were effectively lysed. However, polyacrylate sodium modified nanoparticles did not present such a property as shown in Figure 3-4(c) and (e). To further confirm the result, 100 µL of the mixture from each test vial was extracted and plated on LB agar plates to visualize bacteria colonies after incubating them at 37℃ for 16 hours as shown in Figure 3-5. High resolution TEM was used to examine sections of the samples to have a closer look at the cells after treating them with nanoparticles. In the control sample (Figure 3-6(a) and (b)), characteristics of the untreated bacteria were the well-defined cell membrane as well as the evenly stained interior of the cell, which corresponds to the presence of intracellular materials such as proteins and DNA. After treatment with AuNP+ and TiO2NP+, the cell morphology changed significantly with a noticeable observation that cell membranes were incomplete (Figure 3-6(c), (d), (g), and (h)). Cell membranes remained intact after treatment with AuNP- and TiO2NP- (Figure 3-6(e), (f), (i), and (j)).

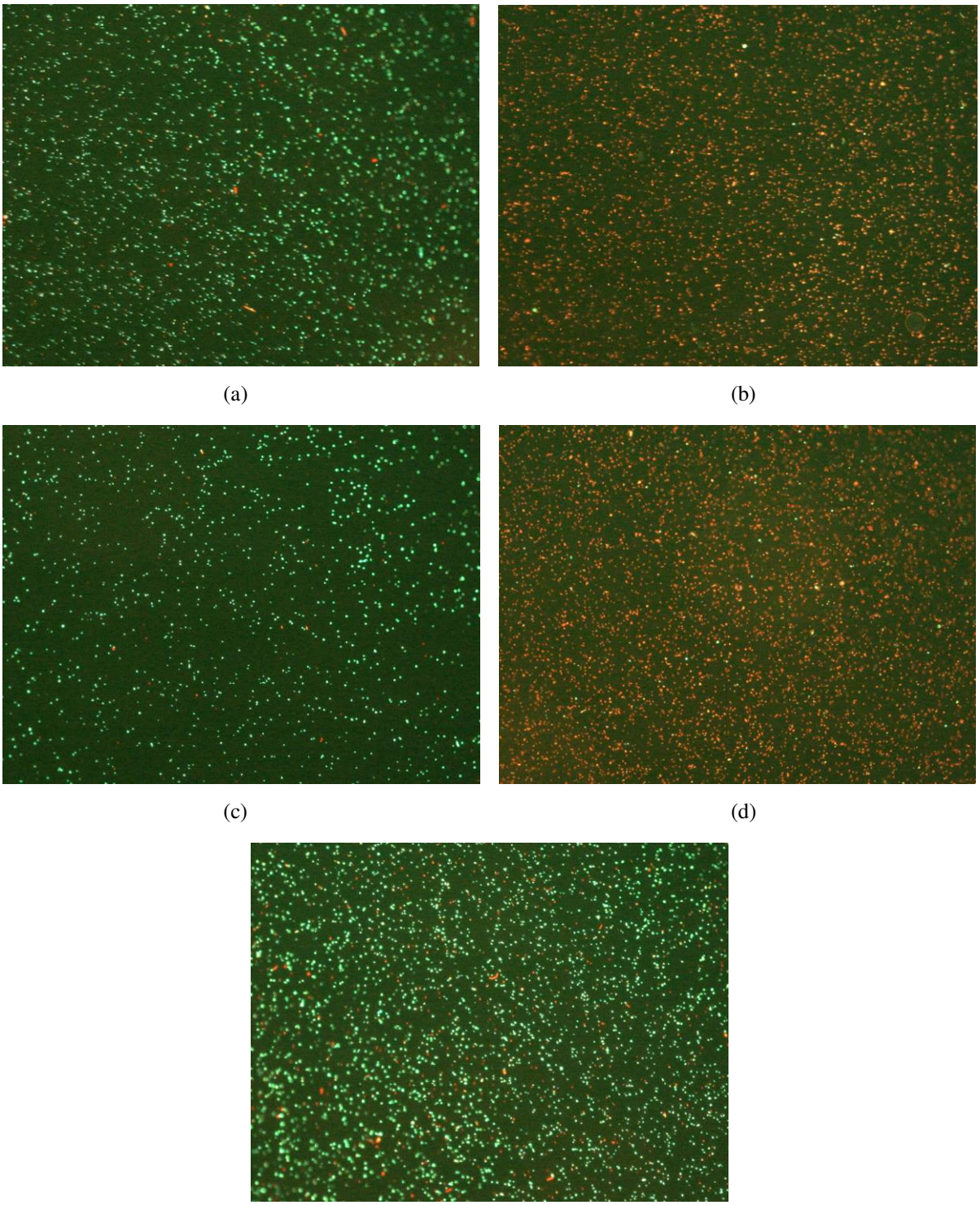

Figure 3-4. Bacteria viability after mixing with gold and titanium dioxide nanoparticles for 10 minutes. (a) Control, (b) AuNP+, (c)AuNP-, (d) TiO2NP+, and (e) TiO2NP-.

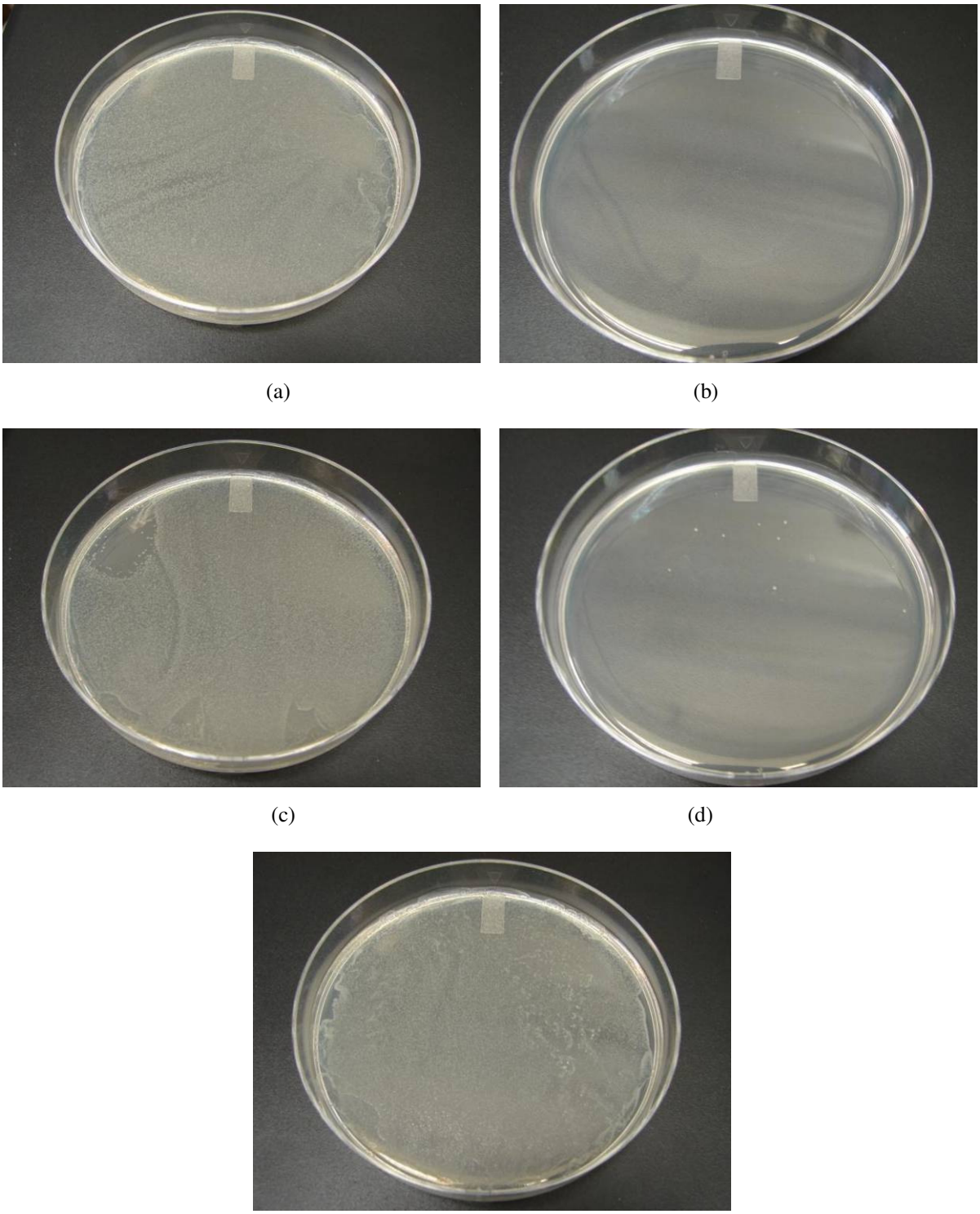

Figure 3-5. Effect of surfactants on *E. coli.* (a) Control, (b) AuNP+, (c)AuNP-, (d) TiO2NP+, and (e) TiO2NP-.

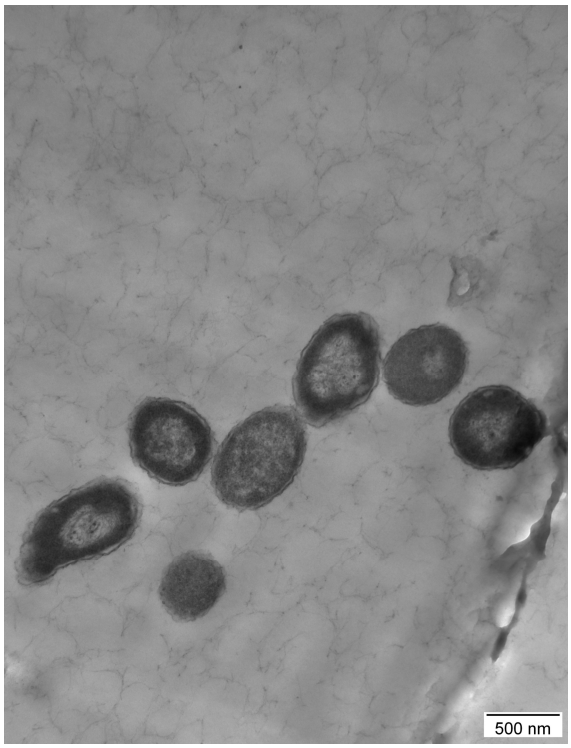

(a)

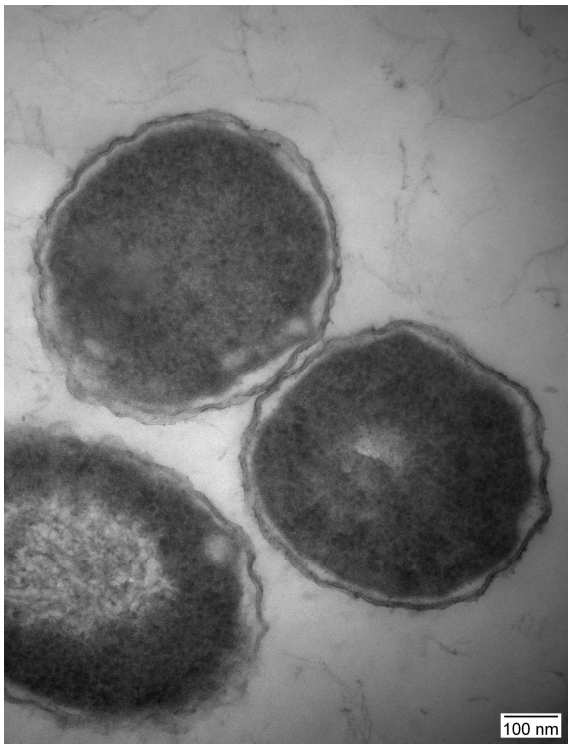

(b)

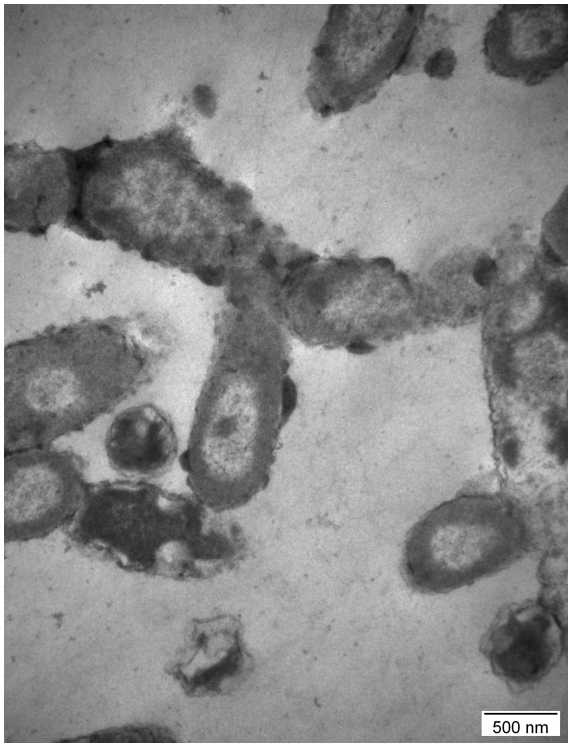

(c)

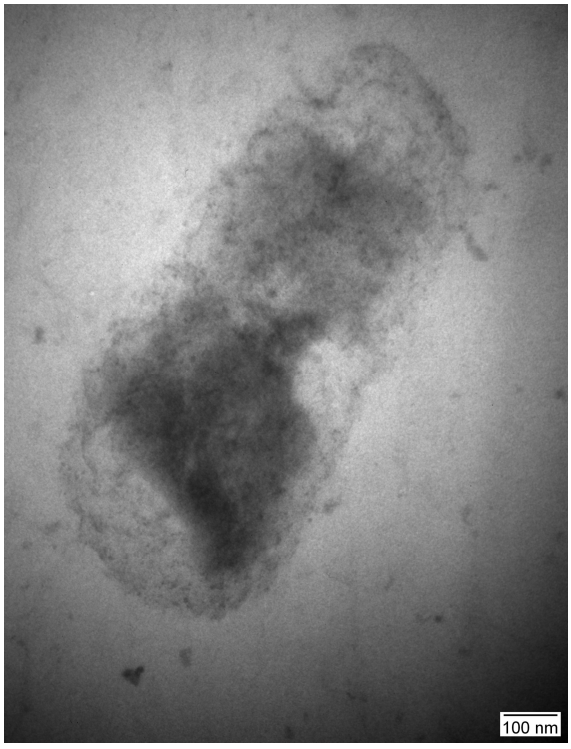

(d)

(e)

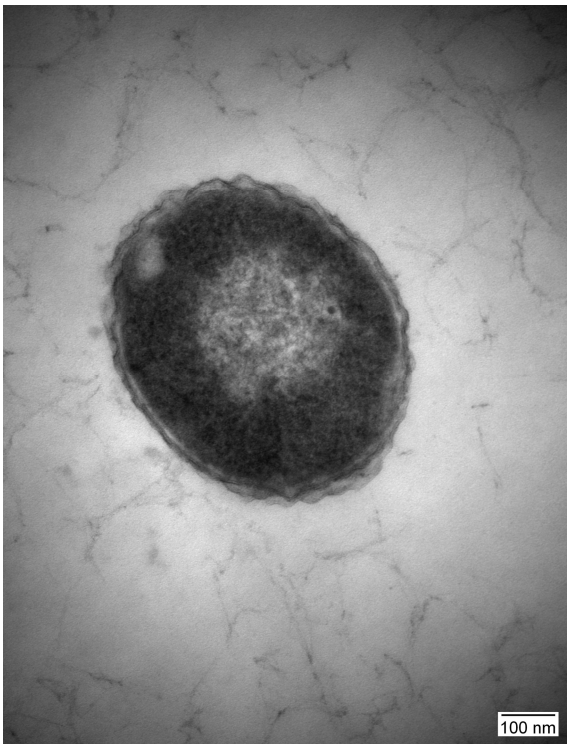

(f)

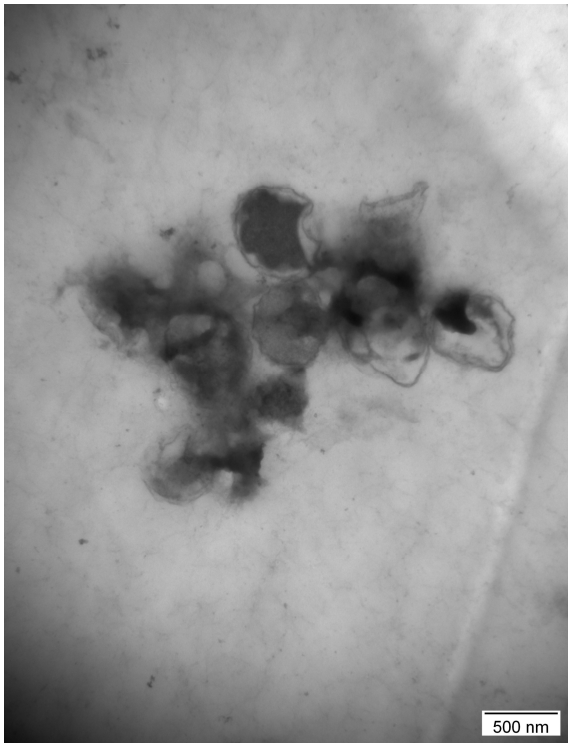

(g)

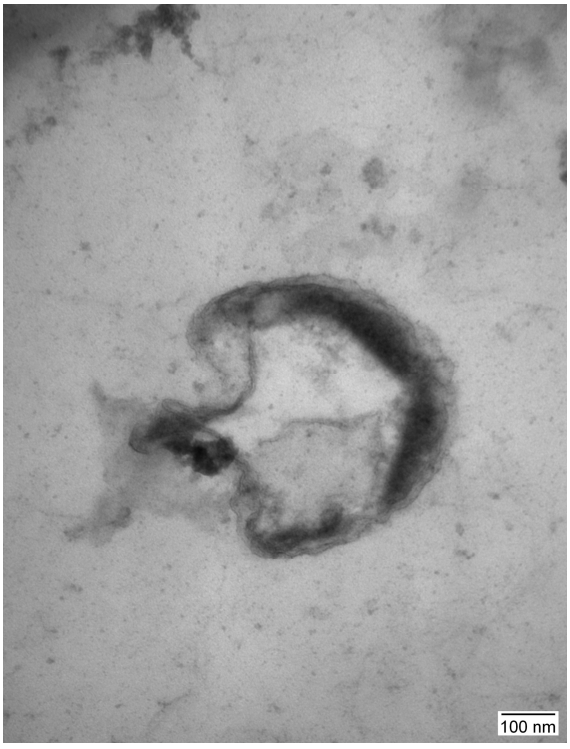

(h)

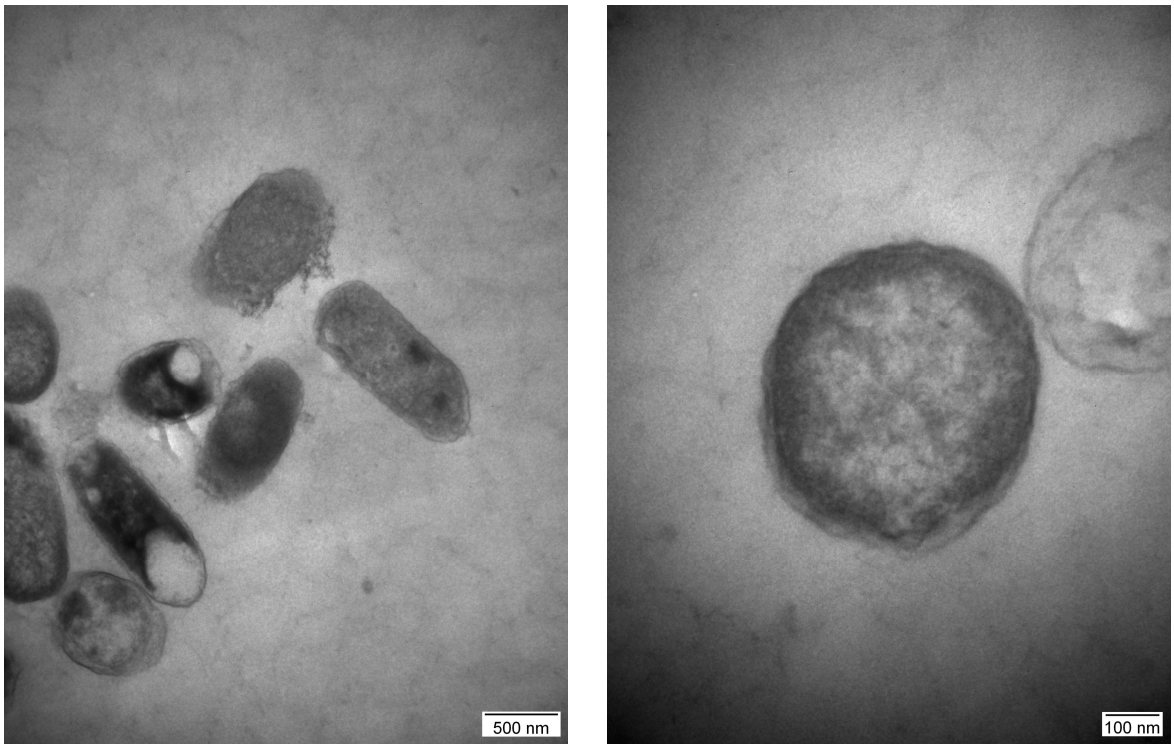

(i) (j)

Figure 3-6. TEM images of *E. coli* treated with different nanoparticles. (a) and (b) Control sample; (c) and (d) AuNP+; (e) and (f) AuNP-; (g) and (h) TiO2NP+; (i) and (j) TiO2NP-.

As demonstrated in the previous experiments, poly(quaternary ammonium) modified gold and titanium dioxide nanoparticles possessed excellent antibacterial property without external excitations. Since the mechanism lies in the direct interaction between poly(quaternary ammonium) functional groups and cell membranes, the number of nanoparticles in the solution determines antibacterial efficiency. Therefore, it was interesting to see how nanoparticle concentration related to the antibacterial efficiency. Poly(quaternary ammonium) modified gold and titanium dioxide nanoparticle colloidal dispersions were mixed with *E. coli* at three different concentrations including 1.36, 0.136 and 0.0136 mg/mL for 10 minutes followed by plating 100 μL of each of the mixtures in LB agar plates at 37℃ for 16 hours. Higher particle concentration led to better antibacterial performance for both gold and titanium dioxide nanoparticles as shown in Figure 3-7 and 3-8. In order to generate a noticeable result in a relatively short period of time, the nanoparticle concentration should be high enough, i.e. it must exceed 0.0136 mg/mL for both gold and titanium dioxide nanoparticles to have

obvious antibacterial effect in 10 minutes. The similarity between Figure 3-7 and 3-8 also indicates that surfactants play a much more important role than carrier materials.

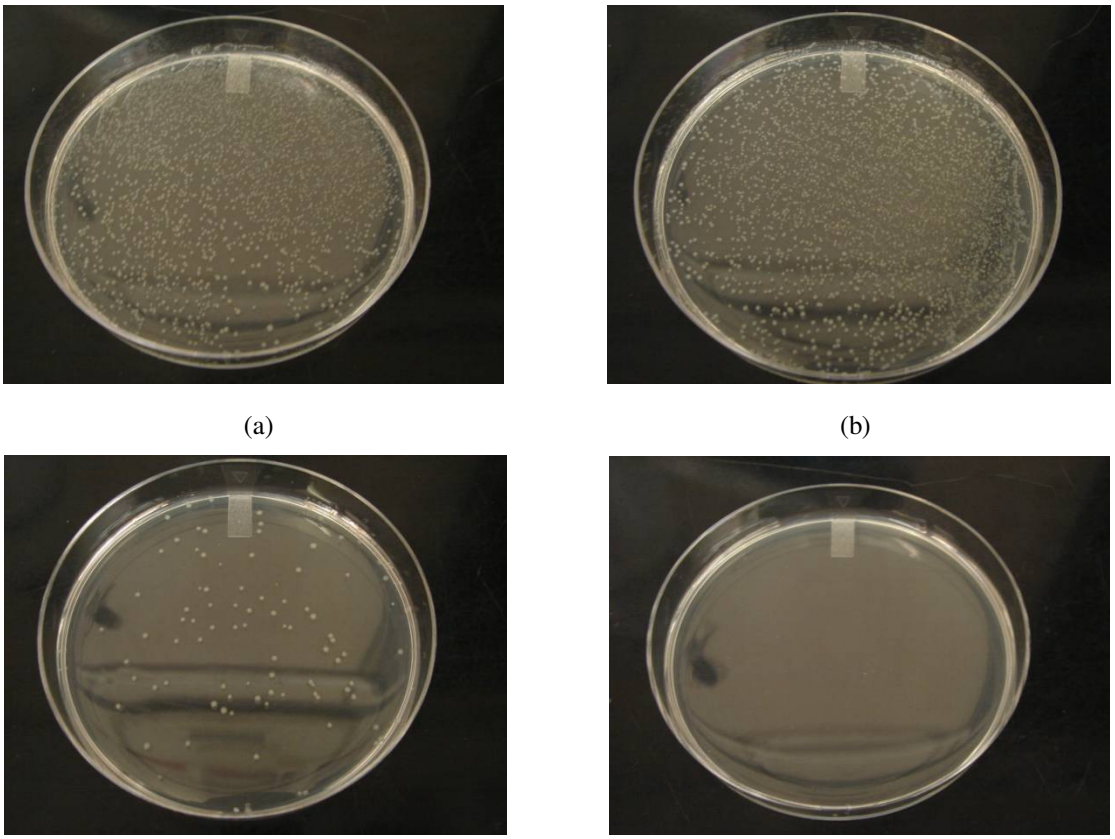

(a) (b)

(c) (d)

Figure 3-7. The effect of poly(quaternary ammonium) modified gold nanoparticles on bacteria after mixing with *E. coli* for 10 minutes. The nanoparticle concentration is (a) 0, (b) 0.0136 mg/mL, (c) 0.136 mg/mL, and (d) 1.36 mg/mL.

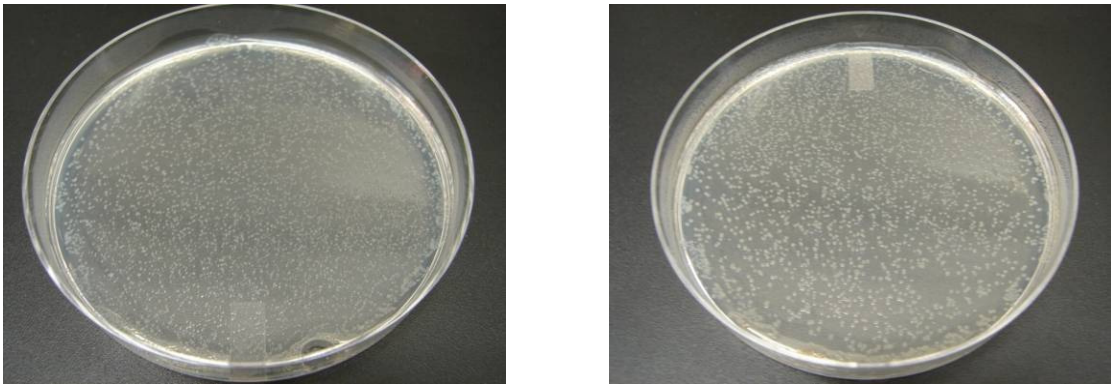

(a) (b)

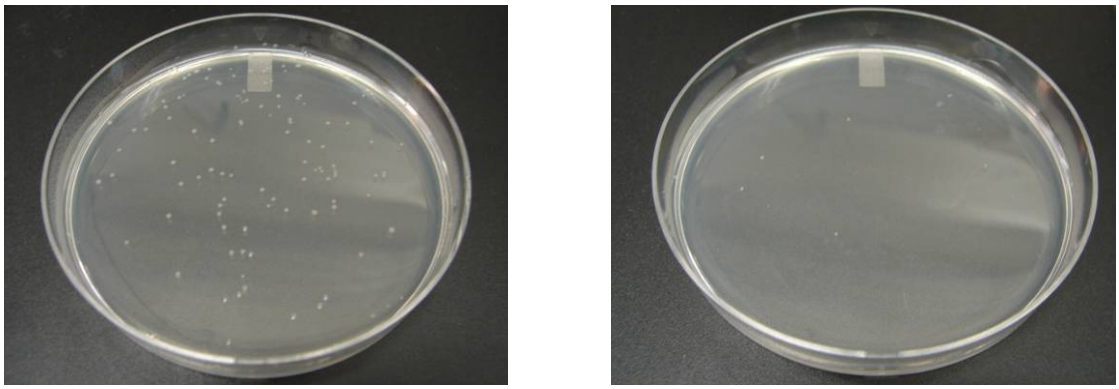

(c) (d)

Figure 3-8. The effect of poly(quaternary ammonium) modified titanium dioxide nanoparticles on bacteria after mixing with *E. coli* for 10 minutes. The nanoparticle concentration is (a) 0, (b) 0.0136 mg/mL, (c) 0.136 mg/mL, and (d) 1.36 mg/mL.

Reaction time was also a factor in determining antibacterial performance as it took time for surfactants to interact with bacteria. As shown in Figure 3-7(c) and 3-8(c), *E. coli* cannot be completely destructed within 10 minutes at the nanoparticle concentration of 0.136 mg/mL for both gold and titanium dioxide. On the other hand, complete bacteria destruction was observed in 60 minutes at the same nanoparticle concentration for both poly(quaternary ammonium) modified gold and titanium dioxide nanoparticles by visualizing bacteria colonies. Same experiments with different controlled reaction time periods were repeated multiple times to get a statistical view towards how bacteria survival rate changed with reaction time period. A traditional way of measuring bacterial survival rates is to count the number of bacteria colonies. However, the method cannot reflect cell condition instantly. A direct technique was used by measuring green and red fluorescence intensities using the bacterial viability kit. Once the ratios of integrated green fluorescence to integrated red fluorescence for different reaction time periods were known, the figure of bacteria survival rate against reaction time period can be plotted. Details about how bacteria survival rate is determined were described in Section 3.1.2.1. Figure 3-9 shows the result for poly(quaternary ammonium) modified gold nanoparticles. It can be seen that extremely efficient cell lysis can be achieved in 10 minutes at the nanoparticle concentration of 1.36 mg/mL.

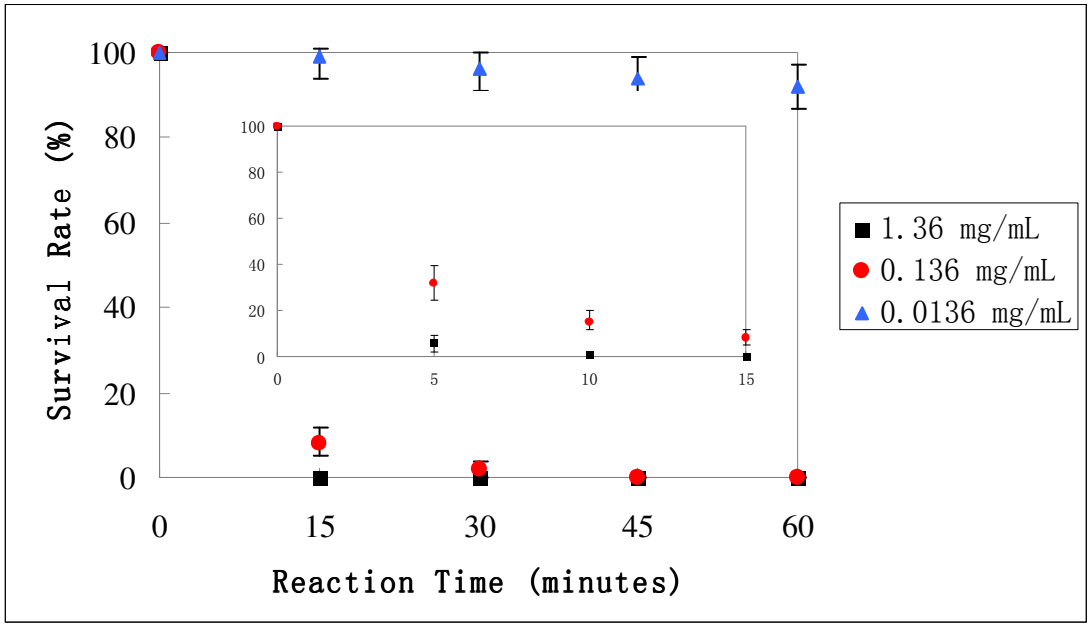

Figure 3-9. Bacteria survival rate against reaction time for poly(quaternary ammonium) modified gold nanoparticles. These surface modified gold nanoparticles showed excellent antibacterial property at the nanoparticle concentration of 1.36 mg/mL in 10 minutes (inset).

3.1.4 Summary

In this study, poly(quaternary ammonium) modified gold and titanium dioxide nanoparticles were demonstrated to be able to destruct *E. coli* within a short period of time without providing external excitations. However, polyacrylate sodium modified gold and titanium dioxide nanoparticles did not present such a property. High resolution TEM images clearly revealed that the mechanism of cell lysis was through cell membrane disruption due to poly(quaternary ammonium) functional groups. Both nanoparticle concentration and reaction time are important to determine cell lysis efficiency. Higher nanoparticle concentration and longer reaction time led to better antibacterial performance. Based on the experimental results, it is reasonable to predict that poly(quaternary ammonium) modified nanoparticles possess efficient antibacterial property no matter what carrier materials are. The proposed method is easy to be implemented in any LOC devices with the only requirement of a reaction chamber of any size. It does not involve any complicated fabrication steps as required in most of current cell lysis methods for LOC applications. The engineered nanoparticles can find

enormous applications such as self-cleaning surfaces, waste water treatment, LOC devices and many more.

3.2 Cell Lysis using Photocatalytic Property of Titanium Dioxide Nanoparticles

Photocatalysis is the acceleration of a photoreaction in the presence of a catalyst which is named photocatalyst in this case. The study of photocatalytic reactions dates back to 1970's when Fujishima and Honda discovered the photocatalytic splitting of water on a titanium dioxide electrode in 1972 [141]. Since then, research efforts in understanding the fundamental processes and in improving the photocatalytic efficiency for real applications have become extensive. In a photocatalysis system, photoinduced reactions take place at the surface of a photocatalyst. Depending on where the initial excitation occurs, photocatalysis can be generally divided into two classes of processes. When the initial photoexcitation occurs in an adsorbate molecule which then interacts with the ground state catalyst substrate, the process is referred to as a catalyzed photoreaction. When the initial photo-excitation takes place in the catalyst substrate and the photoexcited catalyst then transfers an electron or energy into a ground state molecule, the process is referred to as a sensitized photoreaction. The initial excitation of the system is followed by subsequent electron transfer and/or energy transfer. It is the subsequent de-excitation processes, either via electron transfer or via energy transfer, that lead to chemical reactions in the photocatalysis process [142, 143].

Unlike metals which have continuous electronic states, semiconductor materials possess a discrete energy states where no energy levels are available to promote recombination of electrons and holes produced by photoactivation in the solid. The energy gap which extends from the upper-most valence band to the lower-most conduction band is called the band gap. Once excitation occurs across the band gap, electrons in the valence band can be excited to higher energy states in the conduction band leaving electrons in the conduction band and holes in the valence band to form electron-hole pairs. There is a sufficient lifetime, in the nanosecond regime [144], for the created electron-hole pairs to undergo charge transfer to adsorbed species on the semiconductor surface from solution or gas phase contact. Upon excitation, the fate of the separated electron and holes can follow several pathways which are illustrated in Figure 3-10 [142]**.** The enlarged section of Figure 3-10 shows the excitation of

an electron from the valence band to the conduction band initiated by light absorption with energy equal to or greater than the band gap of the semiconductor. Recombination of the separated electron and hole pairs can occur in the volume of the semiconductor material (pathway B) or on the surface (pathway A) with the release of heat. In competition with recombination of electron and hole pairs, the semiconductor can donate electrons to reduce an electron acceptor at the surface, usually oxygen in an aerated solution (pathway C). In turn, a hole can migrate to the surface where an electron from a donor species can combine with the surface hole oxidizing the donor species (pathway D). A series of typical reactions in an aqueous environment are listed as Reaction (1)-(4). The generated highly oxidative radicals are able to oxidize the unsaturated phospholipids of the cell membrane, leading to the compromise of the cell walls and cell membranes, therefore cell lysis.

$$e^- + O_2 \rightarrow O_2^- \qquad \text{Reaction (1)}$$

$$O_2^- + H^+ \rightarrow HO_2^{\bullet} \qquad \text{Reaction (2)}$$

$$h^+ + H_2O \rightarrow {}^{\bullet}OH + H^+ \qquad \text{Reaction (3)}$$

$$h^+ + O_2^- \rightarrow 2{}^{\bullet}O \qquad \text{Reaction (4)}$$

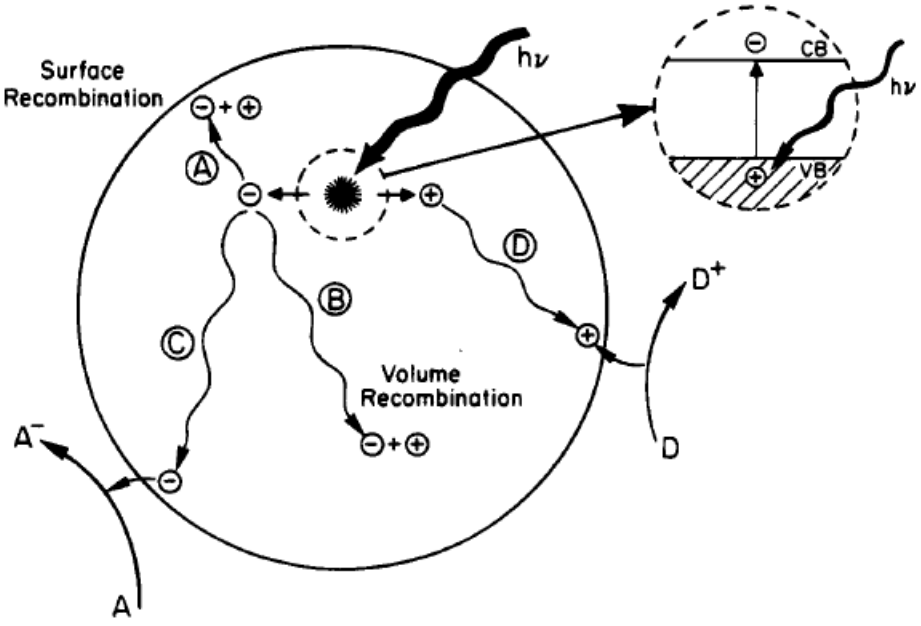

Figure 3-10. Photoexcitation and de-excitation pathways in a semiconductor material [142].

Among photocatalytic semiconductor materials, titanium dioxide is the most commonly used material for disinfection and bactericidal purposes due to its physical and chemical stability, high catalytic activity, high oxidative power and low cost [141, 145-147]. Titanium dioxide has three crystalline structures, named rutile, anatase and brookite. Rutile has the highest photocatalytic efficiency. The excitation light energy falls within UV range which corresponds to the band gap of 3.0 eV for rutile. They are inexpensive and easy to obtain from natural minerals. Conventionally, people use titanium dioxide powders for disinfection purposes. Although the crystallite size of the powders is around 30 nm, in aqueous conditions, they tend to aggregate to form larger groups which are typically 1~3 μm in size [148]. This is undesirable since photocatalytic efficiency is proportional to the surface area while aggregation causes considerable reduction of surface areas. Therefore, titanium dioxide nanoparticles with appropriate surface modifications to avoid aggregation are expected to have better efficiency compared to titanium dioxide powders.

Photocatalytic cell lysis is easy to be implemented on microchips by dispersing titanium dioxide nanoparticles in the solution containing cells to be lysed followed by exposing to UV from a miniaturized light source. A microchannel or a micro reaction chamber is all that is needed. Despite the advantages mentioned, there was no research work done to bring photocatalytic cell lysis to microchip level. Therefore, the research pioneered a novel cell lysis method utilizing photocatalytic effect for LOC applications.

3.2.1 Materials

3.2.1.1 Bacteria samples

E. coli was used in the experiments. They were grown in lysogeny broth (LB) nutrient medium at 37 ℃ over night. To prepare LB, 10 g of tryptone, 5 g of yeast extract, and 10 g of NaCl were dissolved in 1 L of distilled water followed by autoclaving at 121℃. Cells were washed twice with deionized water before experiments and were re-suspended in deionized water afterwards. They were stained using the Live/Dead BacLight bacterial viability kit (L7012, Molecular Probe, USA) to directly view

cell viability before and after experiments. Details about how to use the kit were described in Section 3.1.2.1 in details.

3.2.1.2 Titanium dioxide nanoparticles

Hydrophilic fumed titanium dioxide nanopowders with a specific surface area of 90~100 m^2/g and an average primary particle diameter of 14 nm (AEROXIDE P90) were obtained from Evonik Degussa Corporation. They were dispersed in autoclaved deionized water and were vigorously stirred for 10 minutes followed by ultrasonicating for 10 minutes. The concentration of the dispersion was 0.4 mg/mL. The absorption spectrum of titanium dioxide dispersion was measured using a spectrophotometer (NanoDrop ND-1000) as shown in Figure 3-11.

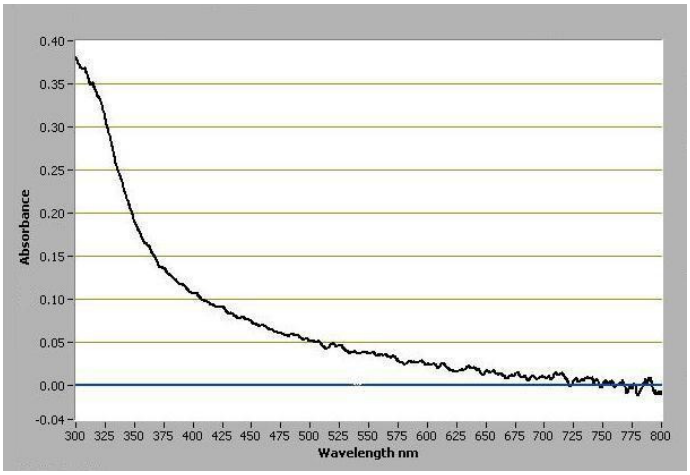

Figure 3-11. Absorption spectrum of titanium dioxide dispersion.

3.2.2 Methods

3.2.2.1 Microchip fabrication

Microchips were fabricated using regular microscope glass slides (75 mm × 25 mm) as substrates. Fabrication process is shown in Figure 3-12. An aluminum mold, which defined the size of the reaction chamber as shown in Figure 3-13, was fabricated by machining. Polydimethylsiloxane (PDMS) mixture was then prepared by well mixing the base and the curing agent at a weight ratio of 10:1 followed by degassing it in a vacuum oven for 60 minutes. After removing from the vacuum

oven, 5 mL of the PDMS mixture was poured on top of the aluminum mold. After curing at 90℃ in an oven for 60 minutes, the cross-linked PDMS layer was carefully peeled off from the aluminum mold. Fluid inlet and outlet were constructed on the PDMS sheet using a hole punch with a diameter of 2 mm. Microscope glass slides were cleaned with acetone and then rinsed with deionized water. Both the PDMS sheet and the clean glass slide were placed in a plasma oven (Harrick plasma cleaner PDC-001) for 45 seconds at a power of 10 W before bonding them together. Plastic tubings with an outer diameter of 2 mm and an inner diameter of 1 mm were inserted to the hole on the PDMS layer and were sealed using epoxy at the connection. Bacteria solution were pumped into the microchip using a peristaltic pump (P720, INSTECH Inc.). Two air tight plugs were then used to cover both flow inlet and outlet to minimize the effect of airflow in the reaction chamber and to prevent solution from evaporating.

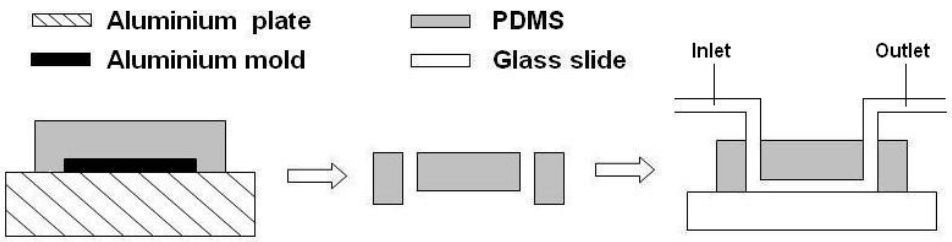

Figure 3-12. Microchip fabrication process.

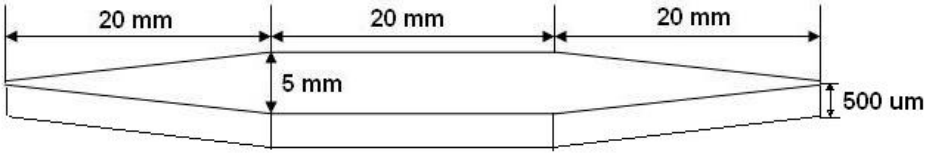

Figure 3-13. Dimension of the reaction chamber.

3.2.2.2 Miniaturized UV light source

In order to generate photocatalytic effect, a miniaturized UV light source is required for LOC applications. Generally speaking, noticeable photocatalytic effect is generated when UV intensity is greater than 1 mW/cm^2 [149-151]. Since a single UV LED did not have the power to generate enough

UV intensity, UV LED array was introduced. A customized PCB board was designed and fabricated. 5 UV LEDs (NSSU100A, Nichia Corporation) were placed on top of the board as shown in Figure 3-14. The size of the PCB board measures 5 cm × 2 cm. UV intensity was determined to be 1.2 mW/cm^2 measured by a radiometer (ILT1700, InternationalLight Technologies Inc.). UV emission spectrum shown in Figure 3-15 was provided by Nichia [152]. By comparing Figure 3-11 and Figure 3-15, it was confirmed that UV emission spectrum fell within the absorption spectrum of the titanium dioxide dispersion.

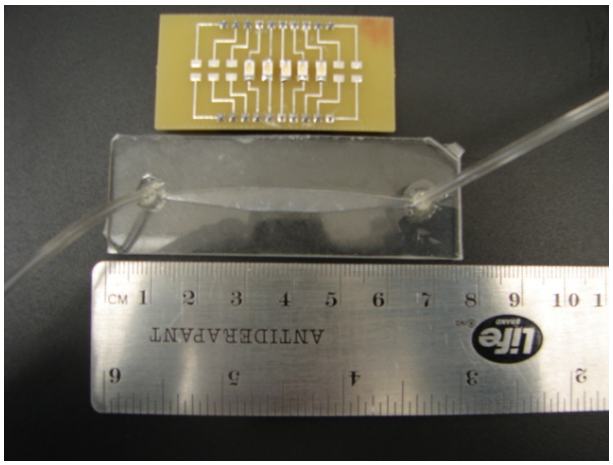

Figure 3-14. UV LED array and a microchip.

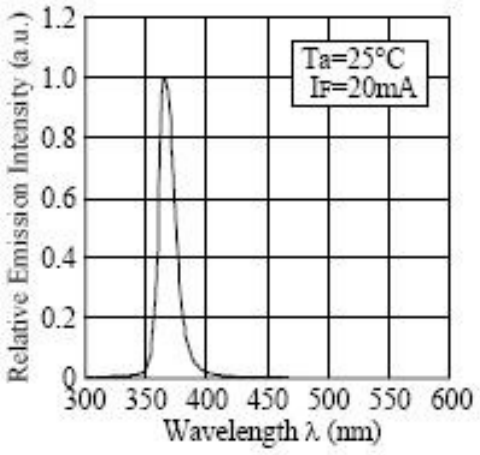

Figure 3-15. UV LED emission spectrum [152].

3.2.3 Results and Discussion

A series of control experiments were conducted before showing that titanium dioxide particles plus UV irradiation were the main cause of cell lysis. In the first control experiment, whether the constructed microchips provided a friendly environment to *E. coli* was evaluated. 50 μL of pure *E. coli* solution was pumped into the microchip which was then placed under an indoor ambient condition for 120 minutes. Figure 3-16(a) and (b) show fluorescent images recorded before and after the experiment. Green dots represent cells with intact cell membranes while red dots represent cells with compromised cell membranes. As shown in the figures, the ratios between green dots and red dots in both images are similar. This implies that cell membranes remained intact during the experiment. To quantify the result, cell viability was determined at different time intervals for the experiment as shown in Figure 3-16(c). The result suggestes that the fabricated microchips provided a friendly environment to *E. coli* at least for 120 minutes.

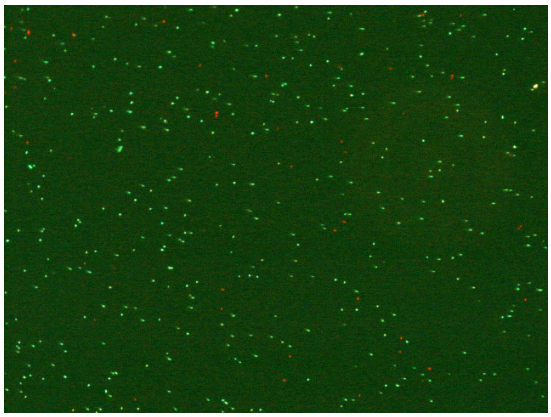

(a)

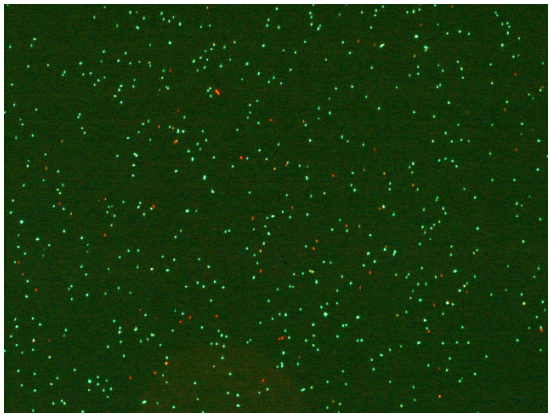

(b)

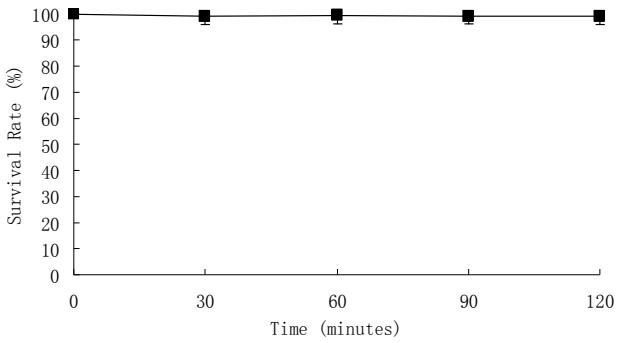

(c)

Figure 3-16. *E. coli* survival rate against UV irradiation time for control experiment 1. (a) Before experiment; (b) After experiment; (c) Cell survival rate against time.

The second control experiment was to evaluate whether UV irradiation alone can induce cell lysis. 50 μL of pure *E. coli* solution was pumped into a microchip. The UV LED array was then placed on top of the microchip from PDMS side as PDMS allows UV to go through [153]. UV irradiation was turned on for 60 minutes. Fluorescent images were recorded before and after the experiment. During the experiments, it was observed that UV LED array generated noticeable heat along with irradiation time. A microchip was used to characterize the temperature variation in the microchannel by embedding a thermocouple directly in the microchannel sandwiched between the top PDMS layer and the bottom glass substrate. Figure 3-17 shows temperature change along with irradiation time. At the steady state, the average temperature of the solution was 39.4℃. Since *E. coli* can survive up to 50℃ [90, 91], the temperature increase caused by UV LED did not induce cell lysis. Both qualitative and quantitative results are shown in Figure 3-18.

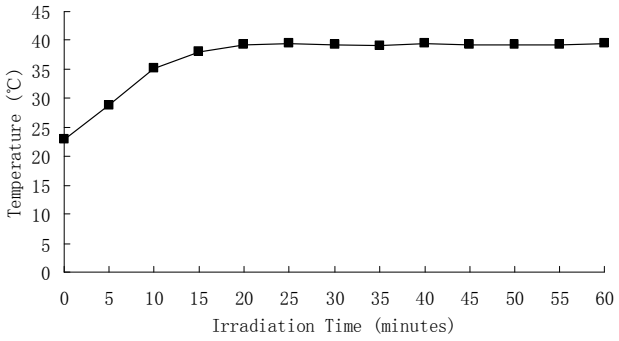

Figure 3-17. Temperature variation in the microchannel due to the heating effect of UV LEDs.

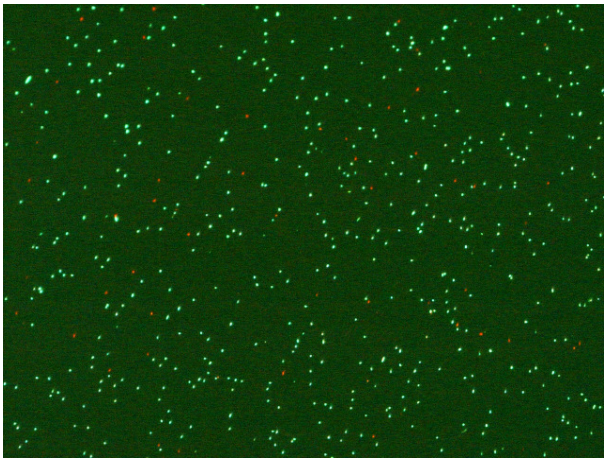

(a)

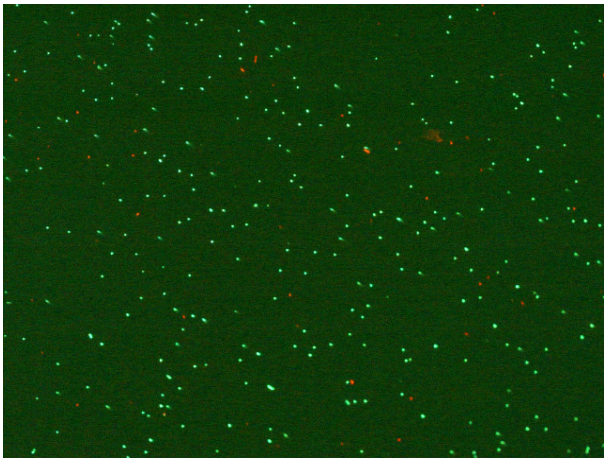

(b)

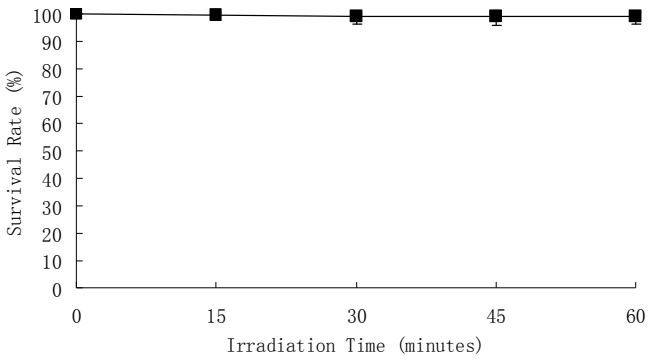

(c)

Figure 3-18. Effect of 365 nm UV on *E. coli*. (a) Before UV irradiation; (b) 60 minutes after UV irradiation; (c) Cell survival rate against UV irradiation time.

In the third control experiment, the effect of titanium dioxide particles without UV irradiation was evaluated. A mixture of *E. coli* and titanium dioxide particles was prepared at a volume ratio of 1:10. 50 μL of the mixture was pumped into a microchip which was then placed in darkness for 60 minutes. Fluorescent images were recorded before and after the experiment. As shown in Figure 3-19 (a) and (b), the ratios of green dots and red dots for both images were almost the same. This indicates that cell membranes remained intact after being placed in darkness for 60 minutes with titanium dioxide particles in the solution. This implies that titanium dioxide particles alone without UV irradiation did not induce cell lysis effect.

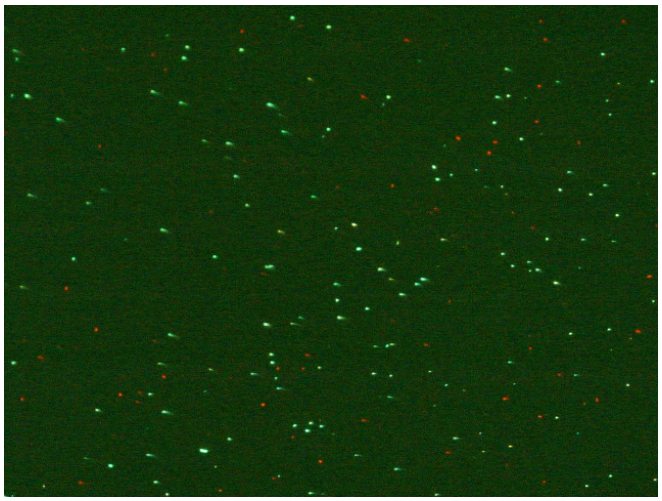

(a)

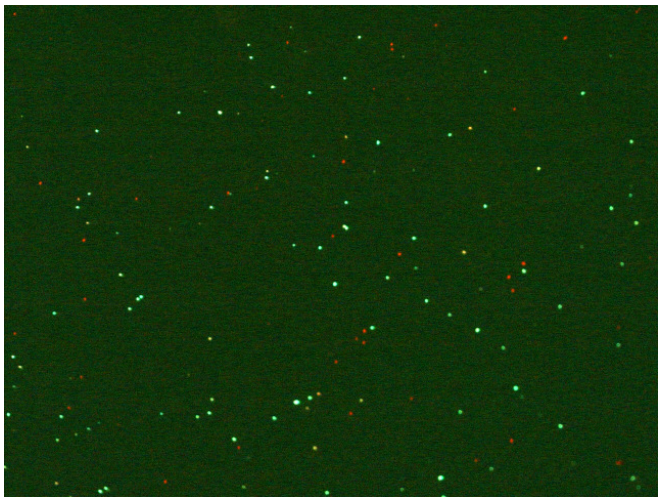

(b)

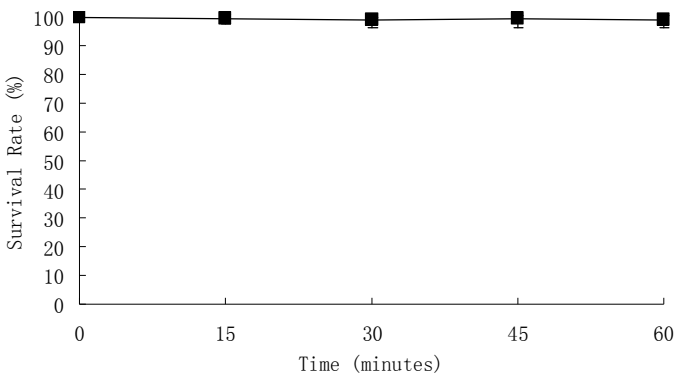

(c)

Figure 3-19. Effect of titanium dioxide particles on *E. coli* in darkness. (a) Before placed in darkness; (b) 60 minutes after being placed in darkness; (c) Cell survival rate against reaction time.

Finally, the effect of both titanium dioxide particles and UV irradiation on *E. coli* at the same time was evaluated. A mixture of *E. coli* and titanium dioxide particles at a volume ratio of 1:10 was pumped into the microchip reaction chamber. UV LED array was placed on top of the microchip from the PDMS side. Figure 3-20(a) and (b) show fluorescent images recorded before and after UV irradiation for 45 minutes in an experiment. As shown in the figures, the number of cells with intact cell membranes (green dots) decreased dramatically along with time. Within 45 minutes, almost neither green nor red dots can be observed in Figure 3-20(c). It has to be mentioned that the bacterial viability kit utilizes mixtures of green-fluorescent and red-fluorescent nucleic acid stains. However, in order to physically see cells, nucleic acid concentration has to be high enough [154]. Therefore, Figure 3-20 suggests that most cells were completely disintegrated therefore nucleic acid concentration was so diluted that fluorescent signals were too weak to discriminate from background signals. Same experiments were repeated 5 times for each time period of 15, 30, 45 and 60 minutes followed by fluorescence protocols to get a statistical view towards how bacteria survival rate changed with irradiation time as shown in Figure 3-20(d). It is clear that titanium dioxide nanoparticles plus UV irradiation resulted in an efficient cell lysis on *E. coli* in 60 minutes. Figure 3-20(b) also reveals a fact that cells were not lysed at the same rate. It is quite possible that titanium dioxide particles at the bottom of the reaction chamber received less UV irradiation compared to the ones at the top therefore cannot keep up the same cell lysis rate. This can cause problems in

applications where DNA and proteins are to be kept intact because oxidizing process can have a detrimental effect on DNA or proteins [148, 155, 156]. However, the first barrier to the oxidizing process is the cell membrane as demonstrated in [157-159] as well as in this work. Based on the evidence, it is reasonable to predict that intracellular materials such as DNA and proteins are intact before cell membranes are disrupted. A potential solution to address the issue is to design a new microchip with a chamber of smaller depth which is close to the dimension of the bacteria. By doing so, all cells and surrounding titanium dioxide particles receive adequate and similar UV irradiation dose so that cells are lysed in a similar rate and we can have control over when cell membranes are disrupted while intracellular materials remain intact by controlling UV irradiation time.

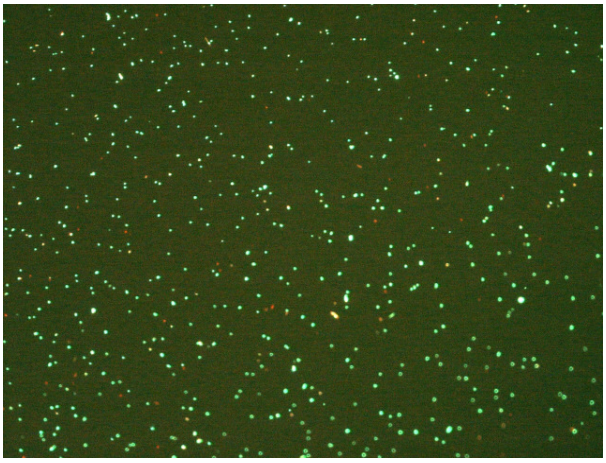

(a)

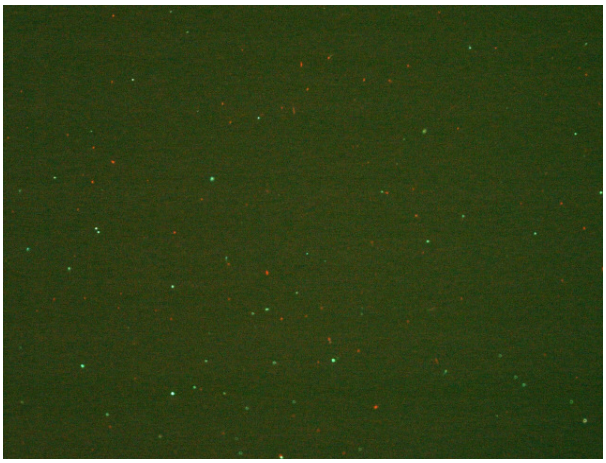

(b)

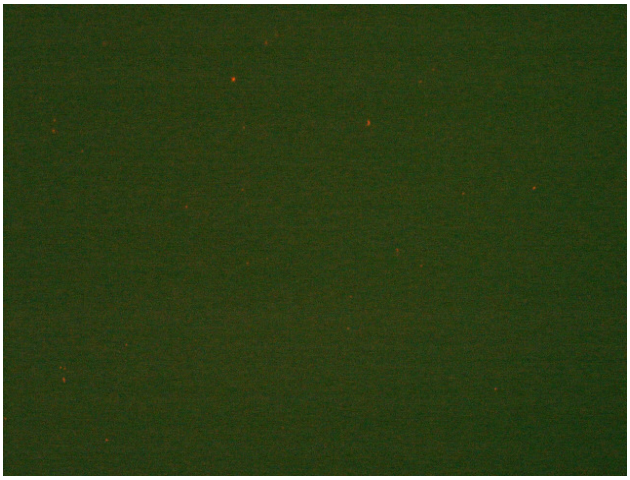

(c)

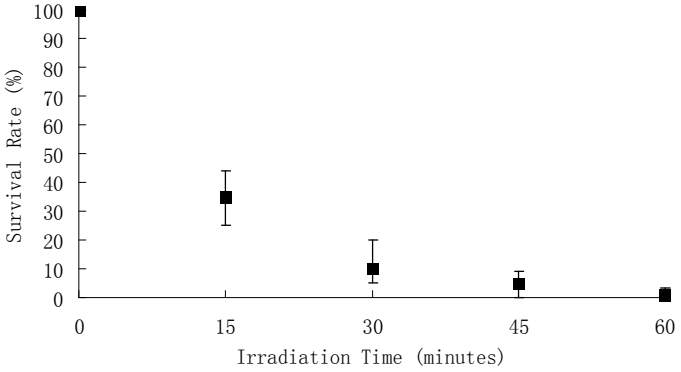

(d)

Figure 3-20. Effect of titanium dioxide particles under 365 nm UV irradiation on *E. coli*. (a) Before UV irradiation; (b) 30 minutes after UV irradiation; (c) 45 minutes after UV irradiation; (d) Cell survival rate against UV irradiation time.

3.2.4 Summary

Experiments were conducted to demonstrate a novel cell lysis method for LOC devices using titanium dioxide particles and a miniaturized UV LED. The cell lysis method is based on photocatalytic effect of titanium dioxide nanoparticles to generate highly oxidative radicals to attack cell membranes. *E. coli* cells were used in the experiments to evaluate cell lysis effect. Several control experiments were conducted first to demonstrate that the fabricated microchips were not the cause of the cell lysis and

UV irradiation alone did not induce cell lysis. It was experimentally determined that most *E. coli* cells can be disrupted in 60 minutes. A potential solution to improve the performance of cell lysis by re-designing the microchip is proposed. The method is easy to be integrated with other functional modules to form a whole LOC system.

Chapter 4

Effects of Nanoparticles on Polymerase Chain Reaction

In Chapter 3, two novel cell lysis methods involving nanoparticles were presented. The next question to answer is what kind of effects these nanoparticles induce when they are part of the PCR reaction. This chapter presents research activities and results towards understanding effects of nanoparticles on PCR. Section 3.1 describes how gold nanoparticles affect PCR. Section 3.2 describes how titanium dioxide nanoparticles affect PCR.

4.1 Effects of Gold Nanoparticles on PCR

Polymerase Chain Reaction (PCR) is a widely used technology that enables researchers to produce millions of copies of a specific region of DNA in vitro. It is marked as one of the most important inventions in Biotechnology in the 20th century and is widely used in gene amplification, DNA cloning, functional analysis of DNA, diagnosis of diseases and so on [45-47]. Nanoparticles possess outstanding properties that are not seen in their bulk forms due to their small sizes. This results in many potential applications in biotechnology [161, 162]. The evaluation of the effect of nanoparticles, especially gold nanoparticles, on PCR is a relatively new research area and is attracting more attention recently. Li *et al.* [162] reported that gold nanoparticles can be added in PCR reagents to avoid non-specific products at lower annealing temperatures. According to the authors, gold nanoparticles' effects similar to single-stranded DNA binding protein should account for the improvement. As for how gold nanoparticles affect PCR efficiency, some researchers found that gold nanoparticles can improve PCR efficiency [163], but some researchers reported contradictory observations [164, 165]. Li *et al.* [163] found that gold nanoparticles can improve the efficiency of PCR at an appropriate concentration when using a fast-speed cycling PCR machine. The authors suspected that the heat conductivity of gold nanoparticles plays the most important role in increasing the efficiency of the PCR by dramatically shortening the time required [166]. Yang *et al.* [164] evaluated gold nanoparticles in PCR with SYBR Green I. They suggested that a complex interaction exists between gold nanoparticles and native Taq DNA polymerase, which can reduce PCR efficiency

at a high concentration of gold nanoparticles. Vu *et al.* [165] demonstrated that gold nanoparticles tend to favor smaller products than larger ones and they inhibit PCR at a certain concentration. Possible reasons concerning the contradiction can be different gold nanoparticles used in terms of surface modification and some other different experimental conditions. This section describes research activities towards understanding how gold nanoparticles interact with PCR components to induce PCR inhibition as well as understanding how induced PCR inhibition can be suppressed. How sizes of gold nanoparticles are related to PCR efficiency was also evaluated. A series of experiments were conducted to explore the mechanism behind the phenomenon.

4.1.1 Materials

4.1.1.1 Gold nanoparticles

Gold nanoparticles used in the experiments described in Chapter 3 were used in the experiments described in this chapter as well. High resolution TEM images and other information can be found in Section 3.1.1.1 in details. To better understand how sizes of gold nanoparticles affected PCR, aqueous solutions of monodispersed gold nanoparticles of 5, 10 and 20 nm in diameter were obtained from Sigma. High resolution TEM images of the samples obtained from Sigma are shown in Figure 4-1. Table 4-1 lists specifications of these gold nanoparticles in details.

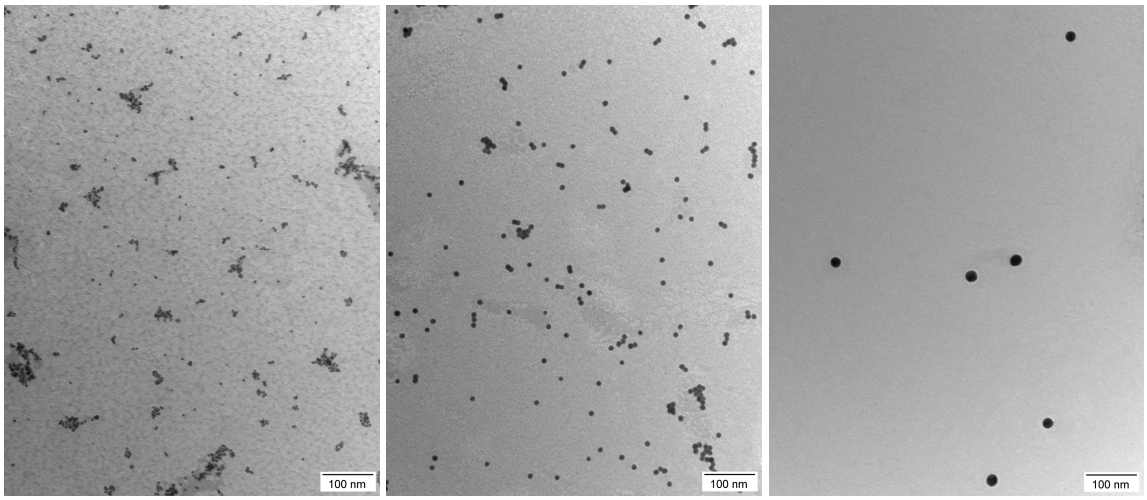

(a) (b) (c)

Figure 4-1. TEM images of the gold nanoparticles obtained from Sigma. (a) 5 nm; (b) 10 nm; (c) 20 nm.

Table 4-1. Specifications of 5, 10 and 20 nm gold nanoparticles used in the experiments

	5 nm nanoparticles	**10 nm nanoparticles**	**20 nm nanoparticles**
Mean diameter (nm)	4.3	9.7	21
Coefficient of variation	19.4%	14%	12%
Concentration (particles/mL)	4.10×10^{13}	5.74×10^{12}	3.63×10^{11}

4.1.1.2 PCR reagents and DNA templates

Salmonella enterica ATCC 13311 was used as DNA templates. The target gene was invasion (*invA*) gene for *Salmonella* species (GenBank accession number: M90846 [167]). Table 4-2 lists the primers and Taqman probe for amplification of a 119-bp sequence [168].

Table 4-2. Primers and Taqman probe used in the experiments

Forward primer	5'-TCGTCATTCCATTACCTACC-3'
Reverse primer	5'-AAACGTTGAAAAACTGAGGA-3'
Taqman probe	FAM-CTGGTTGATTTCCTGATCGCA-BHQ1

Primers, TaqMan probe, dNTP mix (dATP, dCTP, dGTP and dTTP) were obtained from Sigma. iTaq polymerase, 10X PCR buffer and magnesium chloride were obtained from Bio-Rad. PCR was performed in a 25 µL reaction volume. The optimal amount of all reagents and DNA template in each reaction of 25 µL without adding gold nanoparticles was 0.75 µL of each of primer A and B, 0.25 µL of Taqman probe, 200 µM dNTPs, 2.5 µL of 10x PCR buffer, 0.625 U of iTaq polymerase, 3.5 mM $MgCl_2$ and 5 µL of DNA template. In some of the experiments, the concentration of the reagents was changed on purpose to evaluate their interactions with gold nanoparticles. DNA template concentration was adjusted from 30 ng/mL to 30 pg/mL as a standard series with each step differing by 10 fold.

4.1.1.3 Other chemicals

Other chemicals used in the experiments included agarose from VWR, ethidium bromide, Tris-acetate-EDTA (TAE) buffer from Sigma and 100 bp DNA ladder from BioLabs.

4.1.2 Methods

4.1.2.1 Experiment procedures

PCR master mix including forward and reverse primers, Taqman probe, dNTP mix, PCR buffer, magnesium chloride and iTaq polymerase was first prepared and aliquoted into PCR tubes suitable for reaction with a 25 μL volume. Each set of experiments designed to evaluate the effect of nanoparticle sizes contained five tubes. Water was added to the first tube as negative control. DNA template without gold nanoparticles was added to the second tube. DNA template with 5, 10 and 20 nm gold nanoparticles was added to the following tubes consecutively. In the experiments designed to evaluate the effect of poly(quaternary ammonium) modified gold nanoparticles, there were three tubes per experiment run. The first tube had water as negative control. The second tube had DNA template without gold nanoparticles. The third tube had DNA template with gold nanoparticles.

4.1.2.2 PCR programs and real-time PCR system

The PCR program was set as follows: 3 minutes at 95℃ for hot start, 50 cycles of amplification at 95 ℃ for 15 seconds, 60℃ for 30 seconds, 72℃ for 30 seconds, and 10 minutes at 72℃ for final extension. iCycler real-time PCR machine from Bio-Rad was used as shown in Figure 4-2. Fluorescent signal was detected at the end of each cycle. Excitation light was set at 490 nm and emission light was detected at 530 nm. Amplification curves were analyzed at the end.

Figure 4-2. Real-time PCR system used in the experiments.

4.1.2.3 Gel electrophoresis

Gel electrophoresis was used to analyze PCR products in addition to real-time fluorescence monitoring. 2% agarose gel was prepared by dissolving 0.6 g of agarose in 30 mL of distilled water in a 50 mL beaker followed by adding 600 µL of 50X TAE buffer. The beaker was placed on a hot plate until boiling. After cooling down for 5 minutes, the gel liquid was poured in a PMMA mould with a removable comb placed on top to define wells. The comb was carefully removed after 45 minutes when the gel turned to solid. The gel was placed in a gel electrophoresis chamber filled with 1X TAE buffer as shown in Figure 4-3. A constant voltage of 100 V and a running time of 45 minutes were set. The gel was removed from the chamber after gel electrophoresis and was immersed in 0.5 µg/ml ethidium bromide solution for 20 minutes followed by UV imaging process.

Figure 4-3. Gel electrophoresis apparatus used in the experiments.

4.1.3 Results and Discussion

Experiments were conducted to evaluate the effect of sizes of gold nanoparticles on PCR. At low concentrations of gold nanoparticles of all sizes, for example at 3 nM for 5 nm gold nanoparticles, at 0.4 nM for 10 nm gold nanoparticles and at 0.03 nM for 20 nm gold nanoparticles, no obvious effect was observed, neither improving nor inhibitory effect. When the concentration of gold nanoparticles was increased, inhibitory effect was observed. The threshold concentrations causing obvious inhibitory effect for 5, 10 and 20 nm gold nanoparticles were experimentally determined to be 5.5 nM, 1.1 nM and 0.24 nM respectively. PCR is a sensitive chemical reaction and involves many chemical

components. Therefore, experiments were conducted to evaluate which chemical components were responsible for the inhibitory effect. The experiment was performed as follows: at complete PCR inhibition, increasing the concentration of a chemical component one at a time to see whether DNA amplification could be observed. It was first observed that changing the concentration of iTaq polymerase affected the amplification curve. Figure 4-4 shows the PCR amplification curves with 5 nm gold nanoparticles at 13.6 nM and different amounts of iTaq polymerase. Complete PCR inhibition was observed for all standard DNA series when 5 nm gold nanoparticles at 13.6 nM were added to the PCR solution containing 0.625 U of iTaq polymerase as shown in Figure 4-4(a). When the amount of iTaq polymerase was increased to 1.25 U per reaction, DNA amplification was observed although the product yield was suppressed as shown in Figure 4-4(b). Similar behavior was observed for the 10 and 20 nm gold nanoparticles at different concentrations. Figure 4-4 clearly suggests that there was an interaction between gold nanoparticles and iTaq polymerase. Since DNA polymerase is an indispensible component to make PCR work, the interaction between gold nanoparticles and iTaq polymerase should account for the PCR inhibition. Gel electrophoresis was performed to confirm the correct product size after PCR as shown in Figure 4-5.

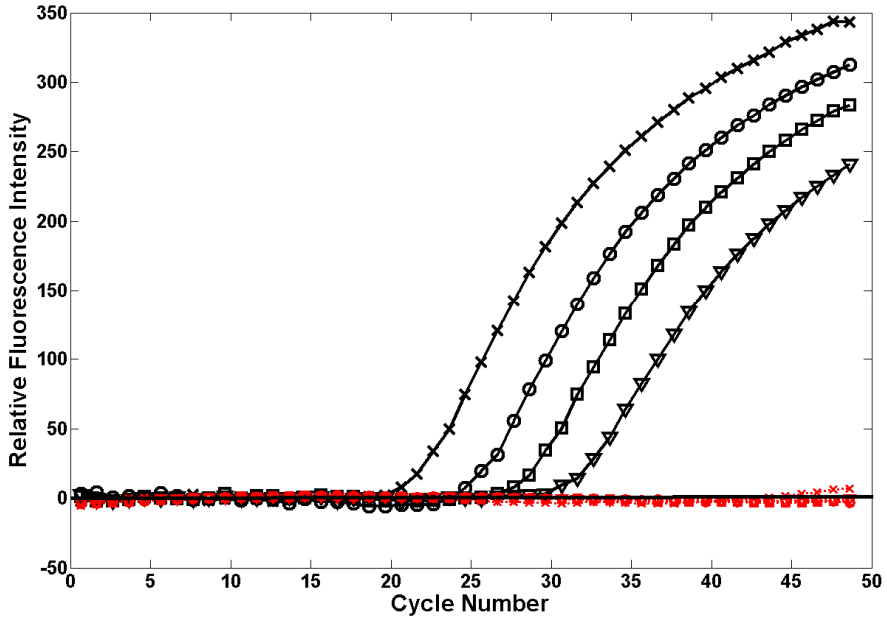

(a)

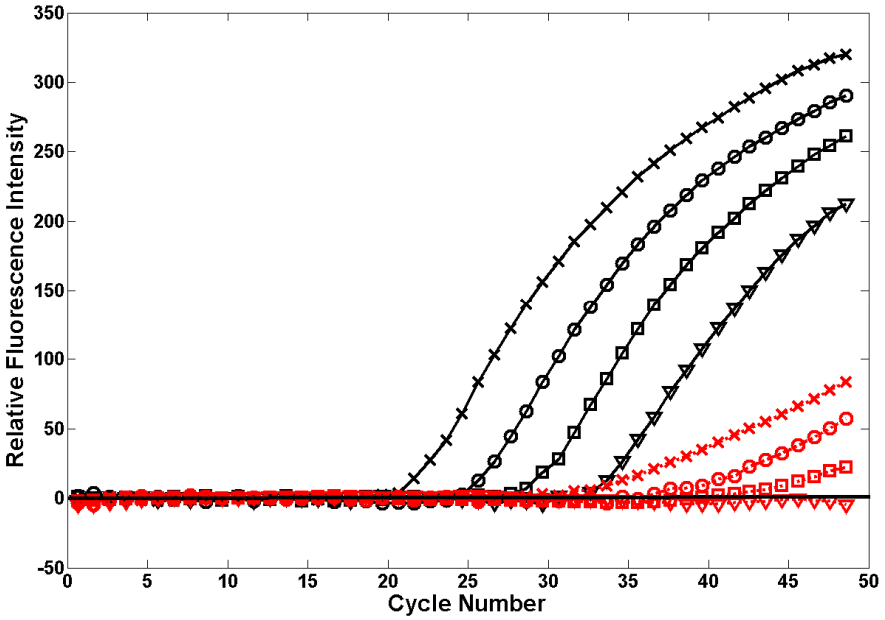

(b)

Figure 4-4. PCR amplification curves with gold nanoparticles and various amounts of iTaq polymerase. ×− Starting DNA concentration was 10^7 cells/mL, ○− Starting DNA concentration was 10^6 cells/mL, □− Starting DNA concentration was 10^5 cells/mL, ▽− Starting DNA concentration was 10^4 cells/mL. Black curves are reference curves without gold nanoparticles and red curves are experimental curves with gold nanoparticles. (a) 0.625 U of iTaq polymerase per reaction; (b) 1.25 U of iTaq polymerase per reaction.

Besides iTaq polymerase, it was also observed that PCR amplification curves could be changed dramatically by changing the amount of BSA in the reaction solution. When 1.25 µL of 5 nm gold nanoparticles was added to the PCR solution containing 2.5 µg of BSA, partial PCR inhibition was observed for all standard DNA series as shown in Figure 4-6(a). However, when the amount of BSA was increased to 10 µg, no PCR inhibition was observed at all in Figure 4-6(b). This suggests that gold nanoparticles can also interact with BSA. PCR inhibition caused by gold nanoparticles can be reversed by adding more BSA to the reaction solution. This is an efficient way of suppressing PCR inhibition caused by gold nanoparticles.

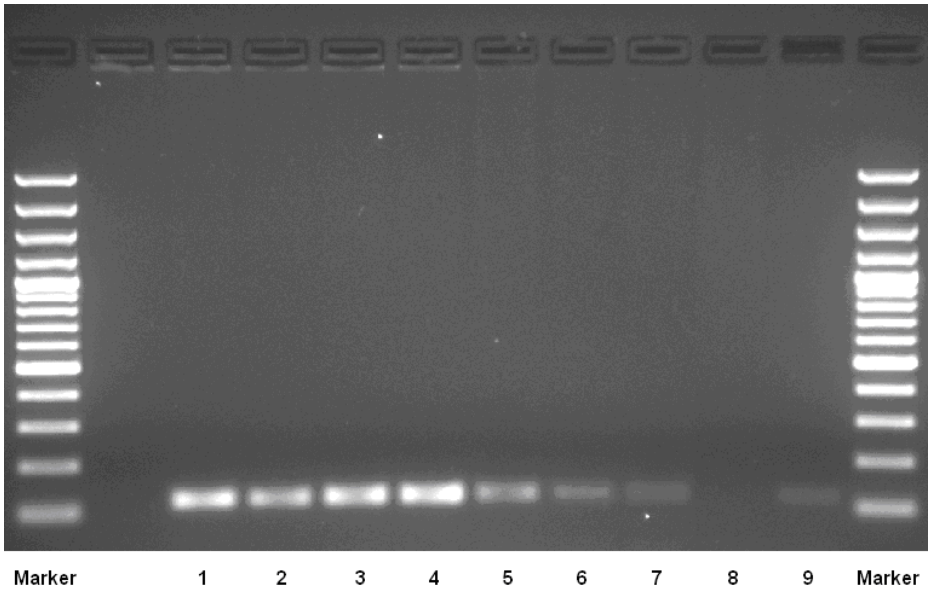

Figure 4-5. Gel electrophoresis result with various experimental conditions. Lane 1-4: DNA template was 30 pg/mL, 300 pg/mL, 3 ng/mL and 30 ng/mL without gold nanoparticles; Lane 5: DNA template was 30 ng/mL with 5 nm gold nanoparticles at 6.8 nM; Lane 6: DNA template was 30 ng/mL with 10 nm gold nanoparticles at 1.9 nM; Lane 7: DNA template was 30 ng/mL with 20 nm gold nanoparticles at 0.24 nM; Lane 8-9: complete and partial PCR inhibition was observed when different amounts of iTaq polymerase was used. Lane 8: DNA template was 30 ng/mL with 5 nm gold nanoparticles at 13.6 nM and 0.625 U (1X) of iTaq polymerase; Lane 9: DNA template was 30 ng/mL with 5 nm gold nanoparticles at 13.6 nM and 1.25 U (2X) of iTaq polymerase.

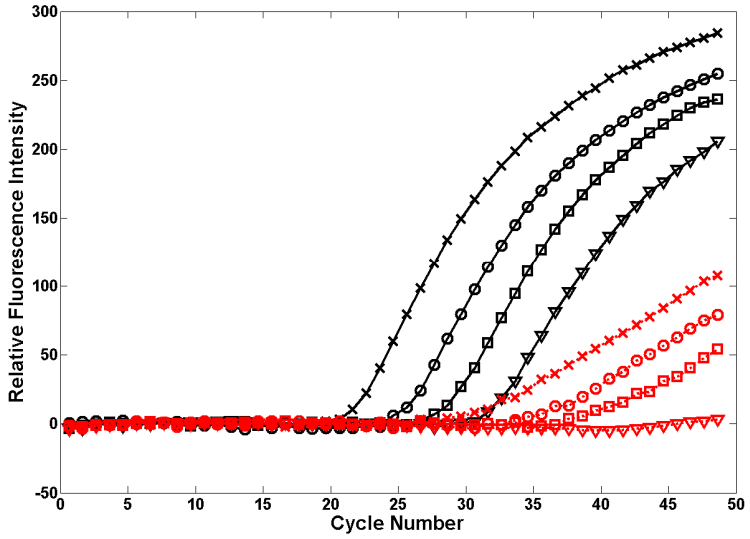

(a)

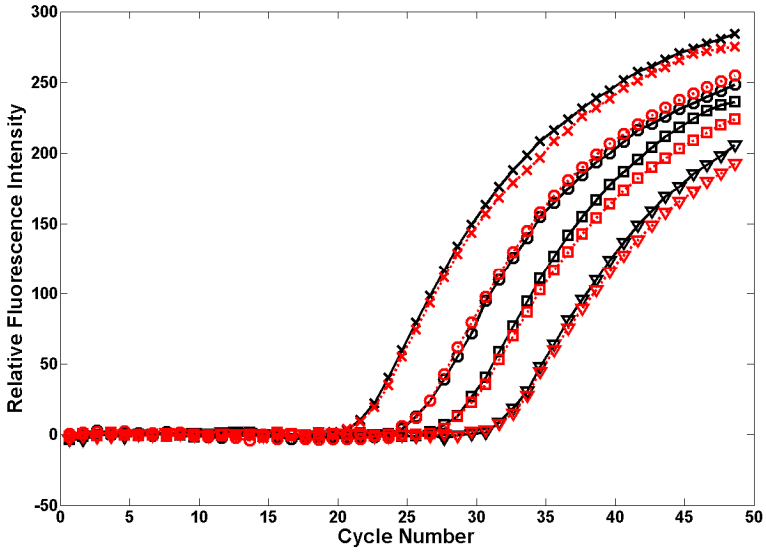

(b)

Figure 4-6. PCR amplification curves with gold nanoparticles and various amounts of BSA. ×− Starting DNA concentration was 10^7 cells/mL, ○− Starting DNA concentration was 10^6 cells/mL, □− Starting DNA concentration was 10^5 cells/mL, ▽− Starting DNA concentration was 10^4 cells/mL. Black curves are reference curves without gold nanoparticles and red curves are experimental curves with gold nanoparticles. (a) 2.5 µg of BSA per reaction; (b) 10 µg of BSA per reaction.

In the next experiment, the effect of gold nanoparticles of different sizes at the same particle concentration was evaluated. Experiments with 5, 10 and 20 nm gold nanoparticles at the same concentration of 1.9 nM in the 25 µL reaction volume were performed. The volumes of the 5 and 10 nm gold nanoparticles at 1.9 nM were 0.7 and 5 µL respectively. The original concentration of the 20 nm gold nanoparticles was too small to be used. Therefore, 8X concentrated solution was prepared and 9.8 µL was needed. To prepare concentrated solution for 20 nm gold nanoparticles, a tube containing 100 µL of the stock nanoparticle dispersion was placed in a tabletop centrifuge at 12,000 rpm for 15 minutes. After repeating the procedure two times, the tube was carefully removed from the centrifuge and 87.5 µL of the supernatant was removed followed by sonicating for 10 minutes. The amplification curves are plotted in Figure 4-7. It clearly shows that nanoparticle size had an impact on the inhibitory effect. At 1.9 nM, 5 nm gold nanoparticles almost had no effect on PCR while 10 nm gold nanoparticles showed partial inhibition with product yield reduced by half. At this concentration,

20 nm gold nanoparticles led to complete inhibition on PCR without DNA amplification. Similar behavior was observed for DNA template from 3 ng/mL to 30 pg/mL. Figure 4-7 suggests that a higher concentration of smaller gold nanoparticles was required to cause complete PCR inhibition than larger gold nanoparticles. In order to explore the probable mechanism of the interaction between DNA polymerase and gold nanoparticles, two experiments were conducted. In the first experiment, a mixture containing iTaq polymerase, water and 20 nm gold nanoparticles was prepared and well mixed. The concentration of iTaq polymerase was ensured to be 0.625 U per reaction. The amount of gold nanoparticles was chosen such that it caused partial PCR inhibition when added to the PCR solution. A centrifugation step was then followed at 12,000 rpm for 8 minutes and the supernatant was carefully transferred to a new tube. Other PCR chemicals were added to the tube at their optimal concentrations. The resulting PCR mix was aliquoted into PCR tubes and DNA template was added to each tube. DNA amplification was observed with partial inhibition after 50 PCR cycles. The observation confirmed that gold nanoparticles interacted with iTaq polymerase to inhibit PCR. The second experiment followed the procedure in the first experiment. The only difference was the amount of gold nanoparticles which was chosen such that it caused complete PCR inhibition when added to the PCR solution. No DNA amplification was observed after 50 cycles. The observations from both experiments led to a hypothesis that is gold nanoparticles and iTaq polymerase bound to each other when mixed together. This could explain why in the first experiment, when limited amount of gold nanoparticles was present, there was still free iTaq polymerase in the supernatant although it was not in the optimal concentration therefore resulting in partial PCR inhibition; in the second experiment, when excessive amount of gold nanoparticles was used, all iTaq polymerase bound to gold nanoparticles leaving no free polymerase in the supernatant to participate in PCR.

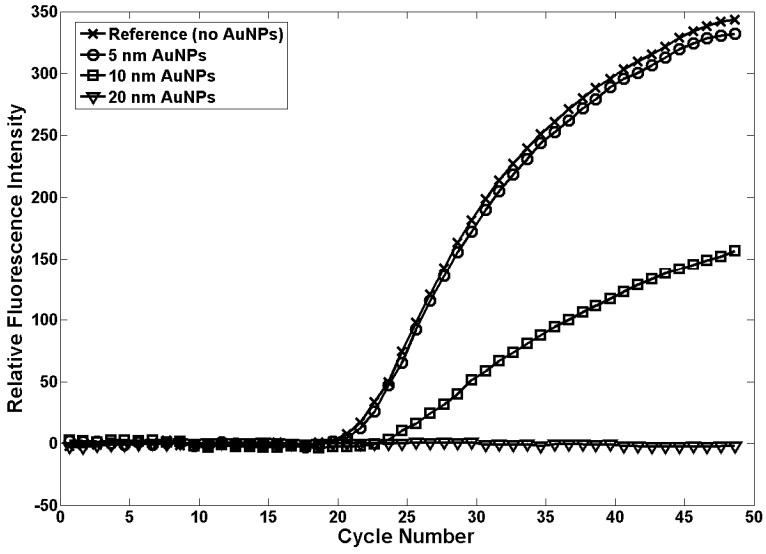
Reference (no AuNPs)
5 nm AuNPs
10 nm AuNPs
20 nm AuNPs
Relative Fluorescence Intensity
Cycle Number
350
300
250
200
150
100
50
0
-50
0
5
10
15
20
25
30
35
40
45
50

(a)

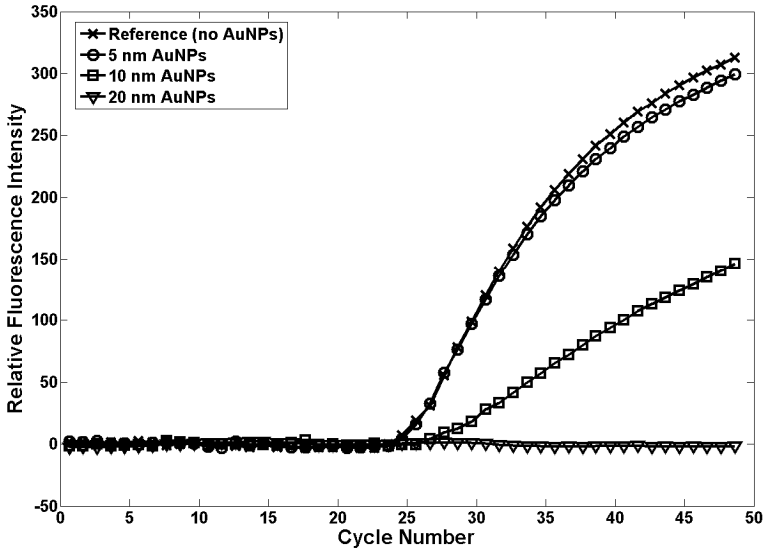
Reference (no AuNPs)
5 nm AuNPs
10 nm AuNPs
20 nm AuNPs
Relative Fluorescence Intensity
Cycle Number
350
300
250
200
150
100
50
0
-50
0
5
10
15
20
25
30
35
40
45
50

(b)

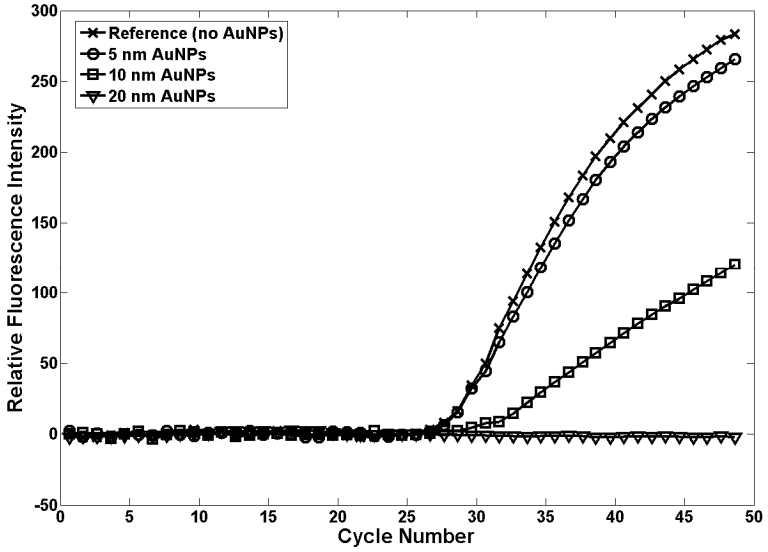

(c)

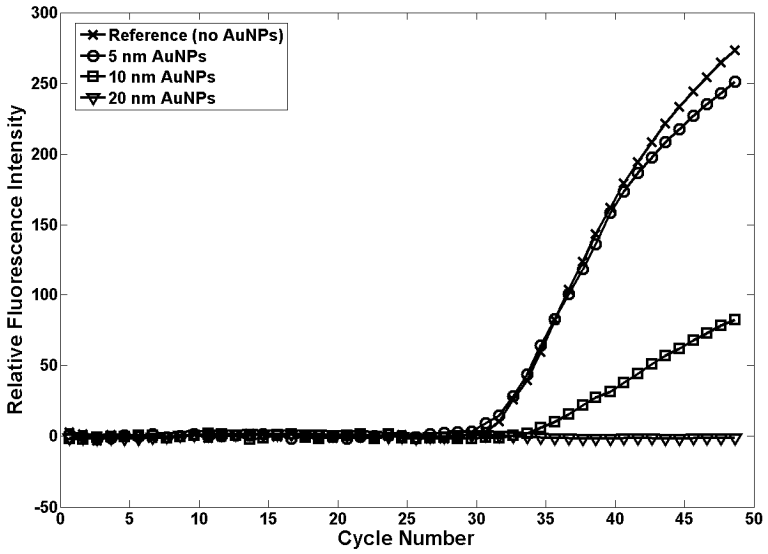

(d)

Figure 4-7. PCR amplification curves with 5, 10 and 20 nm gold nanoparticles at the same nanoparticle concentration of 1.9 nM. ×− No gold nanoparticles, ○− 5 nm gold nanoparticles, □− 10 nm gold nanoparticles, ▽− 20 nm gold nanoparticles. Gold nanoparticles of larger sizes had stronger inhibitory effect on PCR than those of smaller sizes at the same nanoparticle concentration. Starting DNA concentration was (a) 30 ng/mL; (b) 3 ng/mL; (c) 300 pg/mL; (d) 30 pg/mL.

To further testify the hypothesis, a set of experiments were conducted to determine the critical concentration of gold nanoparticles of each size. Critical concentration is defined as the minimum concentration of gold nanoparticles that is required to cause complete PCR inhibition. In other words, complete PCR inhibition was observed when the concentration of gold nanoparticles was larger than the critical concentration while partial PCR inhibition was observed when the concentration of gold nanoparticles was smaller than the critical concentration. It was experimentally determined that the critical concentration of the 5, 10 and 20 nm gold nanoparticles was 13.03 nM, 2.85 nM and 0.63 nM respectively, with $\pm 5\%$ variation. Since nanoparticles have large surface-area-to-volume ratio, interactions between nanoparticles and polymerase are quite likely dominated by surface interaction. Therefore, it is necessary to compare the surface areas of the gold nanoparticles at the critical concentrations. The mean total surface area of the gold nanoparticles of all sizes when complete PCR inhibition just occurs can be calculated based on the data collected in the experiments. Assume all nanoparticles are spheres, mean unit surface area is calculated as

$$\overline{A_u} = E(4\pi(r/2)^2) = \pi[(E(r))^2 + (u \cdot C_v)^2] = \pi[u^2 + (u \cdot C_v)^2]$$

where r is particle diameter, u is mean particle diameter, C_v is coefficient of variation, mean total surface area $\overline{A}$ is calculated as $\overline{A} = L \cdot P \cdot V_c \cdot \overline{A_u}$, where L is the Avogadro constant, P is critical concentration and V_c is reaction volume. Values listed in Table 4-1 are used in the calculation. Table 4-3 shows the critical concentrations, mean unit surface areas and mean total surface areas of the 5, 10, and 20 nm gold nanoparticles that inhibit PCR completely.

Table 4-3. Minimum amount of the 5, 10 and 20 nm Gold nanoparticles required to induce complete PCR inhibition

	5 nm nanoparticles	**10 nm nanoparticles**	**20 nm nanoparticles**
Critical concentration (nM)	13.03	2.85	0.63
Mean unit surface area (nm^2)	60.4	301.2	1404
Mean total surface area (nm^2)	$1.2\times10^{13} \pm 5\%$	$1.3\times10^{13} \pm 5\%$	$1.3\times10^{13} \pm 5\%$

As shown in Table 4-3, the mean total surface areas of the 5, 10 and 20 nm gold nanoparticles at the corresponding critical concentrations are almost equal. The result indicates that no matter what

size they have, the total surface areas of the gold nanoparticles are the same at the point when complete PCR inhibition starts to occur. It is also a perfect match with the proposed hypothesis since binding is a surface interaction and binding capacity is linearly proportional to total surface area. Therefore, given the fact that the amounts of iTaq polymerase used in all reactions were the same, gold nanoparticles of all sizes should have the same total surface area at the corresponding critical concentrations to bind to all polymerase resulting in no free polymerase in the solution to participate in PCR.

Similar experiments were conducted with poly(quaternary ammonium) modified gold nanoparticles. It was experimentally determined that the critical concentration for poly(quaternary ammonium) modified gold nanoparticles was 0.045 mg/mL. BSA was found to be able to minimize PCR inhibition. When the concentration of BSA was over 15 μg/reaction in the presence of poly(quaternary ammonium) modified gold nanoparticles at 0.045 mg/mL, the PCR amplification curve appeared in the same position as that of the reference sample without nanoparticles.

4.1.4 Summary

As a summary, experiments were conducted to evaluate the effect of gold nanoparticles on PCR efficiency. How sizes of gold nanoparticles affected PCR was evaluated by using 5nm, 10nm and 20 nm gold nanoparticles. In general, gold nanoparticles of larger sizes had stronger inhibitory effect on PCR than gold nanoparticles of smaller sizes at the same particle concentration. The mechanism of gold nanoparticles inhibiting PCR was explored, which led to a proposed hypothesis that is gold nanoparticles and iTaq polymerase bound to each other therefore resulting in PCR inhibition by reducing the amount of free polymerase in PCR solution. The proposed hypothesis was supported by several experiments. Methods were discovered and proved to be efficient in suppressing the induced PCR inhibition caused by gold nanoparticles by adding either more polymerase or more BSA. Considering that BSA is much more inexpensive than Taq polymerase, it is a more feasible way to add BSA to improve PCR efficiency. The research paves a way for the integration of nanoparticle cell lysis and PCR for rapid detection of bacteria. Besides, the research alone can help people better

understand how gold nanoparticles interact with biological substances and hence lead to appropriate applications.

4.2 Effects of Titanium Dioxide Nanoparticles on PCR

In Section 3.2, cell lysis using titanium dioxide nanoparticles and a miniaturized UV light source was demonstrated. The next step is to evaluate how titanium dioxide nanoparticles affect PCR when they are part of the reaction solution. There are very few publications in the literature about how PCR is affected in the presence of titanium dioxide nanoparticles. Therefore, similar experiments compared to those described in Section 4.1 were conducted to provide a basic understanding of the problem. It was discovered that there was an interesting interaction between titanium dioxide and silver nanoparticles which under appropriate conditions, can greatly reduce PCR inhibition caused by either one of them.

4.2.1 Materials

4.2.1.1 Titanium dioxide and silver nanoparticles

Aqueous solutions of monodispersed titanium dioxide and silver nanoparticles were prepared by Vive Nano. The sizes of the silver and titanium dioxide nanoparticles fell in the range of 1 to 10 nm. Figure 4-8 shows the high resolution TEM images of both samples used in the experiments.

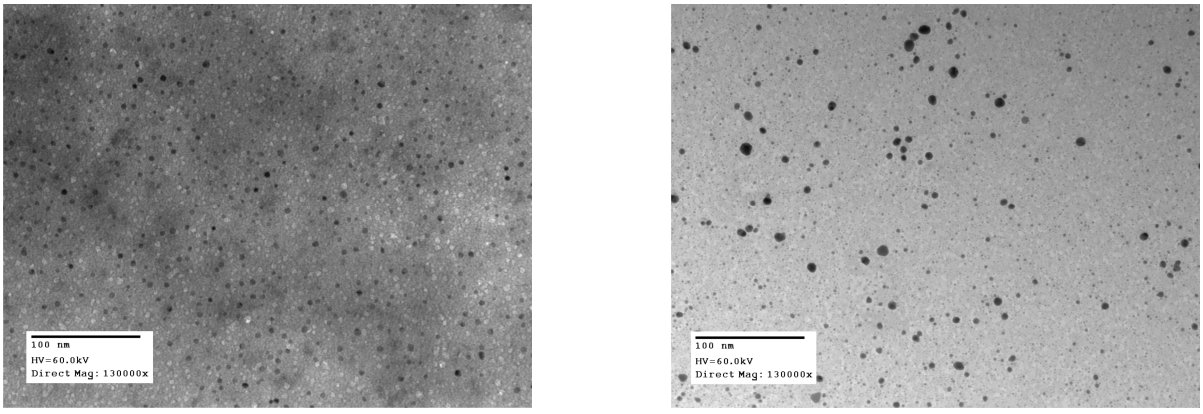

(a) (b)

Figure 4-8. TEM images of titanium dioxide and silver nanoparticles. (a) titanium dioxide nanoparticles; (b) silver nanoparticles.

4.2.1.2 PCR reagents and DNA templates

Salmonella enterica ATCC 13311 was used as DNA templates. The target gene was invasion (*invA*) gene for *Salmonella* species, the same as the one described in Section 4.1.1.2. Table 2-1 lists the sequences of the primers and the Taqman probe in details. iTaq polymerase, 10X PCR buffer and magnesium chloride were obtained from Bio-Rad. Primers, TaqMan probe, dNTP mix (dATP, dCTP, dGTP and dTTP) and bovine serum albumin (BSA) were obtained from Sigma. The optimal amount of all reagents and DNA template in each reaction of 25 μL without adding titanium dioxide and silver nanoparticles was 0.75 μL of each of forward and reverse primers, 0.25 μL of Taqman probe, 200 μM dNTPs, 2.5 μL of 10x PCR buffer, 0.625 U of iTaq polymerase, 3.5 mM $MgCl_2$ and 5 μL of DNA template. In some experiments, the concentration of the reagents was changed on purpose to evaluate their interactions with titanium dioxide and silver nanoparticles. DNA template concentration was adjusted from 30 ng/mL to 30 pg/mL as a standard series with each step differing by 10 fold.

4.2.1.3 Other chemicals

Other chemicals used in the experiments included agarose from VWR, Tris-acetate-EDTA (TAE) buffer from Sigma and GelRed from Biotium.

4.2.2 Methods

4.2.2.1 Experiment procedures

PCR master mix was first prepared and aliquoted into PCR tubes suitable for reaction with a 25 μL volume. Water was added to the first tube as negative control. DNA template without nanoparticles was added to the second tube as reference. DNA template with titanium dioxide nanoparticles alone, silver nanoparticles alone or a combination of both was added to the other tubes consecutively.

4.2.2.2 PCR programs and real-time PCR system

iCycler iQ real-time PCR machine from Bio-Rad was used in the experiments. Fluorescent signal was detected at the end of each cycle. Excitation light was set at 490 nm and emission light was detected

at 530 nm. The PCR program for *Salmonella* DNA was set as follows: 3 minutes at 95℃ for pre-denaturation, 50 cycles of amplification at 95℃ for 15 seconds, 60℃ for 30 seconds, 72℃ for 30 seconds, and 10 minutes at 72℃ for final extension. Details about the real-time PCR system were described in Section 4.1.2.2.

4.2.3 Results and Discussion

Experiments were conducted to determine the effect of titanium dioxide nanoparticles on PCR efficiency. In each run, there were a set of reference tubes containing no titanium dioxide nanoparticles and a set of experimental tubes containing titanium dioxide nanoparticles. The concentrations of PCR chemicals were the same as described in Section 4.2.1.2. Different concentrations of titanium dioxide nanoparticles were tested in the experiments. It was observed that titanium dioxide nanoparticles exhibited a strong PCR inhibitory effect. It was experimentally determined that they caused obvious PCR inhibition starting from 0.8 µg/mL and complete PCR inhibition was observed at 5 µg/mL for titanium dioxide nanoparticles. PCR amplification curves with titanium dioxide nanoparticles at 1.5 µg/mL and 5 µg/mL are plotted in Figure 4-9.

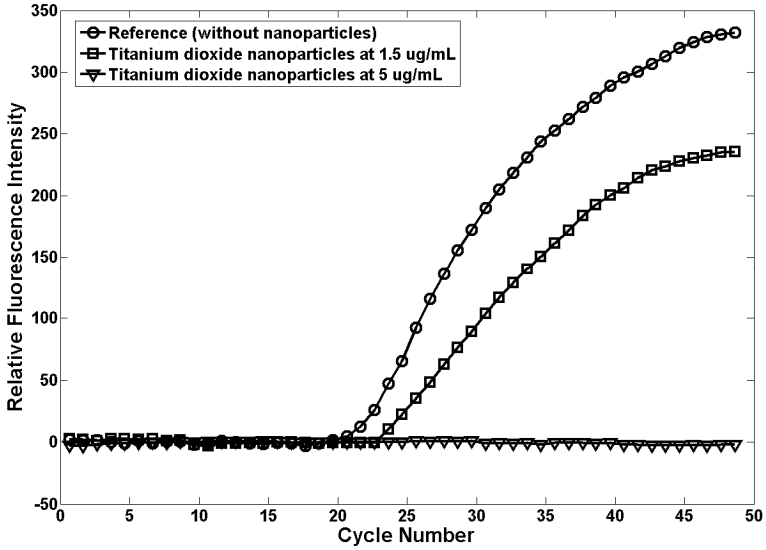

(a)

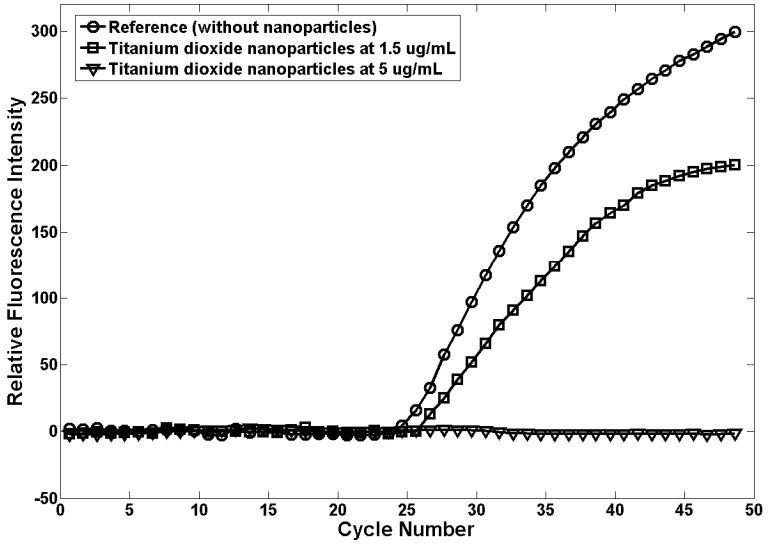

(b)

Figure 4-9. PCR amplification curves with titanium dioxide nanoparticles at 1.5 µg/mL and 5 µg/mL. Starting DNA concentration was (a) 30 ng/mL; (b) 3 ng/mL.

It is worth mentioning an interesting discovery during the experiments to evaluate the effect of a combination of titanium dioxide and silver nanoparticles on PCR. It started with testing 3 µL of several combinations of silver nanoparticles and titanium dioxide nanoparticles. These included pure titanium dioxide nanoparticles at 180 µg/mL (3 µL of silver nanoparticles), pure silver nanoparticles at 180 µg/mL (3 µL of titanium dioxide nanoparticles), a combination of titanium dioxide nanoparticles at 90 µg/mL and silver nanoparticles at 90 µg/mL (1.5 µL of titanium dioxide nanoparticles and 1.5 µL of silver nanoparticles), a combination of titanium dioxide nanoparticles at 120 µg/mL and silver nanoparticles at 60 µg/mL (2 µL of titanium dioxide nanoparticles and 1 µL of silver nanoparticles), a combination of titanium dioxide nanoparticles at 135 µg/mL and silver nanoparticles at 45 µg/mL (2.25 µL of titanium dioxide nanoparticles and 0.75 µL of silver nanoparticles), a combination of titanium dioxide nanoparticles at 60 µg/mL and silver nanoparticles at 120 µg/mL (1 µL of titanium dioxide nanoparticles and 2 µL of silver nanoparticles), and a combination of titanium dioxide nanoparticles at 45 µg/mL and silver nanoparticles at 135 µg/mL (0.75 µL of titanium dioxide nanoparticles and 2.25 µL of silver nanoparticles). Figure 4-10 shows

the corresponding PCR amplification curves. It can be seen from the figure that complete PCR inhibition occurred with titanium dioxide nanoparticles at 180 µg/mL and partial PCR inhibition occurred with silver nanoparticles at 180 µg/mL. This is expected since the concentration of titanium dioxide nanoparticles was larger than 5 µg/mL, which is the critical concentration for titanium dioxide nanoparticles to cause complete PCR inhibition. Complete PCR inhibition was observed for titanium dioxide nanoparticles:silver nanoparticles=2:1 and titanium dioxide nanoparticles:silver nanoparticles=3:1 at 3 µL. This is understandable since the concentration of titanium dioxide nanoparticles was much larger than the threshold concentration. However, partial PCR inhibition was observed for titanium dioxide nanoparticles:silver nanoparticles=1:1, titanium dioxide nanoparticles:silver nanoparticles=1:2 and titanium dioxide nanoparticles:silver nanoparticles=1:3 as opposed to complete PCR inhibition. It is confusing since the concentrations of titanium dioxide nanoparticles in these cases all exceeded the threshold concentration for titanium dioxide nanoparticles to cause complete PCR inhibition.

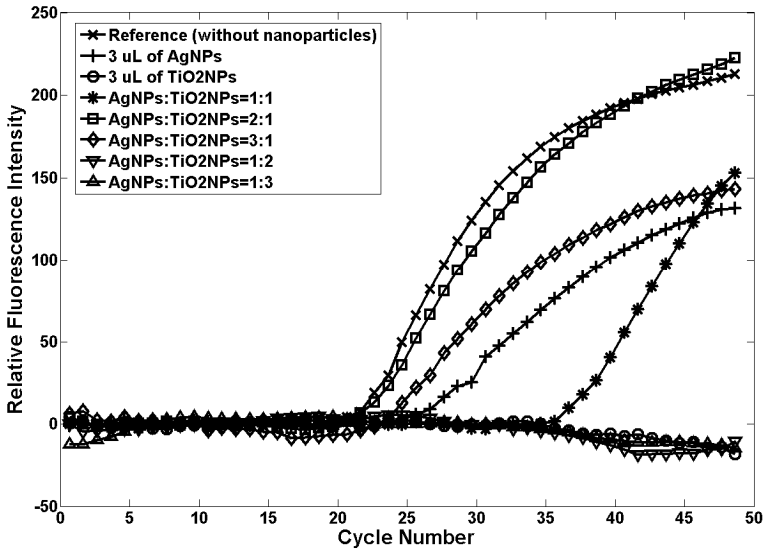

(a)

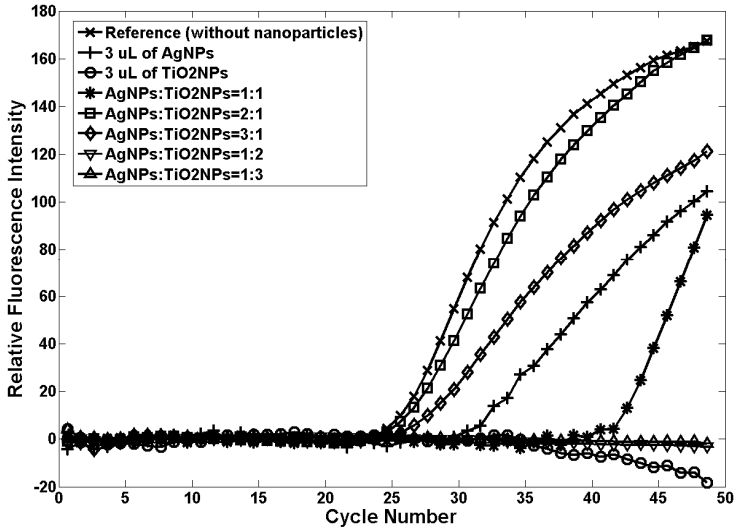

(b)

Figure 4-10. PCR amplification curves with 3 µL of different combinations of titanium dioxide and silver nanoparticles. DNA template concentration was (a) 30 ng/mL; (b) 3 ng/mL.

In the next experiment, same combinations of titanium dioxide and silver nanoparticles as in the previous experiment at 5 µL are tested. The corresponding PCR amplification curves are shown in Figure 4-11. It can be seen from the figure that complete PCR inhibition is occurred with titanium dioxide nanoparticles at 300 µg/mL since the concentration titanium dioxide nanoparticles is larger than the corresponding threshold concentration. Complete PCR inhibition is observed for titanium dioxide nanoparticles:silver nanoparticles=2:1 and titanium dioxide nanoparticles:silver nanoparticles=3:1, the same as the case for the same combinations at 3 µL. Partial PCR inhibition is observed for titanium dioxide nanoparticles:silver nanoparticles=1:2 and titanium dioxide nanoparticles:silver nanoparticles=1:3 at 5 µL, the same as the case for the same combinations at 3 µL. Complete PCR inhibition is observed for titanium dioxide nanoparticles:silver nanoparticles=1:1 instead of partial inhibition as is observed in the case of the same combination at 3 µL. The results obtained from both experiments suggest that the effect of the combination of titanium dioxide and silver nanoparticles is not simply the linear combination of the individual effect of titanium dioxide and silver nanoparticles. The different PCR efficiencies of different combinations of titanium dioxide and silver nanoparticles indicate that there exists an optimal ratio between titanium dioxide and silver

nanoparticles which yields the least PCR inhibition for a specific volume of both nanoparticles. In some cases, titanium dioxide and silver nanoparticles play such a role that they interact to suppress the inhibitory effect of each other. By carefully choosing the combination of titanium dioxide and silver nanoparticles, the strong inhibitory effect caused by any one of them can be minimized. The confusing observation suggests that a complex interaction between titanium dioxide and silver nanoparticles exists and it needs to be explored in the future.

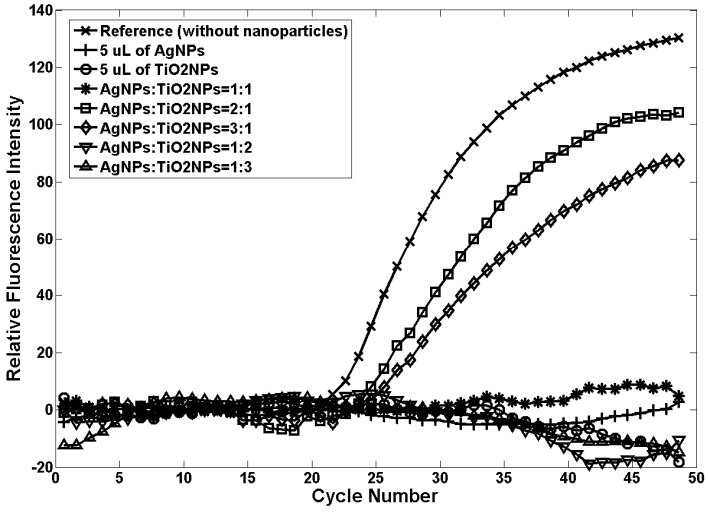

(a)

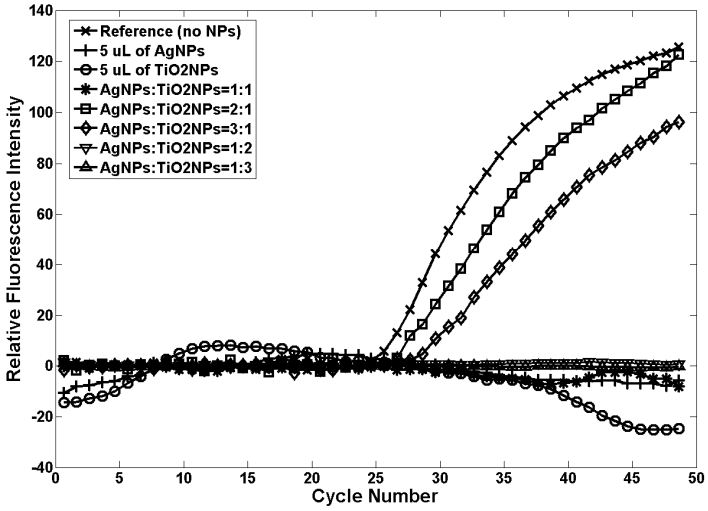

(b)

Figure 4-11. PCR amplification curves with 5 μL of different combinations of titanium dioxide and silver nanoparticles. DNA template concentration was (a) 30 ng/mL; (b) 3 ng/mL.

4.2.4 Summary

Experiments were conducted to demonstrate the PCR inhibitory effect of silver and titanium dioxide nanoparticles. Silver nanoparticles started to cause PCR inhibition at 30 µg/mL while complete PCR inhibition was observed at 240 µg/mL. Titanium dioxide nanoparticles had much stronger inhibitory effect compared to silver nanoparticles. They started to cause PCR inhibition at 0.8 µg/mL while they caused complete PCR inhibition at 5 µg/mL. Effect of the combination of silver and titanium dioxide nanoparticles on PCR was evaluated as well. It was found that different combinations of silver and titanium dioxide nanoparticles had an impact on PCR efficiency. There exists an optimum concentration ratio between silver and titanium dioxide nanoparticles which results in the least inhibitory effect on PCR. However, the actual mechanism of the interaction between silver and titanium dioxide nanoparticles remains to be explored with more solid experiments.

Chapter 5

Integration of Nanoparticle Cell Lysis and Microchip PCR for Rapid Detection of Bacteria

In chapter 3, a novel method using poly(quaternary ammonium) modified gold nanoparticles for efficient cell lysis was demonstrated. In chapter 4, the effect of gold nanoparticles on PCR was evaluated and several methods to suppress the inhibitory effect caused by gold nanoparticles were proposed. This chapter describes activities towards the integration of cell lysis using poly(quaternary ammonium) modified nanoparticles and PCR on the microchip level based on the experience gained in chapter 3 and 4.

5.1 Design Considerations

The microchip design for the integration of nanoparticle cell lysis and PCR is essentially the design for a microchip PCR system because all it takes for nanoparticle cell lysis to work is a reaction chamber which can be shared with the PCR chamber. It is a big advantage in terms of system integration. Therefore, the focus is how to design and fabricate a microchip PCR system in an easy, reliable and inexpensive way. A microchip PCR system consists of a physical microchip PCR device, a temperature control system and necessary interface connections between the physical microchip for PCR and the temperature control system. The physical microchip PCR device should consist of at least the following components, a microheater for generating desired temperatures, a PCR chamber for the reaction to undergo and a temperature sensor to monitor temperature.

5.1.1 Physical Microchip PCR Device

5.1.1.1 Microheater

A microheater is required to generate desired temperatures for a successful PCR. There are two types of microheaters for microchip PCR devices. One is on-chip and the other is off-chip. On-chip microheaters are fabricated directly on the substrate with PCR chamber together. Advantages of on-chip microheaters are that they require less assembly and are more reliable. However, they require

going through time-consuming and relatively expensive clean room fabrication process. They are more suitable when fabricated in large quantities at the final production stage. Off-chip microheaters are fabricated separately from reaction chambers while they are assembled together afterwards. Advantages of off-chip microheaters are that they are readily available as commercial products and there are all kinds of off-chip microheaters that can be chosen to suit the design need. However, assembly with other components needs to be done at a later stage. It is without question that off-chip microheaters are more appropriate at the very first stage for the research work. Therefore, off-chip microheaters were adopted in the fabrication of physical microchips PCR devices. Kapton (polyimide) thermofoil microheaters (Model number: HK5318R15.7L12D) were obtained from Minco. One side of the microheater was backed with 0.76 mm thick aluminum foil for the consideration of the assembly process at a later stage.

5.1.1.2 PCR chamber

PCR chamber is mandatory for PCR to take place. There are many different ways to create a PCR chamber. As mentioned in Section 2.5, clean room microfabrication techniques and polymer techniques are widely used to manufacture micro structures including PCR chambers on microchips. Compared to clean room microfabrication techniques, polymer techniques are less time-consuming and less expensive, therefore considered being a good candidate in this case. PDMS (Polydimethylsiloxane) is the most widely used silicone-based organic polymer in fabricating microfluidics devices. It is optically transparent and has a very interesting property of being able to turn from liquid to solid after polymerization. SYLGARD® 184 SILICONE ELASTOMER KIT was used in the experiment to fabricate PCR chambers. The kit contains two parts. One is PDMS base and the other is PDMS curing agent. They were well mixed with base versus curing agent at a weight ratio of 10:1. After degassing in a vacuum oven for 45 minutes, a constant amount of the mixture was poured into a rectangular mould, in order to create PDMS sheets of constant thickness to be used for the fabrication of microchip PCR chamber. The thickness of the PDMS sheets was determined by the volume of the PDMS mixture as well as the size of the mould and was 0.5 mm in this work. After cured for approximately 60 minutes at 100℃, PDMS sheets were removed from the oven, peeled off

from the mould and cut down to the same size as the off-chip microheater. Parafilm was used to wrap them to ensure clean surfaces to be used at the assembly stage. A PCR chamber was formed by punching a though hole at the center of a PDMS sheet using a metal hole punch.

5.1.1.3 Temperature sensor

PCR is very sensitive to temperature variations therefore temperature monitoring is key to a successful PCR. As the same as microheaters, temperature monitoring can be done either on-chip or off-chip. On-chip temperature monitoring implements temperature sensors on the microchip to directly measure temperature in the reaction chamber. It is reliable and reduces assembly involved in later stages. However, it requires going through complicated and time consuming clean room microfabrication process, the same as on-chip microheaters. Off-chip temperature monitoring usually involves a temperature sensor to measure the temperature of the microheater and a characterization temperature sensor to characterize the temperature in the reaction chamber. Temperature in the reaction chamber is correlated with the temperature of the microheater after characterization by using a look-up table. Although off-chip temperature monitoring needs more work in the assembly and characterization, it was adopted in this work due to the fact that it does not involve the burden of clean room microfabrication and it has much faster turn-around time, which is more suitable for the very first stage of the research work.

5.1.2 Temperature Control System/Thermocycling

Temperature control system is used to automatically control repeated temperature transition between PCR steps and temperature maintaining for each PCR step. The core of the thermocycling is data acquisition and feedback control. It involves providing appropriate driving signals to hardware such as microheater and fan based on the acquired data from the temperature sensor as well as pre-defined parameters such target temperature and lasting time at each PCR stage. A major design consideration for thermocycling is fast temperature transition between each PCR stage and stable temperature maintaining during each PCR stage. These two factors lead to high PCR specificity and fast thermocycling [169-171]. There are all kinds of control mechanism for PCR thermocycling. A simple

strategy is to provide maximum power to the microheater during temperature increase stage to ensure fastest temperature increase. However, maintaining at a temperature needs to be as accurate as possible to minimize temperature variation. This requires a relatively small power supplied to the microheater. A solution to overcome the problem is to use two different control signals and two different power lines for temperature increase and temperature maintaining. A circuit diagram is shown in Figure 5-1. As for temperature decrease stage, no power is supplied to the microheater and another control signal is used to turn on a fan to accelerate air convection.

Data acquisition was accomplished by using a NI 6233 data acquisition card, a NI CB-37F-HVD terminal block, a NI SH37F-37M I/O cable and necessary connections to the driving circuits. There were three output ports/signals used for temperature increase, temperature maintaining and temperature decrease stages as mentioned earlier. There was one input port/signal used to acquire temperature readings from the thermocouple to measure temperature of the microheater. NI LabView 8.2 was used as the software for programming thermocycling. NI LabView is a widely used tool to develop sophisticated measurement, test and control tasks using intuitive graphical icons and wires that resemble a flowchart. The thermocyling was a predefined repeated execution of three modules, one responsible for temperature increase, one responsible for temperature decrease and one responsible for temperature maintaining as shown in Figure 5-2. In the temperature increase operation, a temperature which corresponded to either PCR denaturing stage or PCR extension stage was pre-defined. Control signal V1 was set to be at 5V and V2 was set to be 0, maximum power of 20V was applied to the microheater until the measured temperature reached the pre-defined temperature. When desired temperature was reached, both V1 and V2 were set to be 0 and the next operation was triggered. In the temperature maintaining operation, a time period which corresponded to any one of three PCR stages was pre-defined. Control signal V1 was set to be 0. Within the pre-defined time period, V2 was changing between 0 and 5V based on the measured temperature and the pre-defined temperature. If the measured value was lower than the pre-defined value, V2 was set to be at 5V and if the measured value was higher than the pre-defined value, V2 was set to be 0. Once the pre-defined time target was met, the next operation was triggered. In the temperature dropping operation, a temperature which corresponded to PCR annealing stage was pre-defined. A control signal was set to

turn on the fan for faster cooling. Both V1 and V2 were set to be 0. Once the pre-defined temperature was reached, the next operation was triggered. The control program was written in a "while" loop which cycled among the three basic operations. Hardware part used all necessary electric components to form a driving circuit as shown in Figure 5-1 to control the microheater for temperature increase, to control the fan for cooling down the chamber and to monitor thermocouple readings.

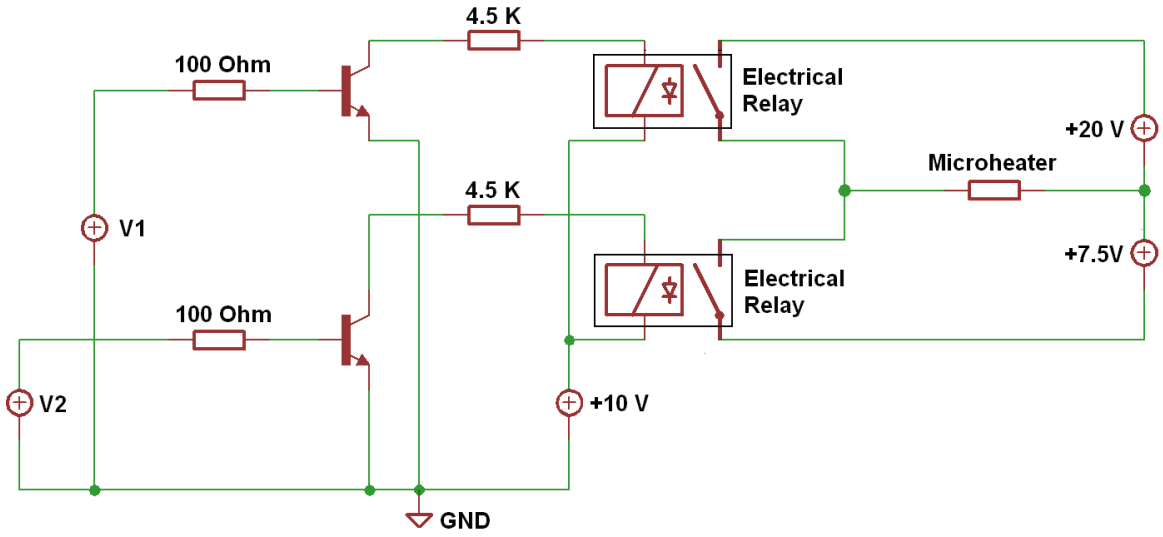

Figure 5-1. Driving circuit for temperature maintaining and temperature transition. V1 is the control signal for temperature transition, either jumping or dropping. V2 is the control signal for temperature maintaining.

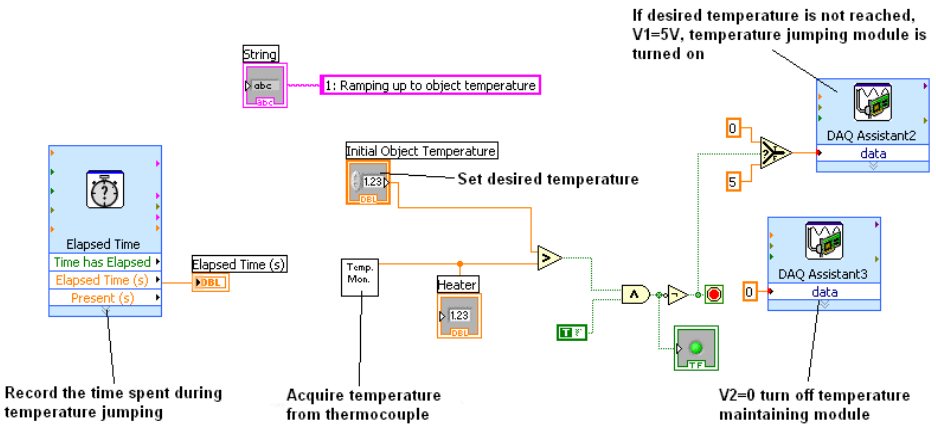

(a)

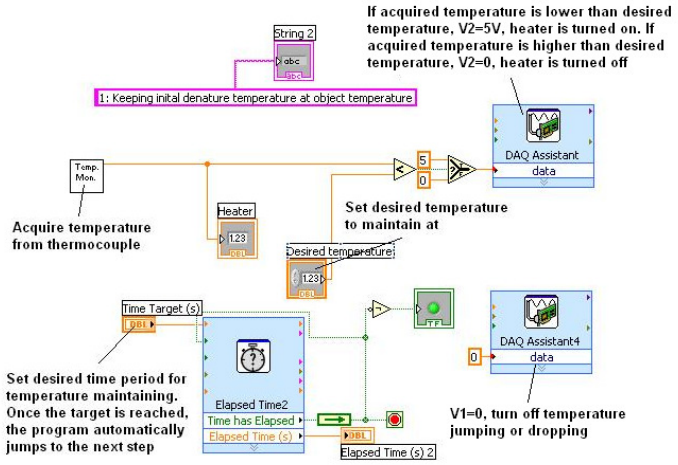

(b)

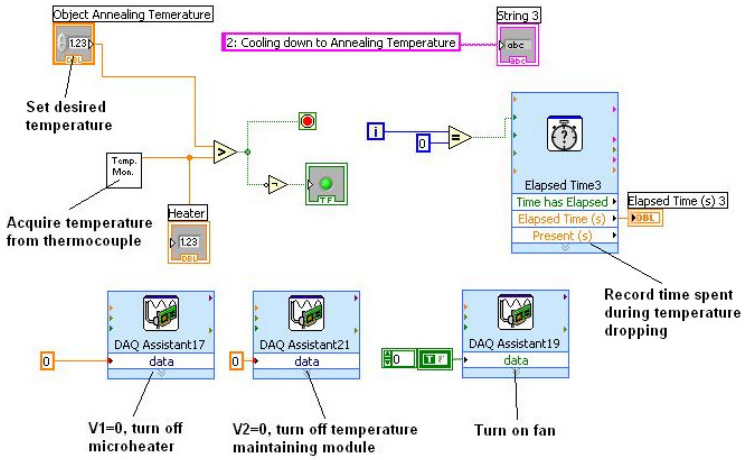

(c)

Figure 5-2. Three basic LabView modules in microchip PCR thermocycling. (a) Temperature increase; (b) Temperature maintaining; (c) Temperature decrease.

5.1.3 System Overview

Figure 5-3 shows the diagram describing the flowchart of the microchip PCR system under working condition. Data acquisition card monitored temperature of the microchip PCR chamber. LabView control program processed the information and output control signal to the driving circuits through interface connections to turn on/off appropriate power lines to drive the microchip PCR device.

During temperature transition stages such as from annealing to extension and from extension to denaturing, Power source 2 was selected. During temperature maintaining stages of annealing, extension and denaturing, Power source 1 was selected. During temperature transition stage from denaturing to annealing, neither power source 1 nor power source 2 was selected and the fan was turned on.

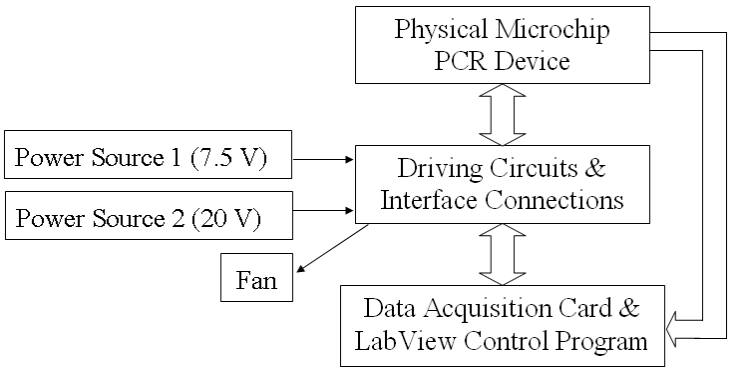

Figure 5-3. Overview of the microchip PCR System.

5.2 Implementation of Microchip PCR System

This section describes the fabrication process of the physical microchip PCR device as well as device assembly. Alpha version was proposed first. Some problems were discovered during fabrication and experiments, which led to the development of the beta version.

5.2.1 Fabrication of Physical Microchip PCR Device

5.2.1.1 Alpha version

The original conceptual design is shown in Figure 5-4. It consisted of a PCR chamber made of PDMS bonded to a microheater with a cover on top as well as a self-adhesive thermocouple to measure temperature. Fabrication process is illustrated in Figure 5-5. It started with making a PDMS sheet with a punched hole in the middle. One side of the sheet was bonded on top of the metal side of the microheater. After loading reagents in the reaction chamber, a PDMS layer or a glass substrate was bonded on the other side of the PDMS sheet to prevent PCR solution from evaporating at high

temperatures. However, some problems were discovered during the fabrication process. First of all, the PDMS/metal bonding problem arose because of the difficulty in producing activated bonding regions between metal and organic ligands. Secondly, placing a cover on top of the PDMS layer after loading reagents was very inconvenient as plasma treatment was required to create strong bonding between PDMS and PDMS or between glass and PDMS. Therefore, a revised beta version was proposed.

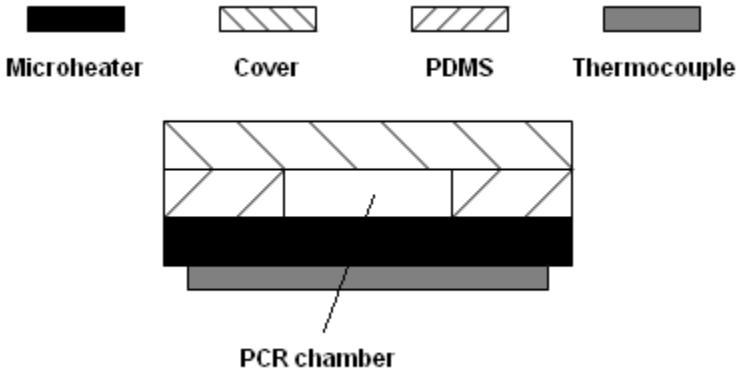

Figure 5-4. Conceptual illustration of the microchip of the alpha version.

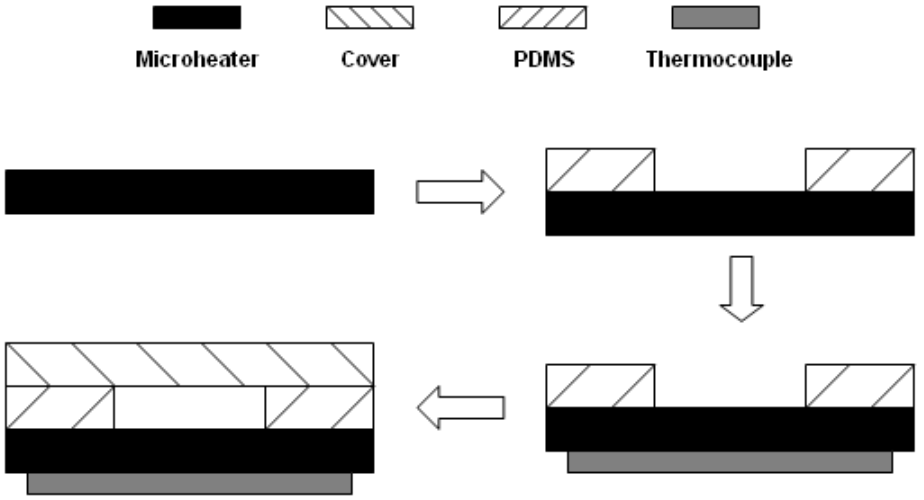

Figure 5-5. Fabrication process of the microchip of the alpha version. It started with bonding a PDMS sheet with a punched hole to the metal side of the microheater. After loading PCR reagents to the PCR chamber, a glass cover was attached on top to prevent PCR solution from evaporating. A self-adhesive thermocouple was attached to the polyimide side of the microheater to measure temperature.

5.2.1.2 Beta version

Based on the experience gained from the alpha version, beta version was proposed as shown in Figure 5-6. The device consisted of two chambers made of PDMS, one as a PCR chamber and the other as a mineral oil chamber to prevent PCR reagents from evaporating. Fabrication process is illustrated in Figure 5-7. It started with coating the metal side of the microheater with a thin layer of PDMS mixture and baking it in the oven. The thickness of the thin PDMS layer was 100~200 μm. It was found that bonding between PDMS and metal in this way was much stronger than bonding between cross-linked PDMS and metal. After baking, two PDMS layers with punched holes of different diameters were bonded to the PDMS side of the microheater sequentially. The thickness of both layers was 500 μm. The PDMS layer in the middle had a smaller hole with a diameter of 3.6 mm than that in the upper PDMS layer with a diameter of 6 mm. PCR chamber had a volume of approximately 5 μL. After that, a self-adhesive thermocouple was attached to the polyimide side of the microheater to measure temperature. PCR reagents were loaded to the chamber located in the middle PDMS layer followed by loading an appropriate amount of mineral oil to the chamber located in the upper PDMS layer to prevent PCR solution from evaporating at high temperatures during PCR. Figure 5-8 shows images of a real device. It is worth mentioning that the device is easy to be reconstructed by peeling off the thin layer of PDMS from the metal side of the microheater and start the process over again.

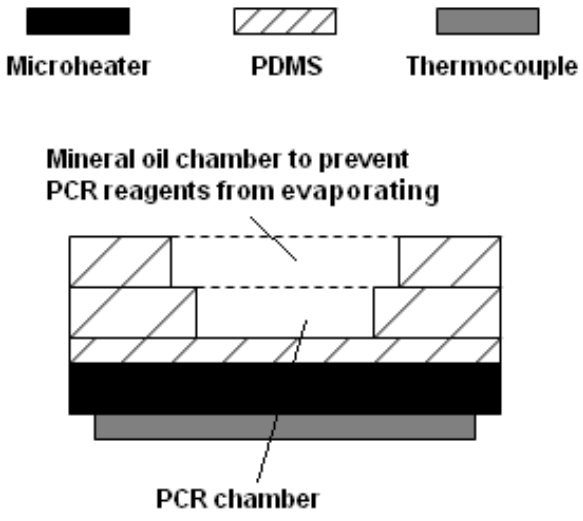

Figure 5-6. Conceptual illustration of the microchip of the beta version.

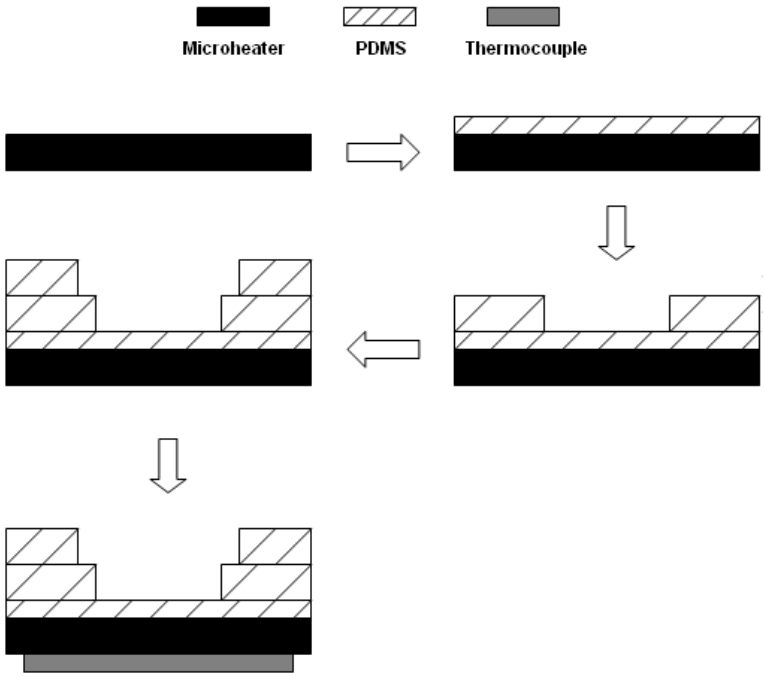

Figure 5-7. Fabrication process of the microchip of the beta version. It started with coating the metal side of the microheater with a thin layer of PDMS mixture and baking it in the oven. After baking, two PDMS layers with punched holes of different diameters were bonded to the PDMS side of the microheater sequentially. PCR reagents were loaded to the chamber located in the middle PDMS layer with a smaller hole followed by loading an appropriate amount of mineral oil to the chamber located in the upper PDMS layer with a larger hole to prevent PCR solution from evaporating at high temperatures during PCR. A self-adhesive thermocouple was attached to the polyimide side of the microheater to measure temperature.

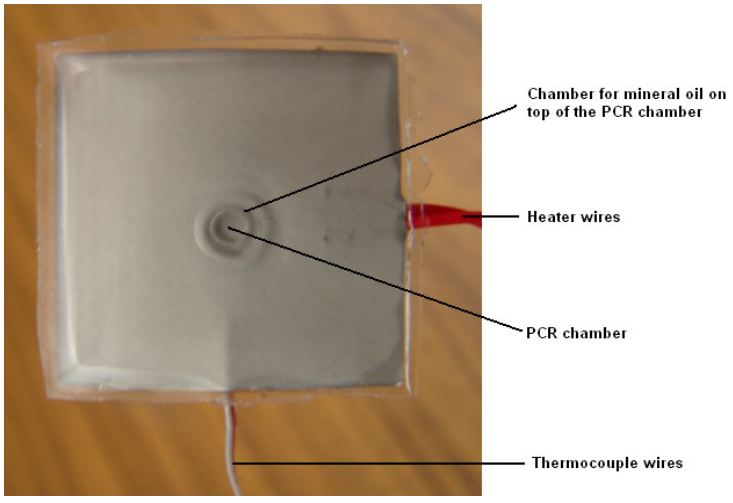

(a)

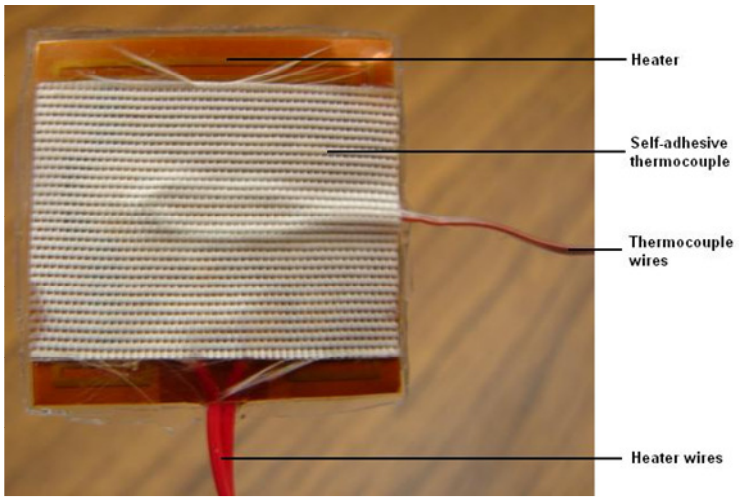

(b)

Figure 5-8. A physical microchip PCR device. (a) View from the metal side of the microheater; (b) View from the polyimide side of the microheater.

5.2.2 Thermocycling Characterization

Thermocycling characterization was mandatory as off-chip temperature sensors were used. The goal of characterization was to establish a relationship between temperature in the reaction chamber and that of the microheater so that temperature in the reaction chamber can be precisely controlled by temperature of the microheater instead. Characterization was carried out in three aspects. The first step was to find a relationship between the temperature in the reaction chamber and that of the microheater at the steady state. This was used to maintain at a specific temperature for any of three PCR cycles. The second step was to characterize temperature transition between each PCR stage such as from denaturing to annealing. The third step was to characterize the thermocycling by combining results obtained from the first two steps.

5.2.2.1 Steady state temperature characterization

A successful PCR depends on accurate control of the temperature in the chamber. However, the off-chip temperature sensor monitors the temperature of the microheater. A temperature difference exists between the temperature in the chamber and that of the microheater. This leads to the mandatory temperature characterization. The characterization was carried out under a mock situation imitating

the working condition. 5 μL of water was loaded in the reaction chamber followed by loading 12 μL of mineral oil. A probe style type J thermocouple was carefully placed in the water to monitor the temperature in the reaction chamber. The temperature of the microheater was raised to a specified value while the temperature in the reaction chamber was recorded when it reached the steady state. Characterization result is listed in Appendix A.

5.2.2.2 Transient temperature characterization

During transition between PCR stages, temperature change of the microheater was faster than that in the chamber. Therefore, transient temperature characterization was necessary. A strategy to achieve fast yet accurate temperature transition was proposed. During temperature increase stages from annealing step to extension step and from extension step to denaturing step, maximum power was supplied to the microheater while temperature in the chamber was monitored. The power was cut off when temperature of the microheater reached a specific value while the temperature in the chamber was increasing to the desired value due to inertia. During temperature decrease stage from denaturing step to annealing step, power was supplied to the fan but not to the microheater. The fan cooled down the device much faster. As the temperature of the microheater changed faster than that in the chamber, the power supplied to the fan was cut off when temperature of the microheater reached a specific value while the temperature in the chamber was decreasing to the desired value due to inertia. Transient speed of up to 6℃/second for temperature increase was achieved while the speed of up to 3 ℃/second for temperature decrease was achieved.

5.2.2.3 Temperature characterization for thermocycling

Thermocycling characterization was carried out after steady state temperature characterization and transient temperature characterization. Figure 5-9 shows the temperature profile of 3 cycles with the following settings: denaturing at 95℃ for 15 seconds, annealing at 60℃ for 30 seconds, extension at 72℃ for 30 seconds. As shown in the figure, the actual temperature profile had a small variance from the desired temperature profile especially during transition between PCR stages. However, temperature maintaining was very close to the desired settings with a small variation of ±1℃.

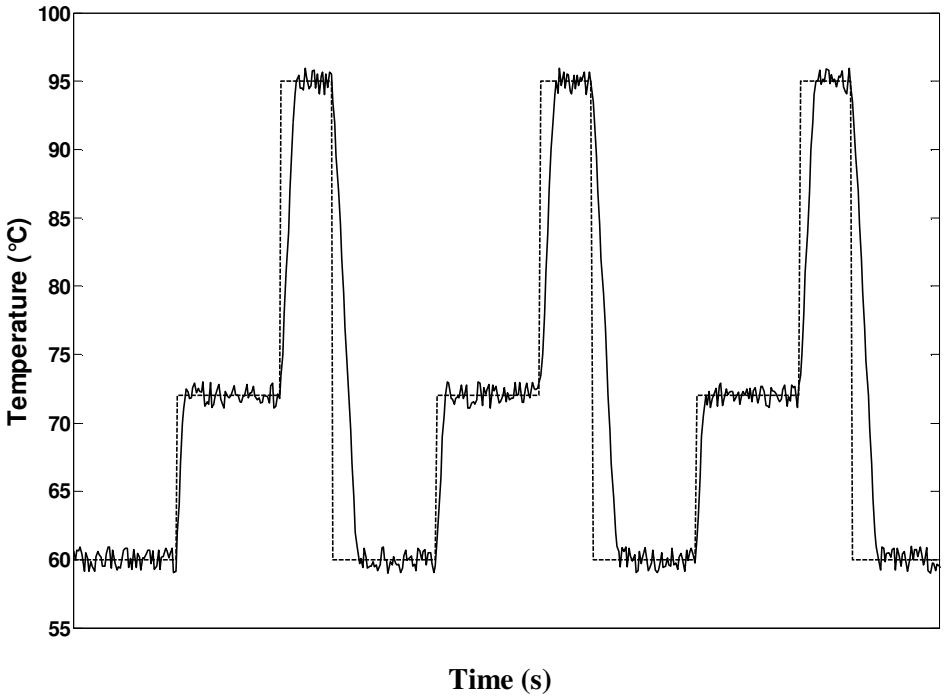

Figure 5-9. Actual temperature profile versus ideal temperature profile. Solid line represents the actual temperature profile. Dotted line represents the ideal temperature profile.

5.3 Materials and Methods

5.3.1 Cell Samples

E. coli was used in the experiments. Cells were grown in lysogeny broth (LB) at 37℃ over night and were washed twice using deionized water before experiments. To prepare LB, 10 g of tryptone, 5 g of yeast extract, and 10 g of NaCl were dissolved in 1 L of distilled water followed by autoclaving at 121℃. Stock cell concentration was adjusted and is determined to be at ~1e7 cells/mL. Cell solution was diluted as needed in different experiments.

5.3.2 Nanoparticles

Poly(quaternary ammonium) functionalized gold nanoparticles were used to perform fast and efficient cell lysis. The stock concentration of the nanoparticle colloidal dispersion was 1.5 mg/mL. High resolution TEM images of the nanoparticles were shown in Section 3.1.1.1.

5.3.3 PCR Reagents and DNA Templates

A 147 bp coding region of the *E. coli* uidA gene, based on the sequence reported by Jefferson *et al.* [172], was used as PCR targets. Table 5-1 lists the 20- and 21-mer primers UAL-754 (forward primer) and UAR-900 (reverse primer) [173]. Primer UAL-754 is located between bp 754 and 773 and primer UAR-900 is located between bp 880 and 900 in the amino-terminal coding region of the uidA gene of *E. coli*. PCR master mix was composed of forward and reverse primers, dNTP mix (dATP, dCTP, dGTP and dTTP), 10x PCR buffer, iTaq polymerase, magnesium chloride and bovin serum albumin (BSA). The concentration of each chemical was varied depending on experiments. Primers, dNTP mix and BSA were obtained from Sigma. iTaq polymerase, 10X PCR buffer and magnesium chloride were obtained from Bio-Rad.

Table 5-1. Primers used in the experiments [173]

Primer A (forward)	5'-AAAACGGCAAGAAAAAGCAG-3'
Primer B (reverse)	5'-ACGCGTGGTTACAGTCTTGCG-3'

5.3.4 Other Chemicals

Other chemicals used in the experiments included agarose from VWR, Tris-acetate-EDTA (TAE) buffer from Sigma, GelRed from Biotium and 100 bp DNA ladder from BioLabs.

5.3.5 Gel Electrophoresis

Gel electrophoresis was used to analyze PCR products. 1.5% agarose gel was prepared by dissolving 0.45 g of agarose in 30 mL of distilled water in a 50 mL beaker followed by adding 600 µL of 50X TAE buffer and 0.5 µL of GelRed. The beaker was placed on a hot plate until boiling. After cooling down for 5 minutes, the gel liquid was poured in a PMMA mould with a removable comb placed on top to define wells. The comb was carefully removed after 45 minutes when the gel turned to solid. The gel was placed in a gel electrophoresis chamber filled with 1X TAE buffer described in Section 4.1.2.3. A constant voltage of 100 V and a running time of 45 minutes were set. The gel was removed from the chamber afterwards and was imaged using a Bio-Rad Doc XR gel imaging system.

5.4 Results and Discussions

Experiments were conducted to demonstrate the successful integration of nanoparticle cell lysis and PCR for rapid detection of *E. coli*. Figure 5-10 shows the experimental setup of the integrated microchip system. As mentioned in Section 5.2.1.2, the volume of the reaction chamber on the microchip was approximately 5 μL. In all experiments, there were 0.8 μL of bacteria sample and 0.2 μL of nanoparticle colloidal dispersion and 4 μL of PCR master mix. PCR master mix was added 10 minutes after adding bacteria sample and nanoparticle dispersion. Concentrations of the chemical components were adjusted throughout experiments. In the first experiment, concentrations of most PCR chemical components were kept the same as that is required in a successful PCR in the regular PCR machine from Bio-Rad as described in Section 4.1.2.2. The composition of PCR master mix is listed in Table 5-2. The default PCR thermocycling was the same as the protocol for the regular PCR machine and was set as follows: 3 minutes at 95℃ for hot start, 50 cycles of amplification at 95℃ for 15 seconds, 60℃ for 30 seconds, 72℃ for 30 seconds, and 10 minutes at 72℃ for final extension. Same experiments were repeated 10 times. No PCR amplification was observed in any one of the samples after gel electrophoresis. Figure 5-11 shows a gel electrophoresis image of 2 samples from different experiment batches.

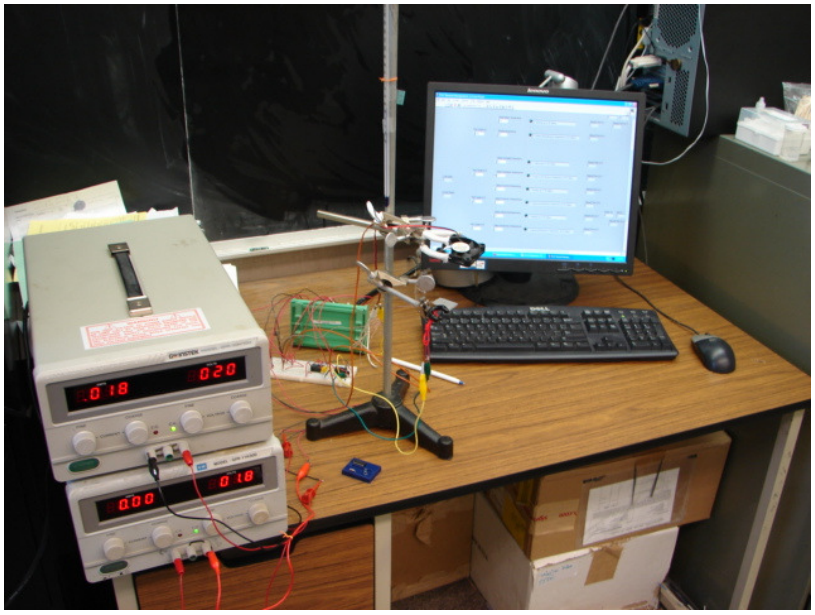

(a)

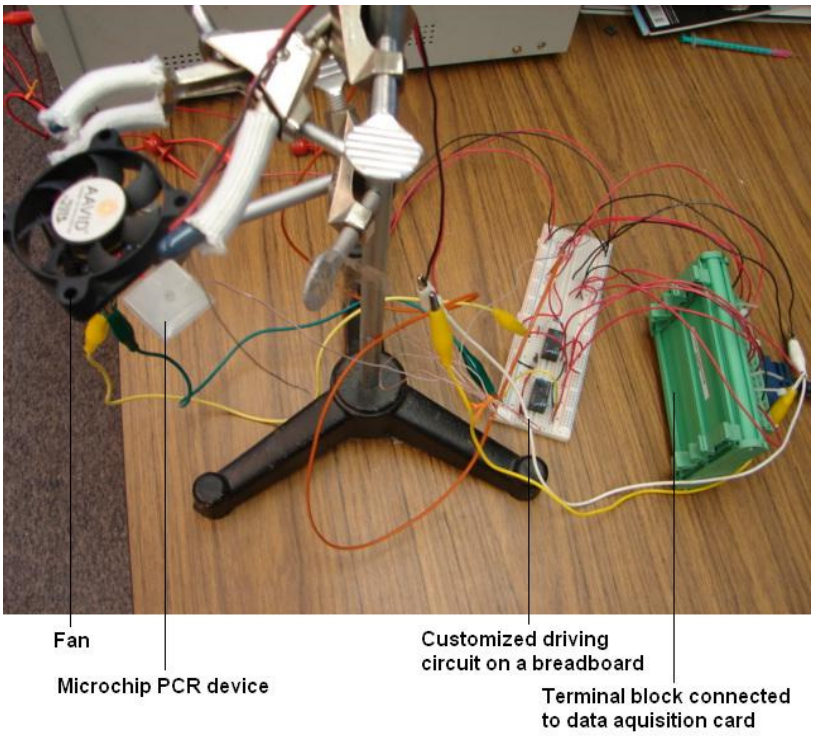

(b)

Figure 5-10. Experimental setup of the integrated microchip system. (a) Overview and (b) Close-look.

Table 5-2. Composition of PCR master mix in the first experiment

Chemicals	Concentration, volume or amount
Forward primer	300 nM
Reverse primer	300 nM
dNTPs	200 µM
Magnesium chloride	3.5 mM
iTaq polymerase	0.125 U/reaction
10X PCR buffer	0.5 µL/reaction
BSA	0

Figure 5-11. Gel electrophoresis image of the experiment (50 cycles) with 0.06 mg/mL poly(quaternary ammonium) modified gold nanoparticles and no BSA. Lane 1 and 2: no BSA is added. They are samples from different experiment batches.

Although the result from the previous experiment is not encouraging, it is not unexpected as gold nanoparticles were demonstrated to induce PCR inhibition in section 4.1.3. The concentration of poly(quaternary ammonium) modified gold nanoparticles in the experiment was 0.06 mg/mL. It was greater than the critical concentration of 0.045 mg/mL as determined in Section 4.1.3. This supports the conclusion made in Section 4.1.4. According to the result obtained in Section 4.1.3, BSA was able to minimize PCR inhibition caused by poly(quaternary ammonium) modified nanoparticles. Therefore, the second experiment was carried out with an increase on the amount of BSA up to 5 µg/reaction while other experimental conditions were kept the same as shown in Table 5-2. The default PCR thermocycling settings in the first experiment were used. Figure 5-12 shows a gel electrophoresis image of different experiment batches at BSA concentrations of 4 and 5 µg/reaction. As shown in the figure, PCR amplification, although not appearing at the desired band, was observed when BSA was increased as compared to no amplification in the first experiment when there was no BSA. Experiments were repeated 10 times at the BSA concentration of 4 µg/reaction. Out of 10 experiments, non-specific amplification was observed 6 times and no amplification was observed 4

times. The result confirms that BSA helps in minimizing PCR inhibition induced by gold nanoparticles. However, some other factors affected microchip PCR to result in non-specific amplification. Experimental conditions need to be optimized to achieve desired amplification.

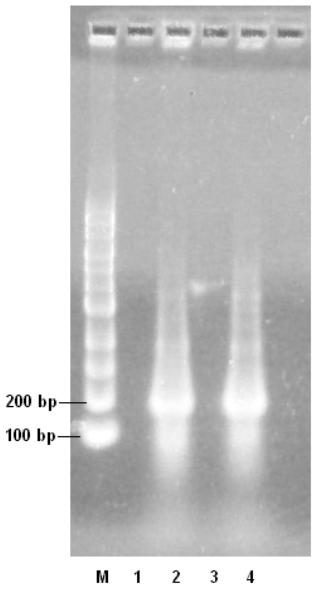

Figure 5-12. Gel electrophoresis image of the experiment (50 cycles) with 0.06 mg/mL poly(quaternary ammonium) modified gold nanoparticles and various amounts of BSA. Lane 1 and 2: BSA concentration was 4 µg/reaction; Lane 3 and 4: BSA concentration was 5 µg/reaction.

As mentioned in Section 2.2, PCR is a very sensitive chemical reaction involving a lot of components to make it work. There are many factors that can potentially result in non-specific DNA amplification such as cross-contamination. However in this case, there was no clue as which one was the most probable cause of the non-specific amplification and there was no existing literature which described solutions to overcome non-specific amplification for PCR involving nanoparticles in a microchip PCR setting. Therefore, a large number of experiments such as varying the amount of PCR reagents as well as changing thermocycling conditions were conducted to explore possible causes and the corresponding solutions. In all experiments, the concentration of poly(quaternary ammonium) modified gold nanoparticles was 0.06 mg/mL and the concentration of BSA was 4 µg/reaction. Table 5-3 summarises the parameters that were evaluated in the experiments and their effects on PCR specificity. It was found that the most efficient method to prevent non-specific DNA amplification

was to immerse PCR chamber with BSA solution prior to loading cells and nanoparticles and to increase annealing temperature from 60℃ to 63℃. However, either operation did not provide any benefits to improve PCR specificity at all. Table 5-4 shows the result of a repeatability test for improving PCR specificity by only immersing PCR chamber with 1~10% BSA prior to loading cells and nanoparticles, by only increasing annealing temperature from 60℃ to 63℃ and by combining both. When PCR chamber was immersed with BSA solution prior to loading cells and nanoparticles without increasing annealing temperature to 63℃, out of 10 experiments, there were 8 experiments with non-specific amplification and 2 experiments with no PCR product at all. When annealing temperature was raised to 63℃ without immersing PCR chamber with BSA solution prior to loading cells and nanoparticles, out of 10 experiments, there were 5 experiments with non-specific amplification and 5 experiments with no PCR product at all. When PCR chamber was immersed with BSA solution prior to loading cells and nanoparticles, and annealing temperature was raised from 60 ℃ to 63℃, out of 10 experiments, desired amplification was observed in 8 experiments with 1 experiment of non-specific amplification and 1 experiment of no amplification. This clearly was a great improvement compared to the previous experiment. Figure 5-13 shows a gel electrophoresis image of samples in different experiments when PCR chamber was immersed with BSA prior to loading cells and nanoparticles, and the annealing temperature was set at 63℃ while the composition of other PCR chemicals was the same as listed in Table 5-2. It clearly shows that desired PCR amplification was achieved when PCR chamber was immersed with 1% and 7.5% BSA prior to loading cells and nanoparticles, and the annealing temperature was set at 63℃. Different concentrations of BSA were tested from 1% to 10%. They all resulted in enhanced PCR specificity. BSA had to stay in PCR chamber long enough to improve PCR specificity. Generally speaking, 1% BSA should stay in PCR chamber for ~10 minutes and 10% BSA should stay in PCR chamber for ~6 minutes to achieve desired PCR amplification.

Table 5-3. Experiments towards finding solutions to improve PCR specificity involving gold nanoparticles in a microchip PCR setting.

Experiments	Does it help minimize non-specificity?
1. dNTPs concentration varied from 50~1500 μM	No
2. Forward primer concentration varied from 50~1500 nM	No
3. Reverse primer concentration varied from 50~1500 nM	No
4. PCR buffer solution varied from 0.1~2.5 μL/reaction	No
5. Magnesium chloride concentration varied from 0.6~15 mM	No
6. Amount of iTaq polymerase varied from 0.1~0.6 U/reaction	No
7. Increasing annealing temperature from 60℃ to 63℃	*Yes, only when combined with 13*
8. Decreasing annealing temperature from 60℃ to 55℃	No
9. Increasing extension temperature from 72℃ to 75℃	No
10. Decreasing extension temperature from 72℃ to 68℃	No
11. Increasing denaturing temperature from 95℃ to 98℃	No
12. Decreasing denaturing temperature 95℃ to 90℃	No
13. Immersing PCR chamber with 1~10% BSA solution 10 minutes prior to loading cells and nanoparticles	*Yes, only when combined with 7*

Table 5-4. Repetitive test results for improving PCR specificity. Experiment 1: Immersed PCR chamber with BSA solution prior to loading cells and nanoparticles only; Experiment 2: Increased annealing temperature to 63℃ only; Experiment 3: Immersed PCR chamber with BSA solution prior to loading cells and nanoparticles and increased PCR annealing temperature to 63℃.

	Experiment 1	Experiment 2	Experiment 3
Total Number of experiments	10	10	10
Number of experiments with non-specific amplification	8	5	1
Number of experiments with desired amplification	0	0	8
Number of experiments with no amplification	2	5	1

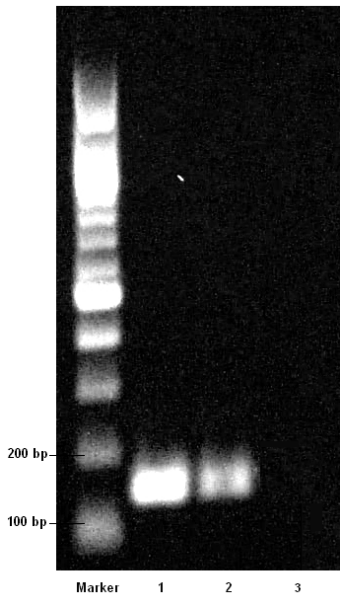

Figure 5-13. Gel electrophoresis image of the experiments (50 cycles) to improve PCR specificity. PCR chamber was immersed with different amounts of BSA prior to loading cells and nanoparticles for 10 minutes and PCR annealing temperature was raised to 63℃. PCR chamber was immersed with 7.5% BSA for 10 minutes (Lane 1), with 1% BSA for 10 minutes (Lane 2) and without BSA (Lane 3).

As demonstrated in the previous experiment, successful PCR with cells and nanoparticles was achieved using the integrated microchip system. However, a question arose as were those nanoparticles really necessary in the system? Therefore, the next experiment was conducted to demonstrate the usefulness of poly(quaternary ammonium) modified gold nanoparticles and the resulting high efficiency of the system. In this experiment, 0.8 μL of *E. coli* solution was mixed with 0.2 μL of sterilized water as a reference instead of mixing with poly(quaternary ammonium) modified gold nanoparticle dispersion followed by adding PCR master mix. The composition of the PCR master mix and experimental conditions were kept the same as that in the previous experiment which led to a successful PCR with desired amplification. The PCR thermocycling settings were as follows: 3 minutes at 95℃ for hot start, 50 cycles of amplification at 95℃ for 15 seconds, 63℃ for 30 seconds, 72℃ for 30 seconds, and 10 minutes at 72℃ for final extension. Gel electrophoresis was conducted after PCR as shown in Figure 5-14. It was clear that poly(quaternary ammonium) modified gold nanoparticles contributed significantly in cell lysis efficiency which improved the efficiency of the

integrated microchip system in terms of PCR yield. This is essential in applications where time is critical as a higher efficiency in yield means an earlier detection.

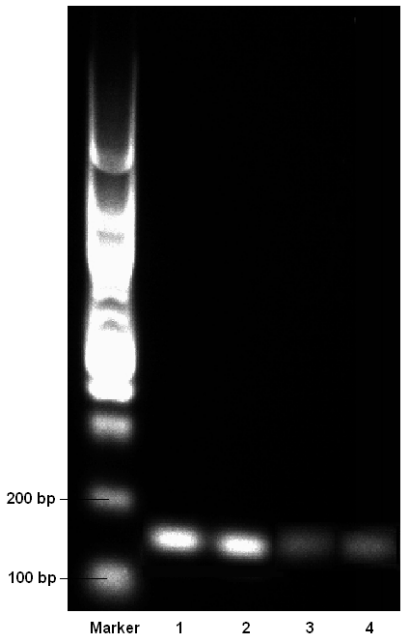

Figure 5-14. Gel electrophoresis image of the experiments (50 cycles) with 0.06 mg/mL poly(quaternary ammonium) modified gold nanoparticles and without nanoparticles. Lane 1 and 2: With nanoparticles; Lane 3 and 4: Without nanoparticles.

To finish a task in a short period of time is always desirable. In the integrated microchip system, the time it takes to complete the task is mostly dependant on the time PCR takes as cell lysis only takes 10 minutes while PCR takes more than an hour for 50 cycles under default settings. The time PCR takes is composed of two parts. One is the time it takes to transit between PCR stages and the other is the time it takes during each PCR stage. In the integrated microchip system, the time it takes to transit between PCR stages has already been optimized. To potentially shorten PCR, the time it takes during each PCR stage must be optimized. In previous experiments, PCR thermocycling was set as follows: hot start for 3 minutes, denaturing for 15 seconds, annealing for 30 seconds, extension for 30 seconds, and final extension for 10 minutes. Hot start for 3 minutes and final extension for 10 minutes are recommended by the supplier of the DNA polymerase so they were kept unchanged. Table 5-5 lists different combinations of time periods for PCR thermocycling. Figure 5-15 shows a

gel electrophoresis image containing experimental samples corresponding to all situations listed in Table 5-5. There were 50 cycles for all experiments. It was clear that time for PCR can be greatly shortened without any sacrifice in PCR yield. The best-case scenario for thermocycling was denaturing at 95℃ for 10 seconds, annealing at 63℃ for 15 seconds, extension at 72℃ for 15 seconds. This means that PCR cycling time can be reduced by almost 50%.

Table 5-5. Experiments with different time settings in PCR thermocycling.

Experiment Number	Annealing Time (s)	Extension Time (s)	Denaturing Time (s)
1 (Reference)	30	30	15
2	15	30	15
3	30	15	15
4	30	30	10
5	15	15	10

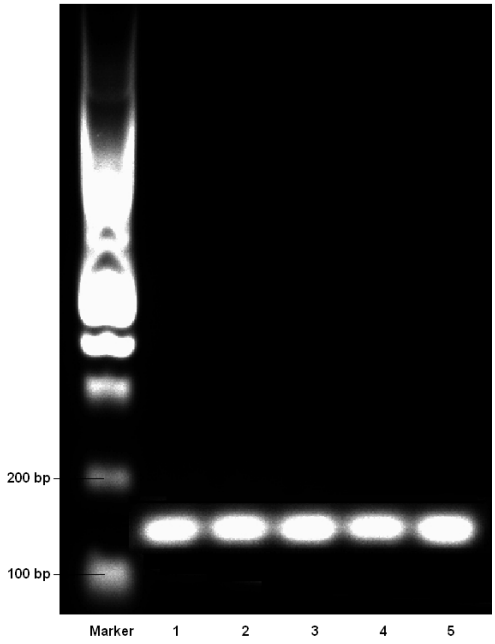

Figure 5-15. Gel electrophoresis image of experiments (50 cycles) with different time settings in PCR thermocycling. Lane 1-5 corresponds to Experiment Number 1-5 in Table 5-5.

5.5 Summary

This chapter described the research work towards prototyping an integrated LOC system involving cell lysis using poly(quaternary ammonium) modified gold nanoparticles and microchip PCR for rapid detection of bacteria. The integrated LOC system was composed of a physical microchip PCR device and a thermocycling system for fast temperature transition and accurate temperature maintaining. The microchip PCR device was easy and inexpensive to fabricate. It consisted of an off-chip microheater, an off-chip temperature sensor and 3 layers of PDMS. It was disposable and was easy to be re-constructed. The thermocycling system consisted of a data acquisition card and a software control program to provide a fast temperature transition between PCR stages and an accurate temperature maintaining during PCR stages. It was successfully demonstrated that the integrated microchip system was capable of performing cell lysis and PCR with a high efficiency. Compared to regular PCR machines, the integrated microchip system required less amounts of PCR reagents as well as reaction time, and provided the same performance if not better. The integrated microchip system can be applied to the detection of virtually any bacteria species. It provided a novel, inexpensive, convenient and point-of-care solution for rapid detection of bacteria. The system can easily be integrated with other analytical functional modules as customized solutions for point-of-care diagnosis and detection.

Chapter 6

Conclusions and Future Work

6.1 Contributions of the Thesis

The scientific contribution of this thesis is summarized as follows,

1) A novel cell lysis method for LOC applications using poly(quaternary ammonium) modified nanoparticles was proposed and demonstrated. Experiments were carried out to explore the mechanism of cell lysis, which was through cell membrane disruption caused by long chains of poly(quaternary ammonium) functional groups. Nanoparticle concentration and reaction time were critical to cell lysis efficiency. Higher nanoparticle concentration and longer reaction time generally resulted in better cell lysis efficiency. Complete *E. coli* destruction was achieved in 10 minutes. The efficient cell lysis was the result of both poly(quaternary ammonium) functional groups and the large surface-area-to-volume ratio of the nanoparticles;
2) A novel cell lysis method for LOC applications involving titanium dioxide nanoparticles and a miniaturized UV LED array was introduced and demonstrated. The mechanism of cell lysis was through cell membrane disruption caused by highly oxidative radicals generated by photocatalytic effect of titanium dioxide under UV irradiation in an aqueous environment. A miniaturized UV LED array was customized for LOC applications. The method was easy to be implemented and integrated with other LOC functions to form more complicated systems.
3) The effect of gold nanoparticles of different sizes on PCR efficiency was evaluated. In general, gold nanoparticles of larger sizes had stronger inhibitory effect on PCR than gold nanoparticles of smaller sizes at the same particle concentration. The mechanism of gold nanoparticles inhibiting PCR was explored. A hypothesis was proposed, that is gold nanoparticles and iTaq polymerase bound to each other therefore resulting in PCR inhibition by reducing the concentration of free polymerase in PCR solution. The hypothesis was well supported by several experiments. Methods were discovered and proved to be efficient in suppressing PCR inhibition induced by gold nanoparticles such as by adding more DNA polymerase and more BSA.
4) The effect of titanium dioxide nanoparticles on PCR efficiency was evaluated for the first time. They started to cause PCR inhibition at 0.8 μg/mL while they caused complete PCR inhibition at

5 μg/mL. It is suspected that there exists an optimal concentration ratio between titanium dioxide and silver nanoparticles which results in the least inhibitory effect on PCR.

5) An integrated system consisting of a physical microchip for nanoparticle cell lysis and microchip PCR, a temperature control system and all necessary connections between the physical microchip and the temperature control system was demonstrated. The demonstrated system was able to perform cell lysis and PCR with a high efficiency without having to remove nanoparticles from the solution. The integrated microchip system needed less amounts of PCR reagents as well as reaction time. It provided a novel, inexpensive, convenient and point-of-care solution for rapid detection of bacteria and can easily be integrated with other analytical functional modules as customized solutions for point-of-care diagnosis and detection.

6.2 Future Work

The following research projects are suggested as a continuation of current research.

1) Experiments are suggested to evaluate the exact mechanism between titanium dioxide nanoparticles and silver nanoparticles for improving PCR efficiency at an optimal combination.
2) Poly(quaternary ammonium) modified titanium dioxide nanoparticles are proven to exhibit excellent antibacterial property. Experiments can be carried out to use poly(quaternary ammonium) modified titanium dioxide nanoparticles in the integrated nanoparticle cell lysis and microchip PCR system instead of using poly(quaternary ammonium) modified gold nanoparticles.
3) In this thesis, it is found that coating BSA prior to experiment and raising annealing temperature at the same time can result in enhanced PCR specificity. However, the exact mechanism has not been explored yet. Experiments are suggested to find out the answer to the question.
4) Photocatalytic effect induced by titanium dioxide nanoparticles is proven to induce cell lysis. It can be integrated with microchip PCR for detection of bacteria.
5) Although an integrated Lab-on-a-Chip system involving nanoparticle cell lysis and microchip PCR is successfully demonstrated in the thesis, more analytical functional modules such as sample preparation and fluorescence detection can be integrated to the existing system to provide a more powerful and versatile product.

6) In many applications, multiplex PCR is desired. Based on the existing system involving nanoparticle cell lysis and microchip PCR, the physical microchip can be modified to accommodate more PCR chambers for the purpose.
7) *E. coli* was used to test antibacterial property of poly(quaternary ammonium) functionalized nanoparticles in Chapter 3. It is suggested that more bacteria species or even other microorganisms of interest be used to test the antibacterial property to explore more potential applications for the use of poly(quaternary ammonium) modified nanoparticles.
8) Poly(quaternary ammonium) functional groups can be introduced on magnetic nanoparticles for LOC cell lysis or antibacterial applications. They are expected to exhibit excellent antibacterial property and are easy to isolate by an external magnetic field such as a magnet.

Bibliography

[1] S.C. Terry (1975) A gas chromatography system fabricated on a silicon wafer using integrated circuit technology, PhD dissertation, Stanford University, Stanford, California.

[2] A. Manz, N. Graber, and H.M. Widmer (1990) Miniaturized total chemical analysis systems: A novel concept for chemical sensors, *Sens. Actuators, B*, vol. 1, pp. 244-248.

[3] J. Clayton (2005) Go with the microflow, *Nature Meth.*, vol. 2, pp. 621-627.

[4] M. Ratner and D. Ratner (2002) Nanotechnology a gentle introduction to the next big idea, Prentice Hall.

[5] Foresight Nanotech Institute Feynman Prize, http://en.wikipedia.org/wiki/Foresight_Nanotech_Institute_Feynman_Prize

[6] R.F. Service (2001) Breakthrough of the year: molecules get wired, *Science*, vol. 294, pp. 2442-2443.

[7] The Nanotech report, 4th edition (2006) Lux Research, Inc., New York.

[8] R. Bawa and S. Johnson (2008) Emerging issues in nanomedicine and ethics, Nanoethics: Emerging Debates, Springer, Dordrecht.

[9] P.H. Raven and G.B. Johnson (1996) Biology, 4th edition, Dubuque, IA, USA: Wm. C. Brown Publishers.

[10] G. Hollis (2003) Rapid bacteria detection using a microwave resonate cavity, Master thesis, University of Cincinnati, Cincinnati, California.

[11] I.E. Tothill (2001) Biosensor developments and potential application in the agricultural diagnostic sector, *Comput Electron. Agr.*, vol. 30, pp. 205-218.

[12] D.R. Walt and D.R. Franz (2001) Biological warfare detection, *Anal. Chem.*, vol. 72, pp.

738A-746A.

[13] G.S. Ignatov, G.A. Voloshin, Y.S. Filippovich, and R. David Walt (2009) Bacteria detection - biosensors, sensors for environment, health and security, *NATO Science for Peace and Security Series C: Environmental Security*, pp. 267-276.

[14] T. Ussing and L.C. v. Gersdorff (2007) Diode laser generated ultrasound for human blood cell lysis, *NSTI Nanotechnology Conference and Trade Show Technical Proceedings*, pp. 232-234.

[15] S. Youn, D. W. Lee, and Y.H. Cho (2008) Cell-deformability-monitoring chips based on strain- dependent cell-lysis rates, *J. Microelectromech. Syst.*, vol. 17, pp. 302-308.

[16] D. Irimia, R.G. Tompkins, and M. Toner (2004) Single-cell chemical lysis in picoliter-scale closed volumes using a microfabricated device, *Anal. Chem.*, vol. 76, pp. 6137-6143.

[17] S.K. Jha, G. Ra, G. Joo and Y. Kim (2009) Electrochemical cell lysis on a miniaturized flow-through device, *Curr. Appl Phys.*, vol. 9, pp. e301-e303.

[18] V. Schneegaß, R. Bräutigam, and J. M. Köhler (2001) Miniaturized flow-through PCR with different template types in a silicon chip thermocycler, *Lab Chip*, vol. 1, pp. 42-49.

[19] J.W. Hong, T. Fujii, M. Seki, T. Yamamoto, and I. Endo (2001) Integration of gene amplification and capillary gel electrophoresis on a polydimethylsiloxane-glass hybrid microchip, *Electrophoresis*, vol. 22, pp. 328-333.

[20] J. El-Ali, I.R. Perch-Nielsen, C.R. Poulsen, D.D. Bang, P. Telleman, and A. Wolff (2004) Simulation and experimental validation of a SU-8 based PCR thermocycler chip with integrated heaters and temperature sensor, *Sens. Actuators, A*, vol. 110, pp. 3-10.

[21] C. Yu, W. Liang, I. Kuan, C. Wei, and W. Gu (2007) Fabrication and characterization of a flow-through PCR device with integrated chromium resistive heaters, *J. Chin. Inst. Chem. Eng.*, vol. 38, pp. 333-339.

[22] J.S.G. Brookman (1974) Mechanism of cell disintegration in a high pressure homogenizer, *Biotechnol. Bioeng.*, vol. 16, pp. 371-383.

[23] T. Sauer, C.W. Robinson, and B.R. Glick (1989) Disruption of native and recombinant Escherichia coli in a high-pressure homogenizer, *Biotechnol. Bioeng.*, vol. 33, pp. 1330-1342.

[24] J. Rehacek and J. Schaefer (1977) Disintegration of microorganisms in an industrial horizontal mill of novel design, *Biotechnol. Bioeng.*, vol. 19, pp. 1523-1534.

[25] J. Limon-Lason, M. Hoare, C.B. Orsborn, D.J. Doyle, and P. Dunnill (1979) Reactor properties of a high-speed bead mill for microbial cell rupture, *Biotechnol. Bioeng.*, vol. 21, pp. 745-774.

[26] W.W. Lepeschkin (1949) The effect of ultrasonic waves on serum proteins, *J. Phys. Chem.*, vol. 53, pp. 335-343.

[27] B.I. Martins, M.R. Raju, T.L. Hayes, and C.A. Tobias (1977) Survival of cultured mammalian cells exposed to ultrasound, *Radiat. Environ. Biophys.*, vol. 14, pp. 243-250.

[28] J. Kim, J.S. Hee, G. Jia, J.V. Zoval, N.A. Da Silva, and M.J. Madou (2004) Cell lysis on a microfluidics CD (compact disc), *Lab Chip*, vol. 4, pp. 516-522.

[29] A.A. Brayman, Y. Doida, and M.W. Miller (1992) Apparent contribution of respiratory gas exchange to the in vitro “cell density effect” in ultrasonic cell lysis, *Ultrasound Med. Biol.*, vol. 18, pp. 701-714.

[30] L.B. Feril, Jr, T. Kondo, Q.L. Zhao, R. Ogawa, K. Tachibana, N. Kudo, S. Fujimoto, and S. Nakamura (2003) Enhancement of ultrasound-induced apoptosis and cell lysis by echo-contrast agents, *Ultrasound Med. Biol.*, vol. 29, pp.331-337.

[31] C. Oginoa, M.F. Dadjourb, K. Takakic, and N. Shimizu (2006) Enhancement of sonocatalytic cell lysis of Escherichia coli in the presence of TiO_2, *Biochem. Eng. J.*, vol. 32, pp. 100-105.

[32] P. Khannaa, N. Ramachandranb, J. Yangc, J. Wanga, A. Kumard, M. Jaroszeskib, and S. Bhansali (2009) Nanocrystalline diamond microspikes increase the efficiency of ultrasonic cell lysis in a microfluidic lab-on-a-chip, *Diamond Relat. Mater.*, vol. 18, pp. 606-610.

[33] P. Belgrader, D. Hansford, G.T. Kovacs, K. Venkateswaran, R. Mariella, Jr, F. Milanovich, S. Nasarabadi, M. Okuzumi, F. Pourahmadi, and M.A. Northrup (1999) A minisonicator to rapidly disrupt bacterial spores for DNA analysis, *Anal. Chem.*, vol. 71, pp. 4232-4236.

[34] G.C. Frye, S.J. Martin, R.W. Cernosek, K.B. Pfeifer, and J.S. Anderson (1991) Portable acoustic wave sensor systems, *IEEE Ultrason. Symp. Proc.*, vol. 1, pp. 311-316.

[35] G. Reed and H.J. Peppler (1973) Yeast Technology, Westport: AVI Publishing Company, pp. 355-366.

[36] J. Darbyshire (1981) Large scale enzyme extraction and recovery. Topics in enzyme and fermentation biotechnology 5. Ellis Horwood, Chichester, pp. 147-186.

[37] H. Jinseok, K.J. Thomas, G.H. Seong, and R.M. Crooks (2003) A microfluidics bioreactor based on hydrogel-entrapped *E. coli*: cell viability, lysis, and intracellular enzyme reactions, *Anal. Chem.*, vol. 75, pp. 22-26.

[38] X. Chen, D. Cui, C.C. Liu, and H.Y. Cai (2006) Microfluidic biochip for blood cell lysis, *Chin. J. Anal. Chem.*, vol. 34, pp. 1656-1660.

[39] Y. Huang, E.L. Mather, J.L. Bell, and M. Madou (2002) MEMS-based sample preparation for molecular diagnostics, *Anal. Bioanal. Chem.*, vol. 372, pp. 49-65.

[40] E.A. Schilling, A.E. Kamholz, and Yager (2002) Cell lysis and protein extraction in a microfluidics device with detection by a fluoregenic enzyme assay, *Anal. Chem.*, vol. 74, pp. 1798-1804.

[41] J.D. Yantzi and J.T.W. Yeow (2005) Carbon nanotube enhanced pulsed electric field

electroporation for biomedical applications, *IEEE ICMA Proc.*, vol. 4, pp. 1872-1877.

[42] D.W. Lee and Y.H. Cho (2007) A continuous electrical cell lysis device using a low dc voltage for a cell transport and rupture, *Sens. Actuators, B*, vol. 124, pp. 84-89.

[43] K. Park, D. Akin, and R. Bashir (2007) Electrical capture and lysis of vaccinia virus particles using silicon nano-scale probe array, *Biomed. Microdevices*, vol. 9, pp. 877-883.

[44] Mullis, Kary (1998) Dancing Naked in the Mind Field, New York: Pantheon Books.

[45] L. Zhang, X. Cui, K. Schmitt, R. Hubert, W. Navidi, and N. Arnheim (1992) Whole genome amplification from a single cell: implications for genetic analysis, *Proc. Natl. Acad. Sci. USA*, vol. 89, pp. 5847-5851.

[46] R.K. Saiki, S. Scharf, F. Faloona, K. B. Mullis, G.T. Horn, H.A. Erlich, and N. Arnheim (1985) Enzymatic amplification of beta-globin genomic sequences and restriction site analysis for diagnosis of sickle cell anemia, *Science*, vol. 230, pp. 1350–1354.

[47] R.K. Saiki, D.H. Gelfand, S. Stoffel, S.J. Scharf, R. Higuchi, G.T. Horn, K.B. Mullis, and H.A. Erlich (1988) Primer-directed enzymatic amplification of DNA with a thermostable DNA polymerase, *Science*, vol. 239, pp. 487-91.

[48] J. Sambrook, E. F. Fritsch, and T. Maniatis (1989) Molecular cloning: a laboratory manual, 2nd edition, Cold Spring Harbor Laboratory Press, Cold Sprig Harbor, New York.

[49] D.M. Coen (2006) The polymerase chain reaction, current protocols in molecular biology, John Wiley & Sons, pp. 15.0.1-15.0.3.

[50] K.B. Mullis and F.A. Faloona (1987) Specific synthesis of DNA in vitro via a polymerase-catalysed chain reaction, *Methods Enzymol.*, vol. 155, pp. 335-350.

[51] S.J. Scharf, G.T. Horn and H.A. Erlich (1986) Direct cloning and sequence analysis of enzymatically amplified genomic sequences, *Science*, vol. 233, pp. 1076-1078.

[52] T. Tanaka and R.L. Letsinger (1982) Syringe method for stepwise chemical synthesis of oligonucleotides, *Nucl. Acids Res.*, vol. 10, pp. 3249-3259.

[53] A. Chien, D.B. Edgar, and J.M. Trela (1976) Deoxyribonucleic acid polymerase from the extreme thermophile Thermus aquaticus, *J. Bact.*, vol. 127, pp. 1550-1557.

[54] F.C. Lawyer, S. Stoffel, R.K. Saiki, S.Y. Chang, P.A. Landre, R.D. Abramson, and D.H. Gelfand (1993) High-level expression, purification, and enzymatic characterization of full-length Thermus aquaticus DNA polymerase and a truncated form deficient in 5' to 3' exonuclease activity, *Genome Res.*, vol. 2, pp. 275-287.

[55] J.A. Rogers and R.G. Nuzzo (2005) Recent progress in soft lithography, *Mater. Today*, vol. 8, pp. 50-56.

[56] L.J. Kricka and P. Wilding (2003) Microchip PCR, *Anal. Bioanal. Chem.*, vol. 377, pp. 820-825.

[57] J.M. Berg, J.L. Tymoczko, and L. Stryer (2002) Biochemistry, 5th edition, New York: W H Freeman.

[58] Gel electrophoresis, http://en.wikipedia.org/wiki/Gel_electrophoresis

[59] There's Plenty of Room at the Bottom, http://en.wikipedia.org/wiki/Plenty_of_Room_at_the_Bottom

[60] N. Taniguchi (1974) On the Basic Concept of “Nano-Technology”, *Proc. Intl. Conf. Prod. Eng. Tokyo*, Part II, Japan Society of Precision Engineering.

[61] K. Eric Drexler (1981) Molecular engineering: An approach to the development of general capabilities for molecular manipulation, *Proc. Natl. Acad. Sci. USA*, vol. 78, pp. 5275-5278.

[62] H.W. Kroto, J.R. Heath, S.C. O’Brien, R.F. Curl, and R.E. Smalley (1985) C60: Buckminsterfullerene, *Nature*, vol. 318, pp. 162-163.

[63] Eric Drexler (1986) Engines of Creation: The Coming Era of Nanotechnology, New York: Anchor Books.

[64] IBM: More than two decades of nanotechnology leadership, http://www.zurich.ibm.com/nano/themes_history.html

[65] Atomic force microscopy, http://en.wikipedia.org/wiki/Atomic_force_microscopy

[66] Cecie Starr (2005) Biology: Concepts and Applications, Thomson Brooks/Cole.

[67] J.C. Hulteen and R.P. Van Duyne (1995) Nanosphere lithography: A materials general fabrication process for periodic particle array surfaces, *J. Vac. Sci. Technol., A*, vol. 13, pp. 1553-1558.

[68] C.L. Haynes and R.P. Van Duyne (2001) Nanosphere lithography: a versatile nanofabrication tool for studies of size-dependent nanoparticle optics, *J. Phys. Chem., B*, vol. 105, pp 5599-5611.

[69] S.I. Stupp, V. LeBonheur, K. Walker, L.S. Li, K.E. Huggins, M. Keser, and A. Amstutz (1997) Supramolecular materials: self-organized nanostructures, *Science*, vol. 276, pp. 384-389.

[70] M. Monthioux and V.L. Kuznetsov (2006) Who should be given the credit for the discovery of carbon nanotubes? *Carbon*, vol. 44, pp. 1621-1623.

[71] M.F. Yu, O. Lourie, M.J. Dyer, K. Moloni, T.F. Kelly, and R.S. Ruoff (2000) Strength and breaking mechanism of multiwalled carbon nanotubes under tensile load, *Science*, vol. 287, pp. 637-640.

[72] S. Hong and S. Myung (2007) Nanotube electronics: a flexible approach to mobility, *Nature Nanotechnol.*, vol. 2, pp. 207-208.

[73] E. Pop, D. Mann, Q. Wang, K. Goodson, and H. Dai (2006) Thermal conductance of an

individual single-Wall carbon nanotube above room temperature, *Nano Lett.*, vol. 6, pp. 96-100.

[74] R.L. Zong, J. Zhou, B. Li, M. Fu, S.K. Shi, and L.T. Li (2005) Optical properties of transparent copper nanorod and nanowire arrays embedded in anodic alumina oxide, *J. Chem. Phys.*, vol. 123, pp. 094710 (5 pages).

[75] R. Narayanan and M.A. El-Sayed (2004) Shape-dependent catalytic activity of platinum nanoparticles in colloidal solution, *Nano Lett.*, vol. 4, pp 1343-1348.

[76] W.Z. Li, C.H. Liang, W.J. Zhou, J.S. Qiu, Z.H. Zhou, G.Q. Sun, and Q. Xin (2003) Preparation and characterization of multiwalled carbon nanotube-supported platinum for cathode catalysts of direct methanol fuel cells, *J. Phys. Chem., B*, vol. 107, pp 6292-6299.

[77] M. Haruta (2005) Catalysis: Gold rush, *Nature*, vol. 437, pp. 1098-1099.

[78] M.D. Hughes, Y.J. Xu, P. Jenkins, P. McMorn, P. Landon, D.I. Enache, A.F. Carley, G.A. Attard, G.J. Hutchings, F. King, E.H. Stitt, P. Johnston, K. Griffin, and C.J. Kiely (2005) Tunable gold catalysts for selective hydrocarbon oxidation under mild conditions, *Nature*, vol. 437, pp. 1132-1135.

[79] R. Dobashi (2009) Risk of dust explosions of combustible nanomaterials, *J. Phys.: Conf. Ser.*, vol. 170, pp. 012029 (6 pages).

[80] M.L. Pantoya and J.J. Granier (2005) Combustion behavior of highly energetic thermites: nano versus micron composites, *Propellants Explos. Pyrotech.*, vol. 30, pp. 53-62.

[81] D.P. Yu, C.S. Lee, I. Bello, X.S. Sun, Y.H. Tang, G.W. Zhou, Z.G. Bai, Z. Zhang, and S.Q. Feng (1998) Synthesis of nano-scale silicon wires by excimer laser ablation at high temperature, *Solid State Commun.*, vol. 105, pp. 403-407.

[82] Y. Cui, Z.H. Zhong, D.L. Wang, W.U. Wang, and C.M. Lieber (2003) High performance

silicon nanowire field effect transistors, *Nano Lett.*, vol. 3, pp. 149-152.

[83] C.J. Brinker and G.W. Scherer (1990) Sol-Gel Science: The Physics and Chemistry of Sol-Gel Processing, 1st edition, Academic Press.

[84] R. Corriu and N.T. Anh (2009) Molecular Chemistry of Sol-Gel Derived Nanomaterials, John Wiley and Sons.

[85] C.N.R. Rao, G.U. Kulkarni, P.J. Thomasa, and P.P. Edwards (2000) Metal nanoparticles and their assemblies, *Chem. Soc. Rev.*, vol. 29, pp. 27-35.

[86] R.A. Sperling, P.R. Gil, F. Zhang, M. Zanella, and W.J. Parak (2008) Biological applications of gold nanoparticles, *Chem. Soc. Rev.*, vol. 37, pp. 1896-1908.

[87] S. Baron (1996) Medical Microbiology, 4th edition, University of Texas Medical Branch at Galveston.

[88] H.E. Kubitschek (1990) Cell volume increase in Escherichia coli after shifts to richer media, *J. Bacteriol.*, vol. 172, pp. 94-101.

[89] Gram-negative bacteria, http://en.wikipedia.org/wiki/File:Gram-Cell-wall.svg

[90] B.M. Mackey, C.A. Miles, D.A. Seymour, and S.E. Parsons (1993) Thermal denaturation and loss of viability in Escherichia coli and Bacillus stearothermophilus, *Lett. Appl. Microbiol.*, vol. 16, pp. 56-58.

[91] U. Fotadar, P. Zaveloff, and L. Terracio (2005) Growth of Escherichia coli at elevated temperatures, *J. Basic Microbiol.*, vol. 45, pp. 403-404.

[92] P. Feng, S.D. Weagant, and M.A. Grant (2002) BAM: Enumeration of Escherichia coli and the Coliform Bacteria, Bacteriological Analytical Manual (chapter 4), U.S. Food and Drug Administration.

[93] R.L Vogt and L. Dippold (2005) Escherichia coli O157:H7 outbreak associated with consumption of ground beef, *Public Health Rep.*, vol. 120, pp. 174-178.

[94] R. Bentley and R. Meganathan (1982) Biosynthesis of vitamin K (menaquinone) in bacteria, *Microbiol. Rev.*, vol. 46, pp. 241-280.

[95] S. Hudault, J. Guignot, and A. Servin (2001) Escherichia coli strains colonising the gastrointestinal tract protect germfree mice against Salmonella typhimurium infection, *Gut.*, vol. 49, pp. 47-55.

[96] G. Reid, J. Howard, and B.S. Gan (2001) Can bacterial interference prevent infection? *Trends Microbiol.*, vol. 9, pp. 424-428.

[97] P. Abgrall and A.M. Gué (2007) Lab-on-chip technologies: making a microfluidic network and coupling it into a complete microsystem - a review, *J. Micromech. Microeng.*, vol. 17, pp. R15-R49.

[98] M. Anduze, S. Colin, R. Caen, H. Camon, V. Conedera, and T. Do Conto (2001) Analysis and testing of a fluidic vortex microdiode, *J. Micromech. Microeng.*, vol. 11, pp. 108-112.

[99] S. Yang and T. Saif (2005) Reversible and repeatable linear local cell force response under large stretches, *Exp. Cell Res.*, vol. 305, pp. 42-50.

[100] K.B. Lee and L. Lin (2004) Surface micromachined glass and polysilicon microchannels using MUMPs for BioMEMS applications, *Sens. Actuators, A*, vol. 111, pp. 44-50.

[101] M. Heckele and W.K. Schomburg (2004) Review on micro molding of thermoplastic polymers, *J. Micromech. Microeng.*, vol. 14, pp. R1-R14.

[102] C.S. Effenhauser, G.J.M. Bruin, A. Paulus, and M. Ehrat (1997) Integrated capillary electrophoresis on flexible silicone microdevices: analysis of DNA restriction fragments and detection of single DNA molecules on microchips, *Anal. Chem.*, vol. 69, pp. 3451-3457.

[103] AXSUN Technologies Inc, http://www.axsun.com/

[104] R. Truckenmüller, Z. Rummler, Th. Schaller, and W.K. Schomburg (2002) Low-cost thermoforming of micro fluidic analysis chips, *J. Micromech. Microeng.*, vol. 12, pp. 375-379.

[105] B. Graß, G. Weber, A. Neyer, M. Schilling, and R. Hergenröder (2002) Micro-structured analytical instrumentation for the analysis of liquids, *Spectrochim. Acta, B*, vol. 57, pp. 1575-1583.

[106] S. Li, L.W. Pan, and L.W. Lin (2003) Frozen water for MEMS fabrication and packaging applications, *Proc. IEEE MEMS 2003*, pp. 650-653.

[107] G. Kotzar, M. Freas, P. Abel, A. Fleischman, S. Roy, C. Zorman, J.M. Moran, and J. Melzak (2002) Evaluation of MEMS materials of construction for implantable medical devices, *Biomaterials*, vol. 23, pp. 2737-2750.

[108] H. Sato, T. Kakinuma, J.S. Go, and S. Shoji (2003) A novel fabrication of in-channel 3-D micromesh structure using maskless multi-angle exposure and its microfilter application, *Proc. IEEE MEMS 2003*, pp. 223-226.

[109] P. Abgrall, H. Camon, V. Conedera, N. Fabre, and A.M. Gue (2005) SU-8 technology for free-standing structures in optical and fluidic MEMS, *Proc. MICRO SYSTEM Technologies 2005*, pp. 40-47.

[110] T.K. Sau, A.L. Rogach, F. Jäckel, T. A. Klar, and J. Feldmann (2010) Properties and applications of colloidal nonspherical noble metal nanoparticles, *Adv. Mater.*, vol. 22, pp. 1805-1825.

[111] J.S. Kim, E. Kuk, K.N. Yu, J.H. Kim, S.J. Park, H.J. Lee, S.H. Kim, Y.K. Park, Y.H. Park, C.Y. Hwang, Y.K. Kim, Y.S. Lee, D.H. Jeong, and M.H. Cho (2007) Antimicrobial effects of silver nanoparticles, *Nanomed. Nanotechnol. Biol. Med.*, vol. 3, pp. 95-101.

[112] C.N. Lok, C.M. Ho, R. Chen, Q.Y. He, W.Y. Yu, H. Sun, P.K.H. Tam, J.F. Chiu, and C.M. Che (2007) Silver nanoparticles: partial oxidation and antibacterial activities, *J. Biol. Inorg. Chem.*, vol. 12, pp. 527-534.

[113] P.K. Stoimenov, R.L. Klinger, G.L. Marchin, and K.J. Klabunde (2002) Metal oxide nanoparticles as bactericidal agents, *Langmuir*, vol. 18, pp 6679-6686.

[114] H. Gu, P.L. Ho, E. Tong, L. Wang, and B. Xu (2003) Presenting Vancomycin on nanoparticles to enhance antimicrobial activities, *Nano Lett.*, vol. 3, pp. 1261-1263.

[115] G. Applerot, A. Lipovsky, R. Dror, N. Perkas, Y. Nitzan, R. Lubart, and A. Gedanken (2009) Enhanced antibacterial activity of nanocrystalline ZnO due to increased ROS-mediated cell injury, *Adv. Funct. Mater.*, vol. 19, pp. 842-852.

[116] L. Balogh, D.R. Swanson, D.A. Tomalia, G.L. Hagnauer, and A.T. McManus (2001) Dendrimer−Silver complexes and nanocomposites as antimicrobial agents, *Nano Lett.*, vol. 1, pp. 18-21.

[117] C.Z. Chen and S.L. Cooper (2000) Recent advances in antimicrobial dendrimers, *Adv. Mater.*, vol. 12, pp. 843-846.

[118] P. Dallas, J. Tucek, D. Jancik, M. Kolar, A. Panacek, and R. Zboril (2010) Magnetically controllable silver nanocomposite with multifunctional phosphotriazine matrix and high antimicrobial activity, *Adv. Funct. Mater.*, vol. 20, pp. 2347-2354.

[119] H. Zhang, D. Wang, R. Butler, N.L. Campbell, J. Long, B. Tan, D.J. Duncalf, A.J. Foster, A. Hopkinson, D. Taylor, D. Angus, A.I. Cooper, and S.P. Rannard (2008) Formation and enhanced biocidal activity of water-dispersable organic nanoparticles, *Nat. Nanotechnol.*, vol. 3, pp. 506-511.

[120] L. Liu, K. Xu, H. Wang, P.K.J. Tan, W. Fan, S.S. Venkatraman, L. Li, and Y. Yang (2009) Self-assembled cationic peptide nanoparticles as an efficient antimicrobial agent, *Nat.*

Nanotechnol., vol. 4, pp. 457-463.

[121] R.S. Norman, J.W. Stone, A. Gole, C.J. Murphy, and T.L. Sabo-Attwood (2008) Targeted photothermal lysis of the pathogenic bacteria, Pseudomonas aeruginosa, with gold nanorods, *Nano Lett.*, vol. 8, pp. 302-306.

[122] K.H. Cheong, D.K. Yi, J. Lee, J. Park, M.J. Kim, J.B. Edel, and C. Ko (2008) Gold nanoparticles for one step DNA extraction and real-time PCR of pathogens in a single chamber, *Lab Chip*, vol. 8, pp. 810-813.

[123] N. Jones, B. Ray, K.T. Ranjit, and A.C. Manna (2008) Antibacterial activity of ZnO nanoparticle suspensions on a broad spectrum of microorganisms, *FEMS Microbiol. Lett.*, vol. 279, pp. 71-76.

[124] Y. Tsuang, J. Sun, Y. Huang, C. Lu, W.H. Chang, and C. Wang (2008) Studies of photokilling of bacteria using titanium dioxide nanoparticles, *Artif. Organs*, vol. 32, pp. 167-174.

[125] A.D. McNaught and A. Wilkinson (2009) IUPAC. Compendium of Chemical Terminology, 2nd edition, Blackwell Scientific Publications.

[126] Y.B. Acheampong (1980) The antibacterial action of short and long chain quaternary ammonium compounds, Ph.D. thesis, University of Bradford, Bradford, United Kingdom.

[127] S.P. Denyer, and G.S.A.B. Stewart (1998) Mechanisms of action of disinfectants, *Int. Biodeterior. Biodegrad.*, vol. 41, pp. 261-268.

[128] C.J. Ioannou, G.W. Hanlon, and S.P. Denyer (2007) Action of disinfectant quaternary ammonium compounds against Staphylococcus aureus, *Antimicrob. Agents Chemother.*, vol. 51, pp. 296-306.

[129] C.Z. Chen, N.C. Beck-Tan, P. Dhurjati, T.K. van Dyk, R.A. LaRossa, and S.L. Cooper (2000)

Quaternary ammonium functionalized poly(propylene imine) dendrimers as effective antimicrobials: structure-activity studies, *Biomacromolecules*, vol. 1, pp 473-480.

[130] C.Z. Chen, N.C. Beck-Tan, and S.L. Cooper (1999) Incorporation of dimethyldodecylammonium chloride functionalities onto poly(propylene imine) dendrimers significantly enhances their antibacterial properties, *Chem. Commum.*, pp. 1585-1586.

[131] M. Ghosh (1988) Synthetic macromolecules as potential chemotherapeutic agents, *Polym. News*, vol. 13, pp. 71-77.

[132] N. Kawabata and M. Nishiguchi (1988) Antibacterial activity of soluble pyridinium-type polymers, *Appl. Environ. Microbiol.*, vol. 54, pp. 2532-2535.

[133] Y. Ohta, Y. Kondo, K. Kawada, T. Teranaka, and N. Yoshino (2008) Synthesis and antibacterial activity of quaternary ammonium salt-type antibacterial agents with a phosphate group, *Journal of Oleo Science*, vol. 57, pp. 445-452.

[134] S.S. Block (1991) Disinfection, sterilization, and preservation, 4th edition, Philadelphia: Lea & Febiger, pp. 225-255.

[135] F. Kopecky (1996) Micellization and other associations of amphiphilic antimicrobial quanternary ammonium salts in aqueous solutions, *Pharmazie*, vol. 51, pp. 135-144.

[136] T. Tashiro (2001) Antimicrobial and bacterium adsorbing macromolecules, *Macromol. Mater. Eng.*, vol. 286, pp. 63-87.

[137] T. Thorsteinsson, M. Masson, K. Kristinsson, M.A. Hjalmarsdottir, H. Hilmarsson, and T. Loftsson (2003) Soft antimicrobial agents: synthesis and activity of labile environmentally friendly long chain quaternary ammonium compounds, *J. Med. Chem.*, vol. 46, pp. 4173-4181.

[138] A.J. McBain, R.G. Ledder, L.E. Moore, C.E. Catrenich, and P. Gilbert (2004) Effects of

quaternary-ammonium-based formulations on bacterial community dynamics and antimicrobial susceptibility, *Appl. Environ. Microbiol.*, vol. 70, pp. 3449-3456.

[139] R. Roy (1996) Glycodendrimers A new class of biopolymers, *Polym. News*, vol. 21, pp. 226-232.

[140] D.K. Ellsworth, D. Verhulst, T.M. Spitler, and B.J. Sabacky (2000) Titanium nanoparticles move to the marketplace, *Chem. Innov.*, vol. 30, pp. 30-35.

[141] A. Fujishima and K. Honda (1972) Electrochemical photolysis of water at a semiconductor electrode, *Nature*, vol. 238, pp.37-38.

[142] A.L. Linsebigler, G. Lu, and J.T. Yates, Jr. (1995) Photocatalysis on TiO_2 surfaces: principles, mechanisms, and selected results, *Chem. Rev.*, vol. 95, pp. 735-758.

[143] S.J. Teichner (2008) The origins of photocatalysis, *J. Porous Mater.*, vol. 15, pp. 311-314.

[144] Y. Nosaka and M.A. Fox (1988) Kinetics for electron transfer from laser-pulse irradiated colloidal semiconductors to adsorbed methylviologen: dependence of the quantum yield on incident pulse width, *J. Phys. Chem.*, vol. 92, pp. 1893-1897.

[145] A. Fujishima, T. N. Rao, and D. A. Tryk (2000) Titanium dioxide photocatalysis, *J. Photochem. Photobiol., C*, vol. 1, pp. 1-21.

[146] M.R. Hoffmann, S.T. Martin, W. Choi, and D.W. Bahnemann (1995) Environmental applications of semiconductor photocatalysis, *Chem. Rev.*, vol. 95, pp. 69-96.

[147] T. Hisanga, K. Harada, and K. Tanaka (1990) Photocatalytic degradation of organochlorine compounds in suspended TiO_2, *J. Photochem. Photobiol., A*, vol. 54, pp. 113-118.

[148] D.M. Blake, P.C. Maness, Z. Huang, E.J. Wolfrum, and J. Huang (1999) Application of the photocatalytic chemistry of titanium dioxide to disinfection and the killing of cancer cells, *Sep. Purif. Methods*, vol. 28, pp. 1-50.

[149] T. Asahara, H. Koseki, T. Tsurumoto, K. Shiraishi, H. Shindo, K. Baba, H. Taoda, and N. Terasaki (2009) The bactericidal efficacy of a photocatalytic TiO_2 particle mixture with oxidizer against Staphylococcus aureus, *Jpn. J. Infect. Dis.*, vol. 62, pp. 378-380.

[150] K. Page, R.G. Palgrave, I.P. Parkin, M. Wilson, S.L.P. Savin, and A.V. Chadwick (2007) Titania and silver–titania composite films on glass - potent antimicrobial coatings, *J. Mater. Chem.*, vol. 17, pp. 95-104.

[151] M.P. Reddy, A. Venugopal, and M. Subrahmanyam (2007) Hydroxyapatite-supported Ag–TiO_2 as Escherichia coli disinfection photocatalyst, *Water Res.*, vol. 41, pp. 379-386.

[152] Specifications for Nichia chip type UV LED, Model: NSSU100AT, http://www.nichia.co.jp/specification/en/product/led/NSSU100A-E.pdf

[153] T.K. Shih, C.F. Chen, J.R. Ho, and F.T. Chuang (2006) Fabrication of PDMS (polydimethylsiloxane) microlens and diffuser using replica molding, *Microelectron. Eng.*, vol. 83, pp. 2499-2503.

[154] LIVE/DEAD BacLight Bacterial Viability Kits, http://probes.invitrogen.com/media/pis/mp07007.pdf

[155] G. Gogniat and S. Dukan (2007) TiO_2 photocatalysis causes DNA damage via Fenton reaction-generated hydroxyl radicals during the recovery period, *Appl. Environ. Microbiol.*, vol. 73, pp. 7740-7743.

[156] I. Paspaltsis, K. Kotta, R. Lagoudaki, N. Grigoriadis, I. Poulios, and T. Sklaviadis (2006) Titanium dioxide photocatalytic inactivation of prions, *J. Gen. Virol.*, vol. 87, pp. 3125-3130.

[157] T. Saito, T. Iwase, J. Horie, and T. Morioka (1992) Mode of photocatalytic bactericidal action of powdered semiconductor TiO_2 on mutans streptococci, *J. Photochem. Photobiol., B*, vol. 14, pp. 369-379.

[158] H. Sakai, E. Ito, R.X. Cai, T. Yoshioka, Y. Kubota, K. Hashimoto, and A. Fujishima (1994) Intracellular Ca2+ concentration change of T24 cell under irradiation in the presence of TiO_2 ultrafine particles, *Biochim. Biophys. Acta*, vol. 1201, pp. 259-265.

[159] K. Sunada, Y. Kikuchi, K. Hashimoto, and A. Fujishima (1998) Bactericidal and detoxification effects of TiO_2 thin film photocatalysts, *Environ. Sci. Technol.*, vol. 32, pp. 726.

[160] R.W. Whatmore (2006) Nanotechnology-what is it? Should we be worried? *Occupational Medicine*, vol. 56, pp. 295-299.

[161] S.E. McNeil (2005) Nanotechnology for the biologist, *J. Leukocyte Biol.*, vol. 78, pp. 585-594.

[162] H. Li, J. Huang, J. Lv, H. An, X. Zhang, Z. Zhang, C. Fan, and J. Hu (2005) Nanoparticle PCR: nanogold-assisted PCR with enhanced specificity, *Angew. Chem. Int. Edit.*, vol. 44, pp. 5100-5103.

[163] M. Li, Y. Lin, C. Wu, and H. Liu (2005) Enhancing the efficiency of a PCR using gold nanoparticles, *Nucleic Acids Res.*, vol. 33, pp. e184.

[164] W. Yang, L. Mi, X. Cao, X. Zhang, C. Fan, and J. Hu (2008) Evaluation of gold nanoparticles as the additive in real-time polymerase chain reaction with SYBR Green I dye, *Nanotechnology*, vol. 19, 255101(9 pp.).

[165] B.V. Vu, D. Litvinov, and R.C. Willson (2008) Gold nanoparticle effects in polymerase chain reaction: favoring of smaller products by polymerase adsorption, *Anal. Chem.*, vol. 80, pp. 5462-5467.

[166] P. Keblinski, S.R. Phillpot, S.U.S. Choi, and J.A. Eastman (2002) Mechanism of heat flow in suspension of nano-sized particles (nanofluids), *Int. J. Heat Mass Transf.*, vol. 45, pp. 855-863.

[167] J.E. Galán, C. Ginocchio, and P. Costeas (1992) Molecular and functional characterization of

the Salmonella invasion gene invA: homology of InvA to members of a new protein family, *J. Bacteriol.*, vol. 174, pp. 4338-4349.

[168] J. Hoorfar, P. Ahrens, and P. Rådström (2000) Automated 5' nuclease PCR assay for identification of Salmonella enterica, *J. Clin. Microbiol.*, vol. 38, pp. 3429-3435.

[169] C.T. Witter, B.C. Marshall, G.H. Reed, and J.L. Cherry (1993) Rapid cycle allele-specific amplification: studies with the cystic fibrosis locus, *Clin. Chem.*, vol. 39, pp. 804-809.

[170] C.T. Witter and D.J. Garling (1991) Rapid cycle DNA amplification: time and temperature optimization, *Biotechniques*, vol. 10, pp. 76-83.

[171] R.S. Cha and W.G. Thilly (1993) Specificity, efficiency, and fidelity of PCR, *Genome Res.*, vol. 3, pp. S18-S29.

[172] R.A. Jefferson, S.M. Burgess, and D. Hirsh (1986) beta-Glucuronidase from Escherichia coli as a gene fusion marker, *Proc. Natl. Acad. Sci. USA*, vol. 83, pp. 8447-8451.

[173] A.K. Bej, J.L. DiCesare, L. Haff, and R.M. Atlas (1991) Detection of Escherichia coli and Shigella spp. in water by using the polymerase chain reaction and gene probes for uid, *Appl. Environ. Microbiol.*, vol. 57, pp. 1013-1017.

Appendices

Appendix A

Steady State Temperature Characterization Result

Chamber (℃)	Microheater (℃)	Chamber (℃)	Microheater (℃)	Chamber (℃)	Microheater (℃)
25	25	50	54.8	75	85
26	26	51	56	76	86
27	27.5	52	57	77	87.5
28	28.5	53	58.5	78	88.5
29	29.5	54	59.5	79	89.5
30	30.5	55	60.5	80	91
31	31.5	56	61.5	81	92
32	33	57	62.5	82	93
33	34.5	58	63.5	83	94
34	35.5	59	65	84	95
35	36.5	60	66	85	96.5
36	37.5	61	67.5	86	98
37	39	62	69	87	99.5
38	40.5	63	70.5	88	101
39	41.5	64	72	89	102
40	42.5	65	73.5	90	103.5
41	44	66	74.5	91	105
42	45	67	76	92	106
43	46.5	68	77	93	107.5
44	47.5	69	78.5	94	109
45	48.5	70	79.5	95	110
46	49.5	71	80.5	96	111.5
47	51	72	82	97	113
48	52.5	73	83	98	115
49	53.5	74	84	99	117